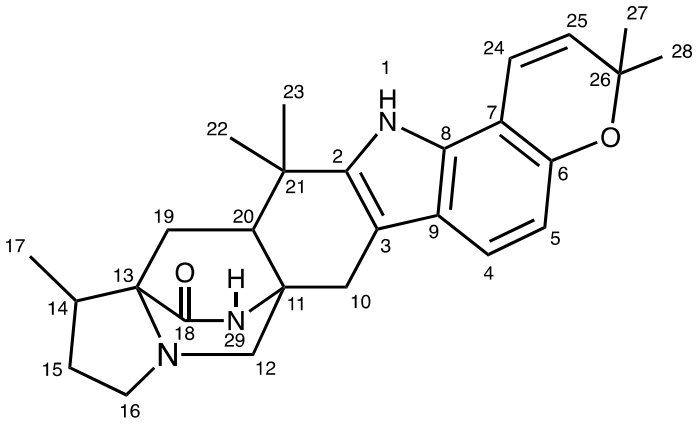

Figure S1. Numbering scheme for paraherquamide K (**14**).

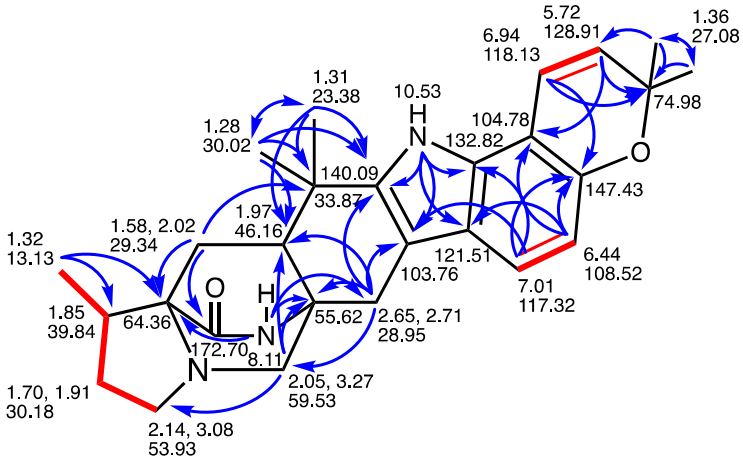

Figure S2. gHMBCAD and gCOSY correlations for paraherquamide K (**14**) in $(CD_3)_2SO$-d_6.

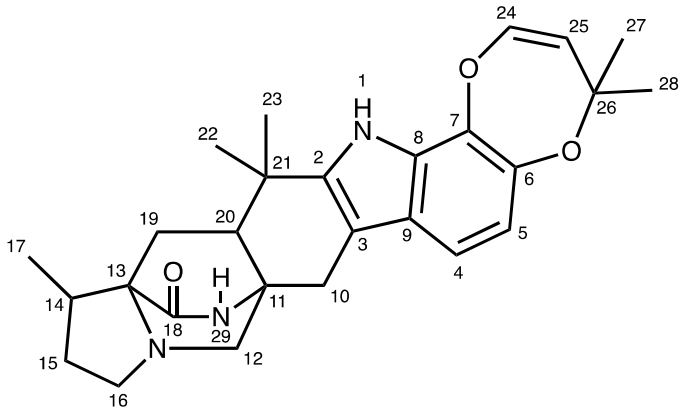

Figure S3. Numbering scheme for paraherquamide L (**15**).

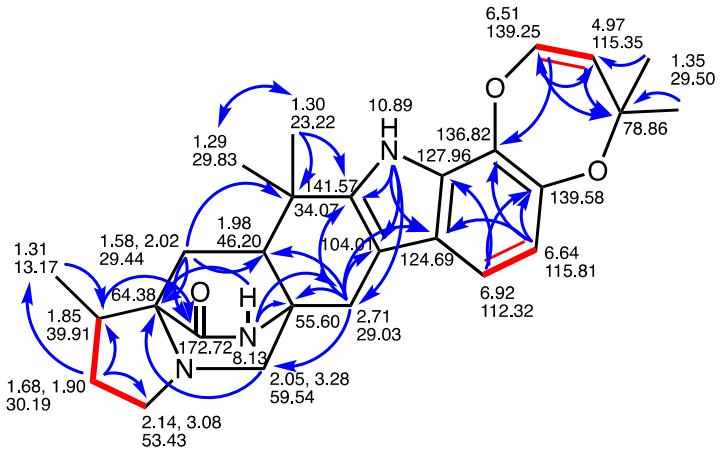

Figure S4. gHMBCAD and gCOSY correlations for paraherquamide L (**15**) in $(CD_3)_2SO$-d_6.

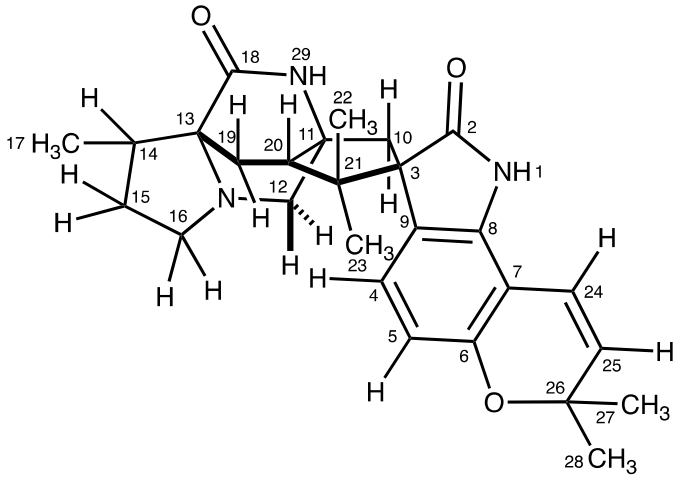

Figure S5. Numbering scheme for paraherquamide M (**16**).

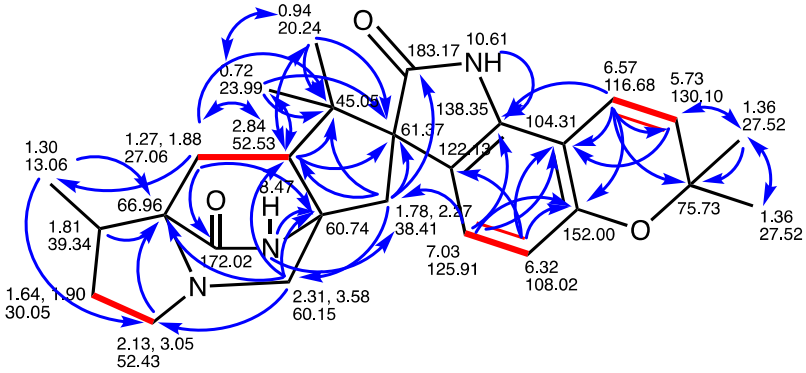

Figure S6. gHMBCAD and gCOSY correlations for paraherquamide M (**16**) in $(CD_3)_2SO$-d_6.

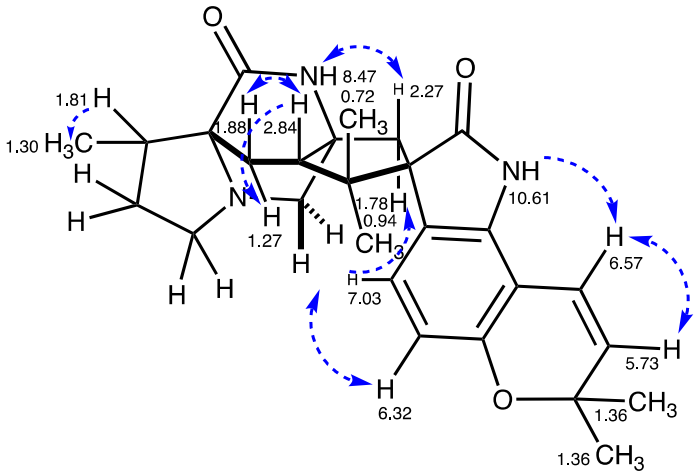

Figure S7. NOESY correlations for paraherquamide M (**16**) in $(CD_3)_2SO$-d_6.

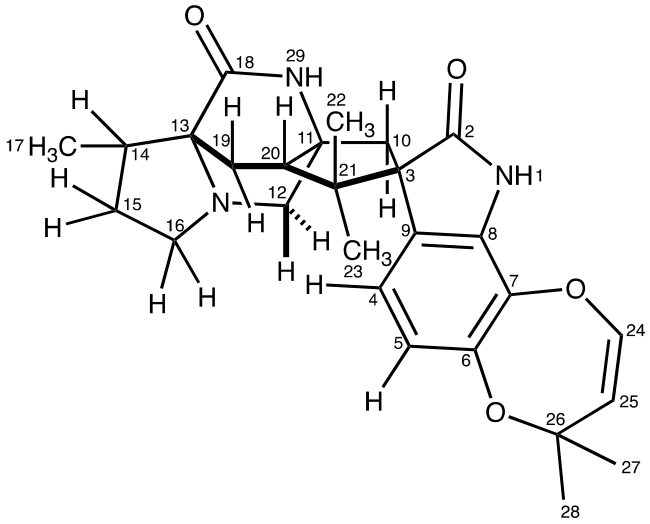

Figure S8. Numbering scheme for paraherquamide N (**17**).

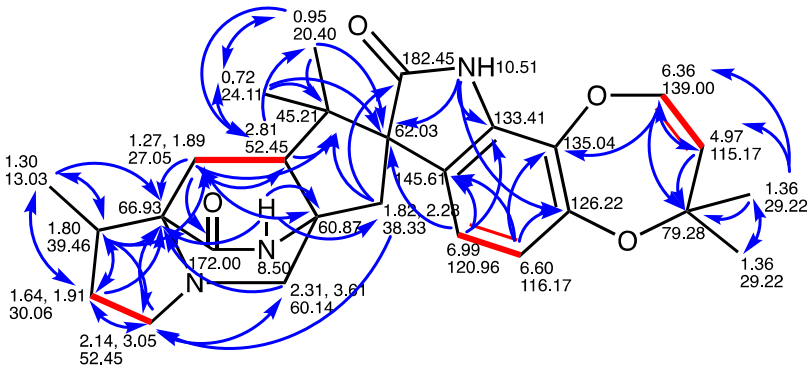

Figure S9. gHMBCAD and gCOSY correlations for paraherquamide N (**17**) in $(CD_3)_2SO$-d_6.

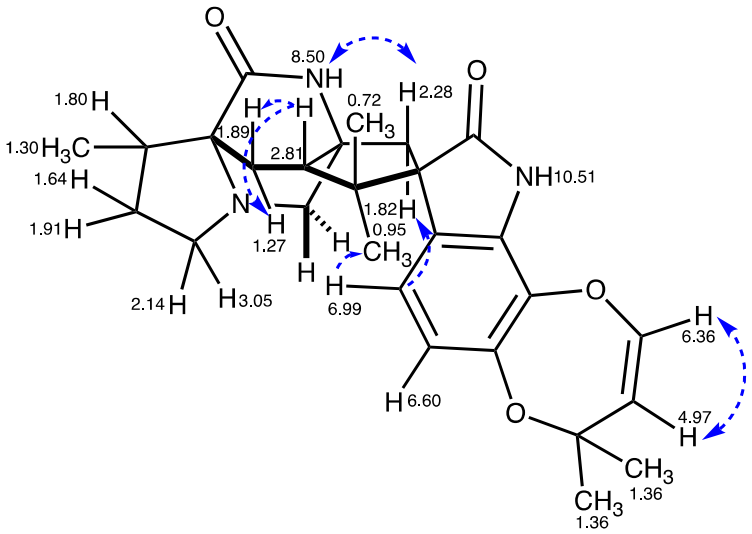

Figure S10. NOESY correlations for paraherquamide N (**17**) in $(CD_3)_2SO$-d_6.

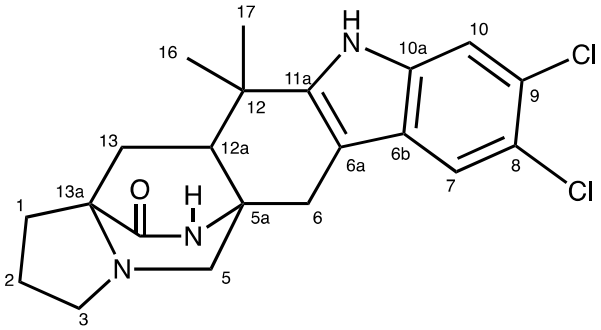

Figure S11. Numbering scheme for malbrancheamide (**19**).

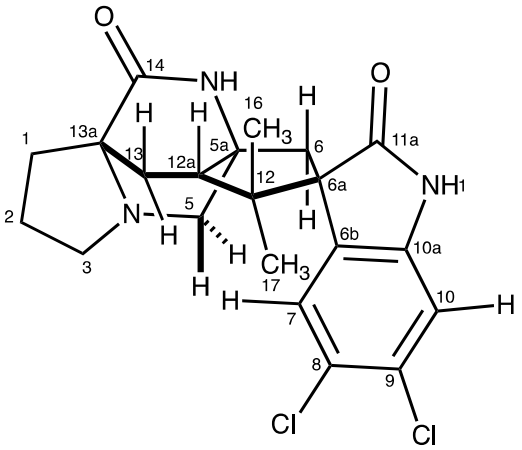

Figure S12. Numbering scheme for spiromalbramide (**20**).

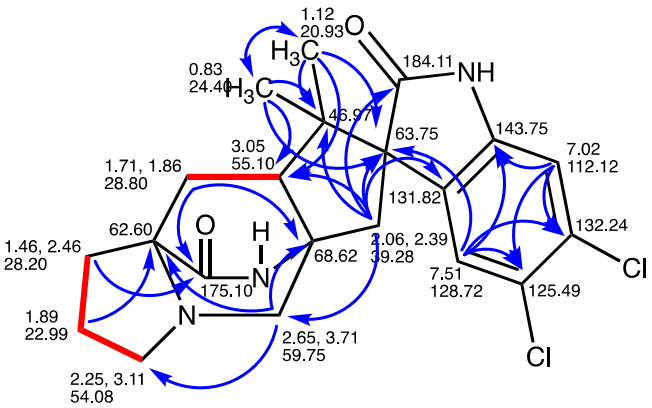

Figure S13. gHMBCAD and gCOSY correlations for spiromalbramide (**20**) in CD_3OD.

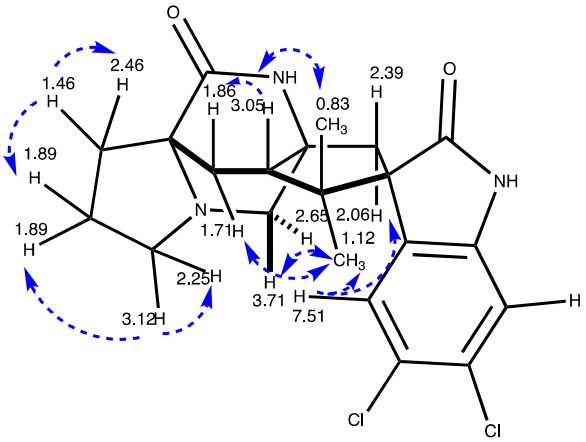

Figure S14. NOESY correlations for spiromalbramide (**20**) in CD_3OD.

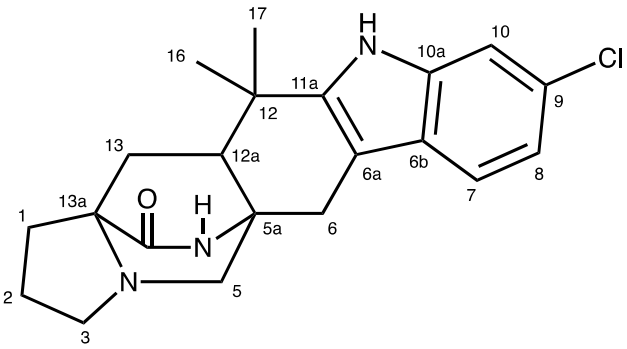

Figure S15. Numbering scheme for malbrancheamide B (**21**).

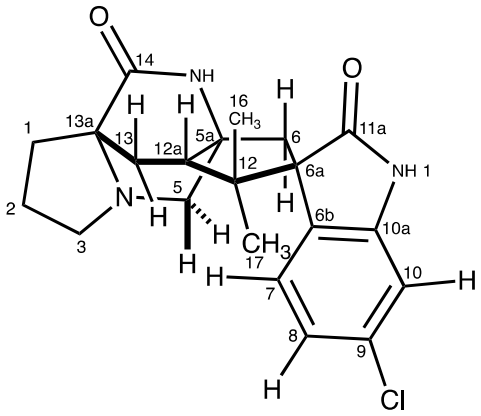

Figure S16. Numbering scheme for spiromalbrancheamide B (**25**).

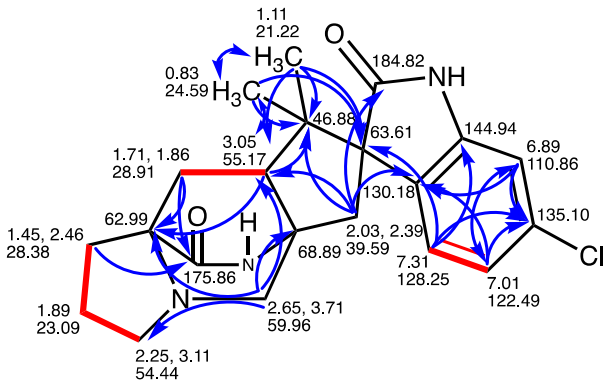

Figure S17. gHMBCAD and gCOSY correlations for spiromalbrancheamide B (**25**) in CD_3OD.

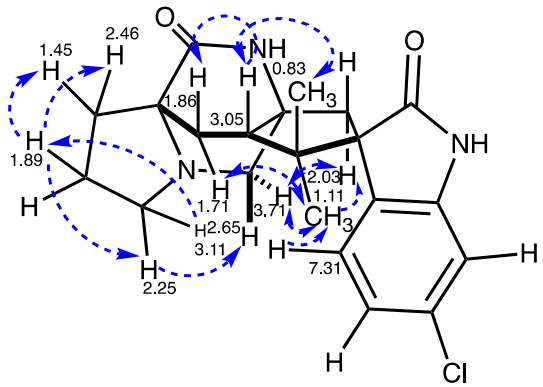

Figure S18. NOESY correlations for spiromalbrancheamide B (**25**) in CD_3OD.

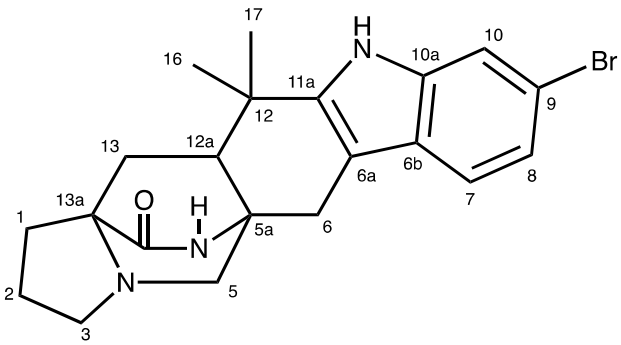

Figure S19. Numbering scheme for malbrancheamide C (**22**).

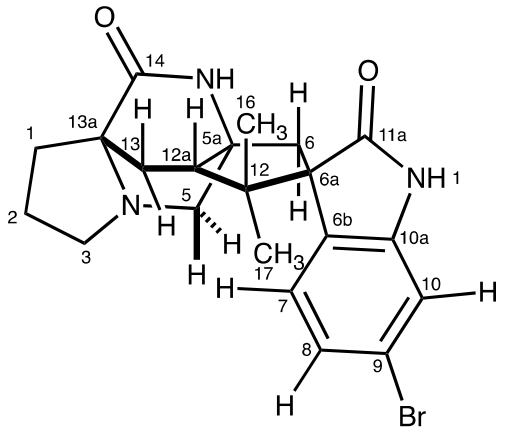

Figure S20. Numbering scheme for spiromalbrancheamide C (**26**).

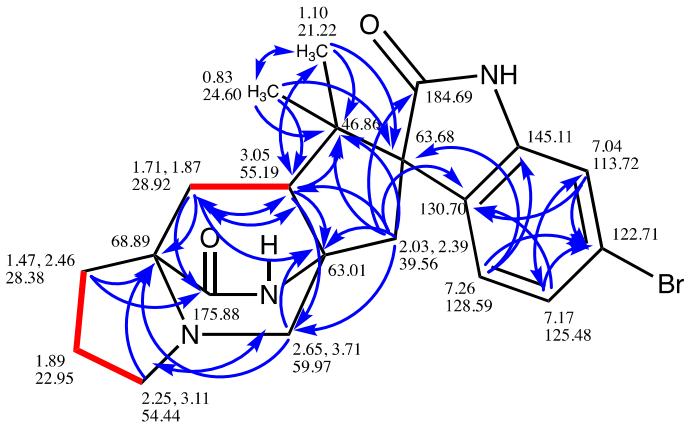

Figure S21. gHMBCAD and gCOSY correlations for spiromalbrancheamide C (**26**) in CD_3OD.

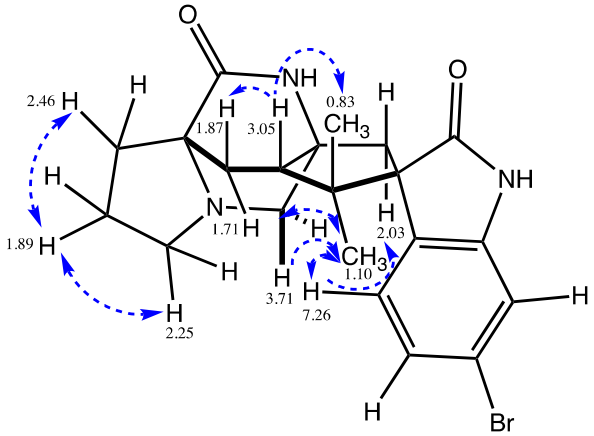

Figure S22. NOESY correlations for spiromalbrancheamide C (**26**) in CD_3OD.

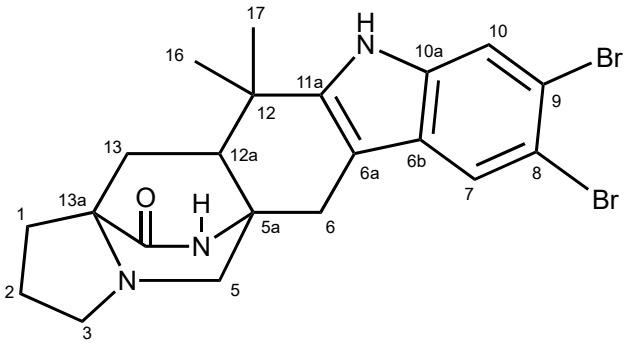

Figure S23. Figure S19. Numbering scheme for malbrancheamide E (**23**).

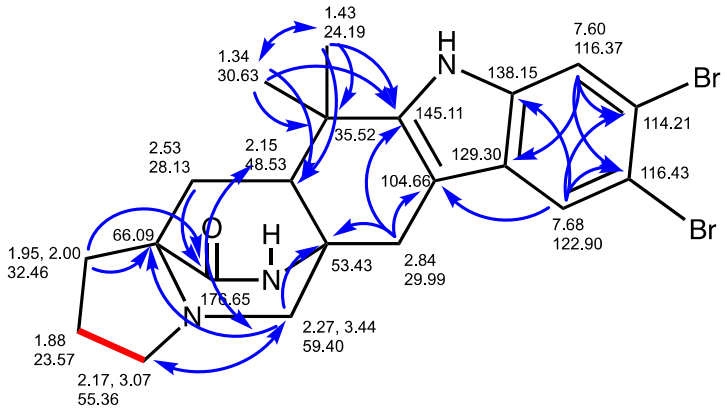

Figure S24. gHMBCAD and gCOSY correlations for malbrancheamide E in CD_3OD (**23**).

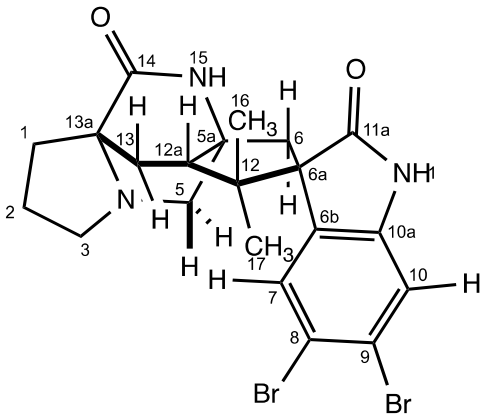

Figure S25. Numbering scheme for spiromalbrancheamide E (**27**).

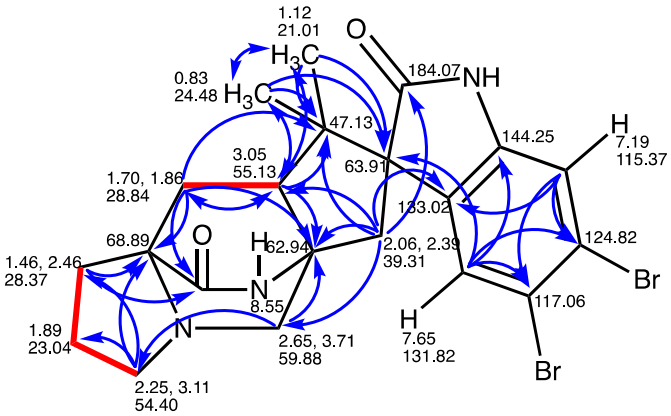

Figure S26. gHMBCAD and gCOSY correlations for spiromalbrancheamide E in CD_3OD (**27**).

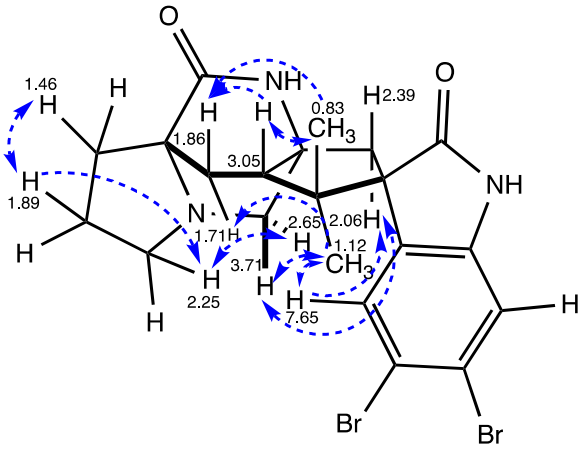

Figure S27. NOESY correlations for spiromalbrancheamide E in CD_3OD (**27**).

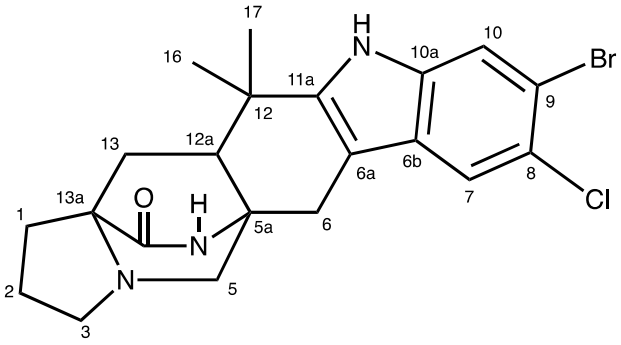

Figure S28. Numbering scheme for isomalbrancheamide D (**24**).

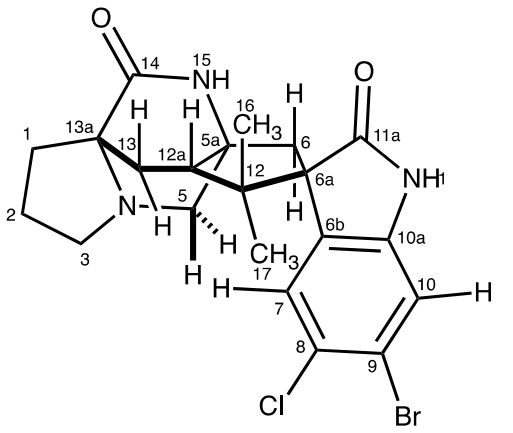

Figure S29. Numbering scheme for spiroisomalbrancheamide D (**28**).

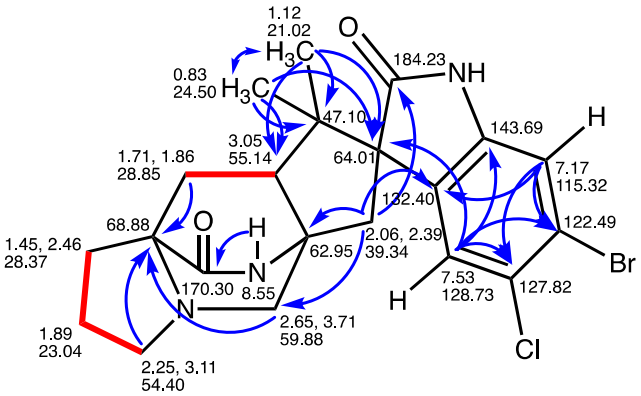

Figure S30. gHMBCAD and gCOSY correlations for spiroisomalbrancheamide D in CD_3OD (**28**).

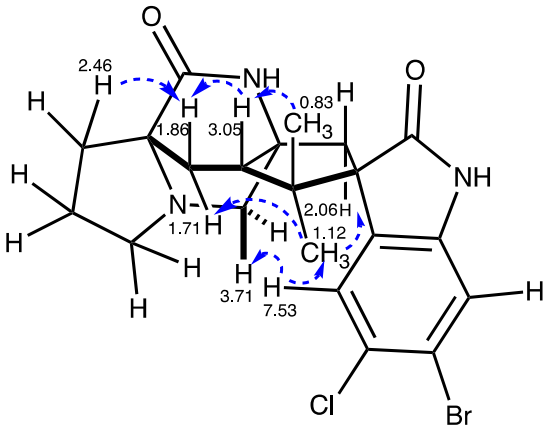

Figure S31. NOESY correlations for spiroisomalbrancheamide D in CD_3OD (**28**).

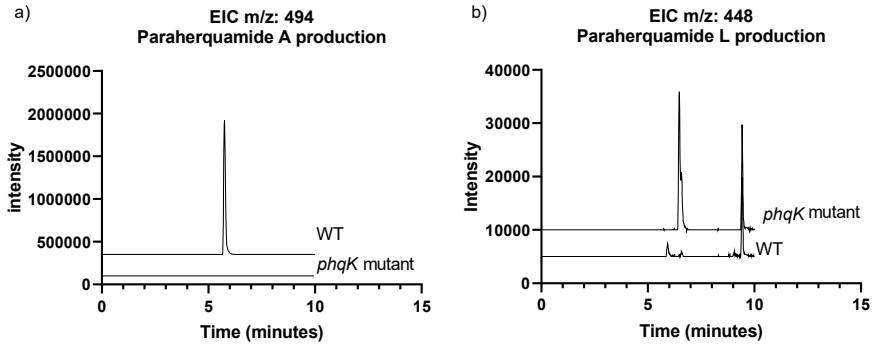

Figure S32. Q-TOF LC/MS EIC from Δ*phqK P. simplicissimum,* indicating that a) paraherquamide A (**13**) is no longer produced, and b) that paraherquamide L (**15**) is produced.

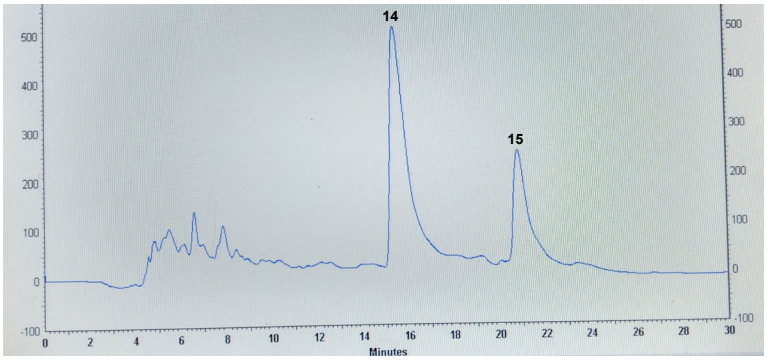

Figure S33. Chiral separation of paraherquamide K (**14**) and L (**15**) from the extract of Δ*phqK P. simplicissimum.*

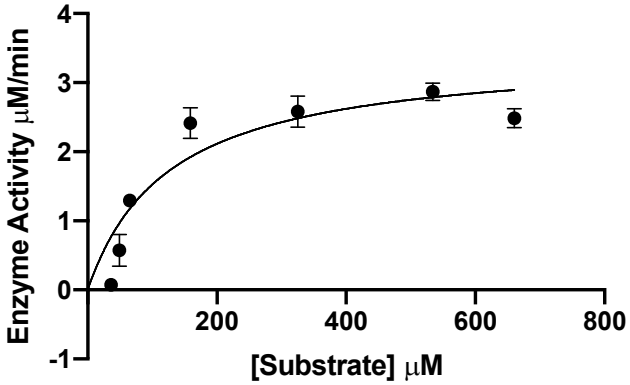

Figure S34. Michaelis-Menten model kinetics for paraherquamide K (**14**).

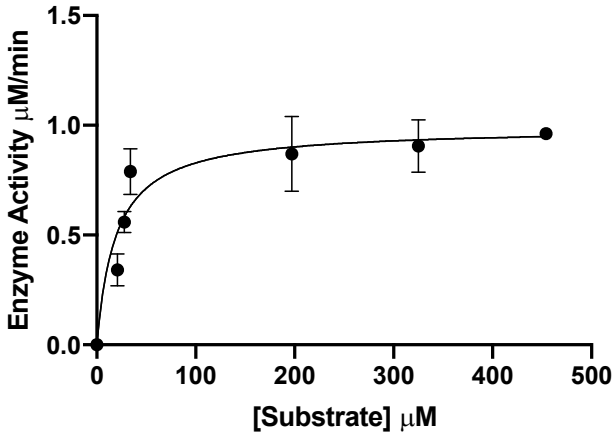

Figure S35. Michaelis-Menten model kinetics for paraherquamide L (**15**).

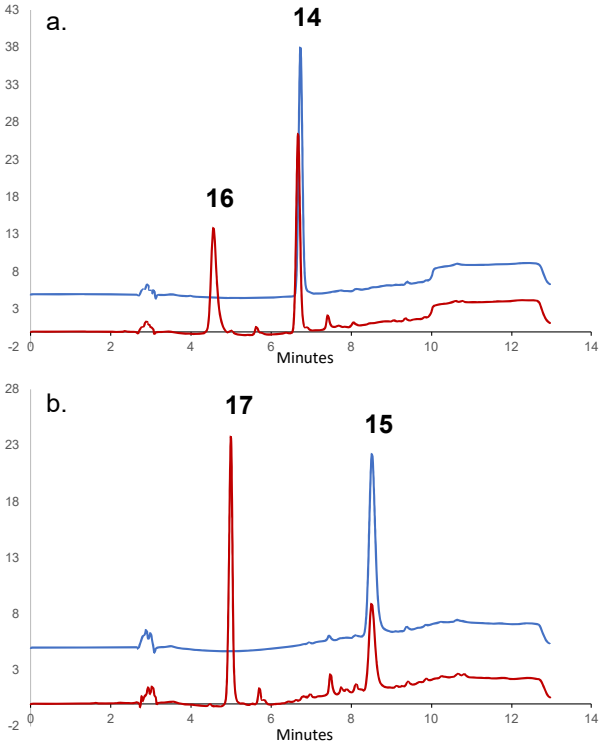

Figure S36. PhqK reactions with paraherquamide K (**14**) (a) and paraherquamide L (**15**) (b) with no enzyme control in blue and the reaction shown in red. Traces listed from top (blue) to bottom (red).

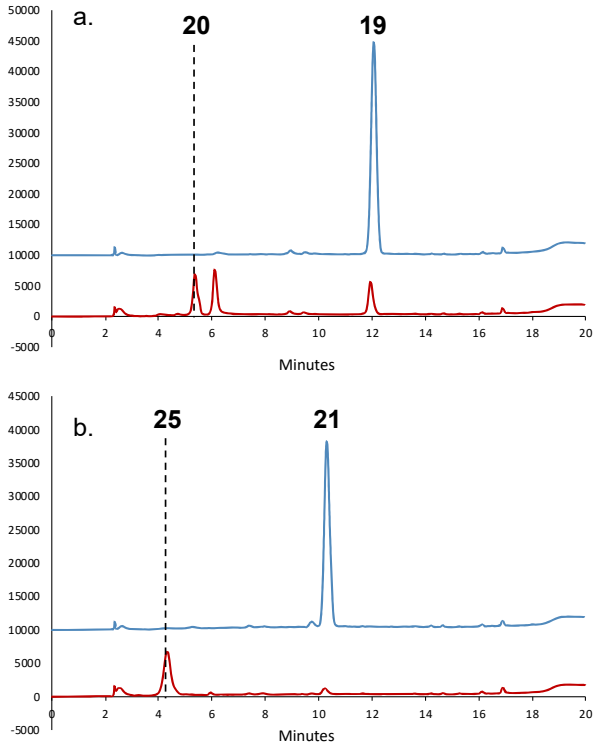

Figure S37. PhqK reactions with malbrancheamide (**19**) (a) and malbrancheamide B (**21**) (b) with no enzyme control in blue and the reactions shown in red.

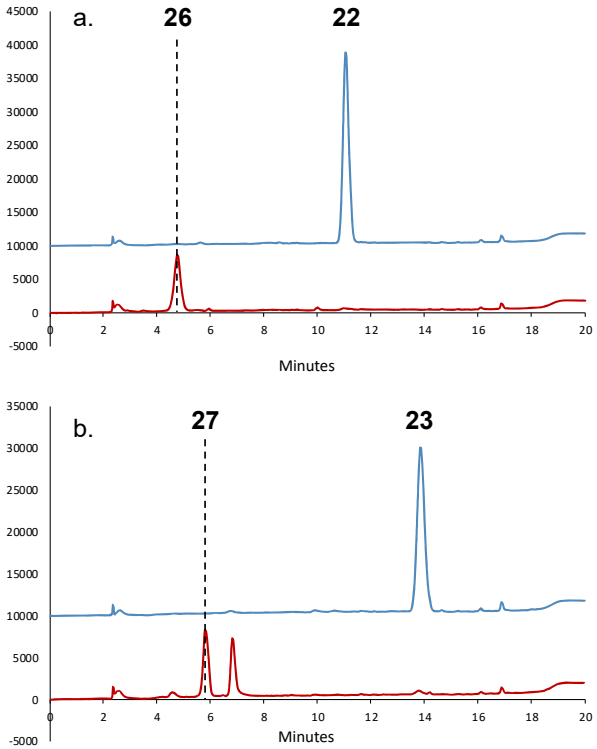

Figure S38. PhqK reactions with malbrancheamide C (**22**) (a) and malbrancheamide E (**23**) (b) with no enzyme control in blue and the reactions shown in red.

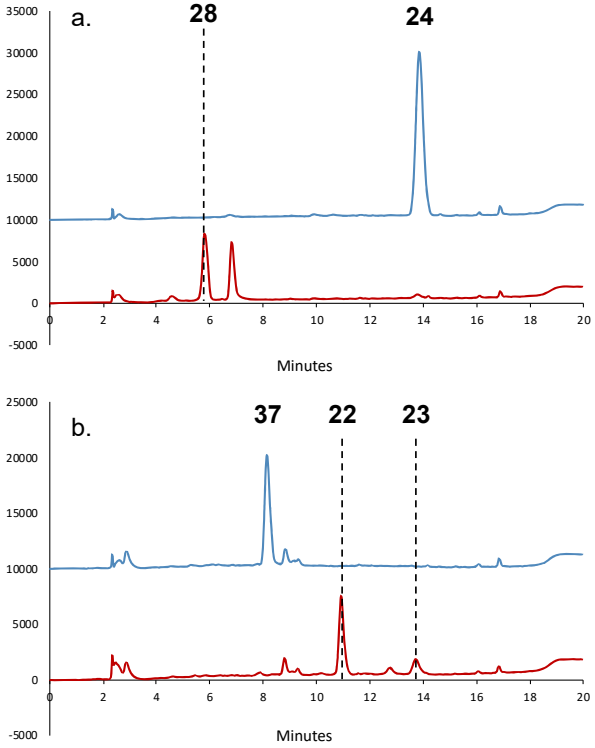

Figure S39. PhqK reaction with isomalbrancheamide D (**24**) (a) and MalA bromination reaction with premalbrancheamide (**37**) to produce the new dibrominated malbrancheamide E (**23**) (b) with no enzyme control in blue and the reactions shown in red.

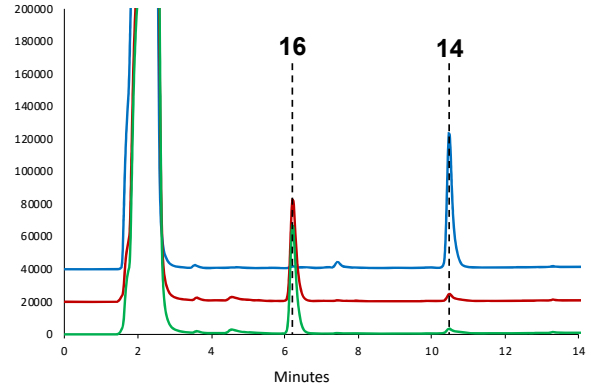

Figure S40. PhqK reaction with paraherquamide K (**14**) in the presence of catalase to produce paraherquamide M (**16**). The no enzyme control is in blue, reaction without catalase is in red (92% conversion), and the reaction with catalase is in green (94% conversion).

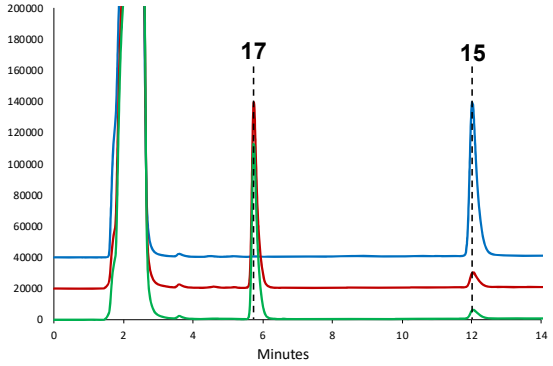

Figure S41. PhqK reaction with paraherquamide L (**15**) in the presence of catalase to produce paraherquamide N (**17**). The no enzyme control is in blue, reaction without catalase is in red (90% conversion), and the reaction with catalase is in green (93% conversion).

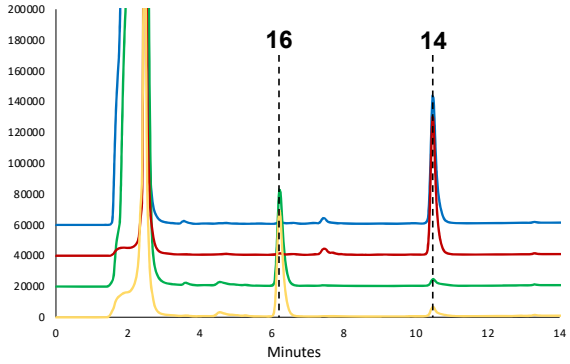

Figure S42. PhqK reaction with paraherquamide K (**14**) in the presence of glucose-6-phosphate dehydrogenase to produce paraherquamide M (**16**). The no PhqK control is in blue, no PhqK/NADH control is in red, reaction with PhqK/NADH is in green (92% conversion), and reaction with glucose-6-phosphate/glucose-6-phosphate dehydrogenase is in yellow (92% conversion).

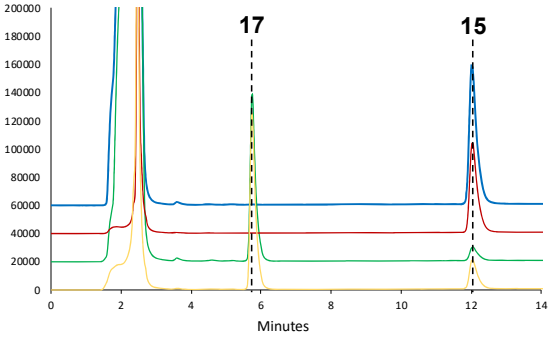

Figure S43. PhqK reaction with paraherquamide L (**15**) in the presence of glucose-6-phosphate dehydrogenase to produce paraherquamide N (**17**). The no PhqK control is in blue, no PhqK/NADH control is in red, reaction with PhqK/NADH is in green (90% conversion), and reaction with glucose-6-phosphate/glucose-6-phosphate dehydrogenase is in yellow (68% conversion).

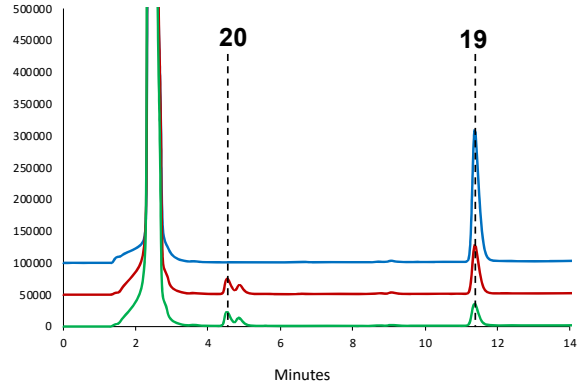

Figure S44. PhqK reaction with malbrancheamide (**19**) in the presence of catalase to produce spiromalbramide (**20**). The no enzyme control is in blue, reaction without catalase is in red, and the reaction with catalase is in green.

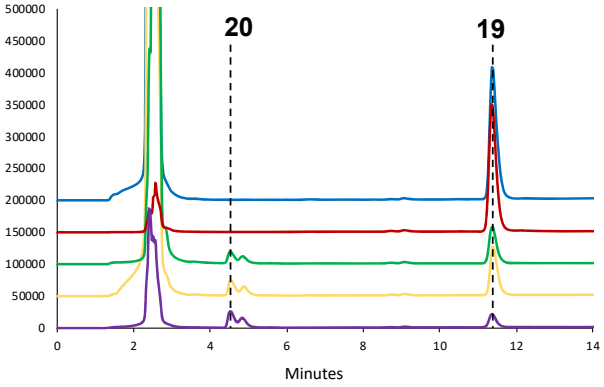

Figure. S45. PhqK reaction with malbrancheamide (**19**) in the presence of glucose-6-phosphate (G-6-P) and glucose-6-phosphate dehydrogenase (G-6-P dehydrogenase) to produce spiromalbramide (**20**). The no NADPH/NADH and no G-6-P DH/G-6-P control is in blue, no PhqK control is in red, PhqK reaction with NADPH is in green, PhqK reaction with NADH is in yellow, and the PhqK reaction in the presence of G-6-P DH/G-6-P with the addition of $NADP^+$ is in purple.

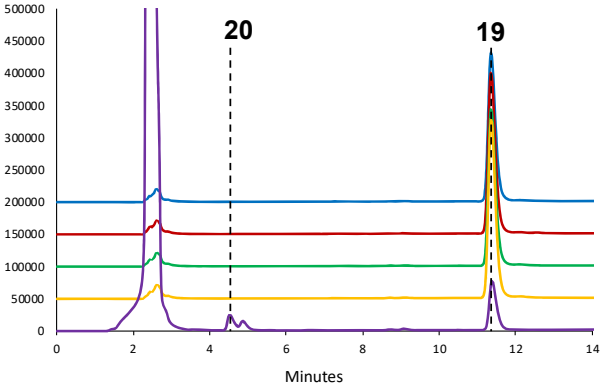

Figure S46. Hydrogen peroxide and malbrancheamide (**19**) reactions. The control with no hydrogen peroxide is in blue and varying concentrations of hydrogen peroxide were added (red: 1 mM, green: 500 µM, yellow: 250 µM). A positive control reaction with PhqK and no added hydrogen peroxide is shown in purple.

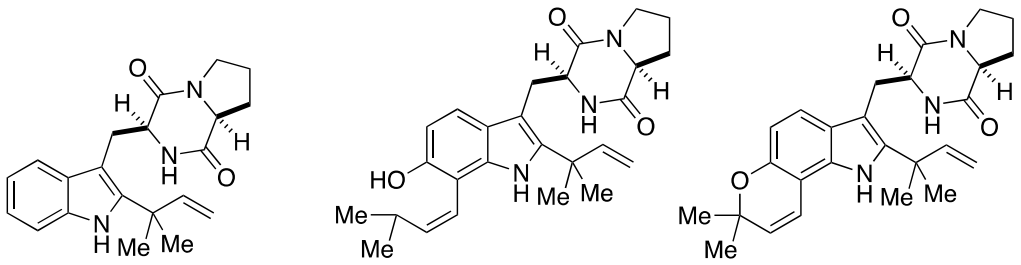

*Deoxybrevianamide E (**37**)* *Notoamide S (**38**)* *Notoamide E (**1**)*

*1,2,3,4-tetrahydro-carbazole (**39**)* *6-chloro-2,3,4,9-tetrahydro-1H-carbazole (**40**)*

Figure S47. Chemical structures of small molecules used in substrate scope of PhqK.

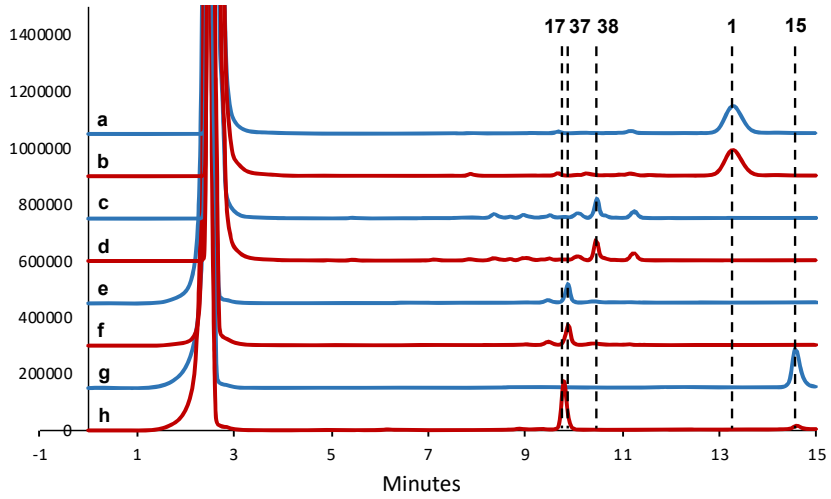

Figure S48. Reactions of PhqK with early intermediates in fungal indole alkaloid biosynthesis. a) notoamide E (**1**) control, b) reaction with **1**, c) notoamide S (**38**) control, d) reaction with **38**, e) deoxybrevianamide E (**37**) control, f) reaction with **37,** g) paraherquamide L (**15**) control, h) reaction with **15**. Conversion was only observed for the complex molecule **15**.

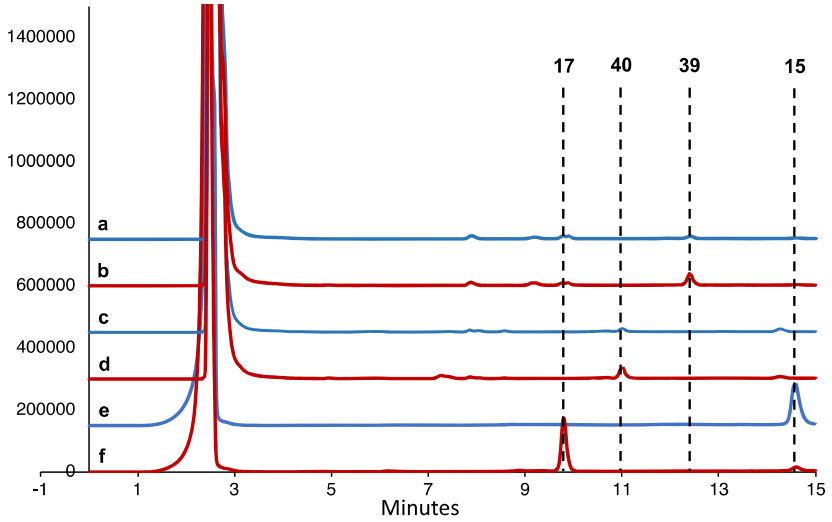

Figure 49. Reactions of PhqK with smaller, less complex substrates. a) 1,2,3,4-tetrahydrocarbazole (**39**) control, b) reaction with **39**, c) 6-chloro-2,3,4,9-tetrahydro-1H-carbazole (**40**) control, d) reaction with **40**, e) paraherquamide L (**15**) control, f) reaction with **15**. Conversion was only observed for the complex molecule **15**.

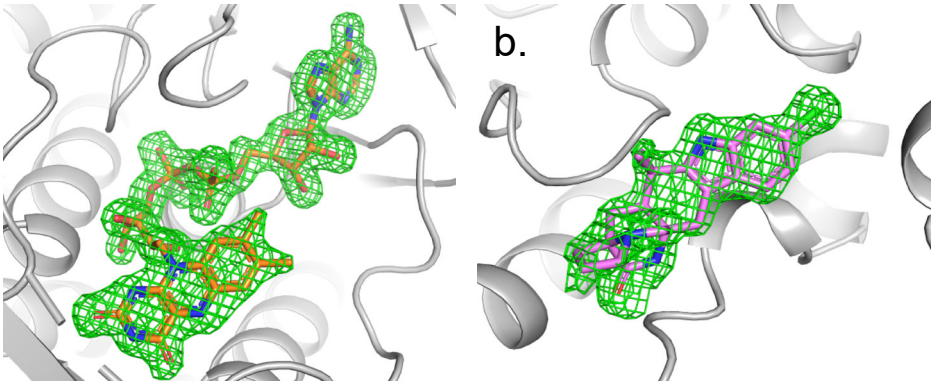

Figure S50. Omit map contoured at 3σ for FAD (a) and malbrancheamide B (**21**) (b) in PhqK cocrystal structure.

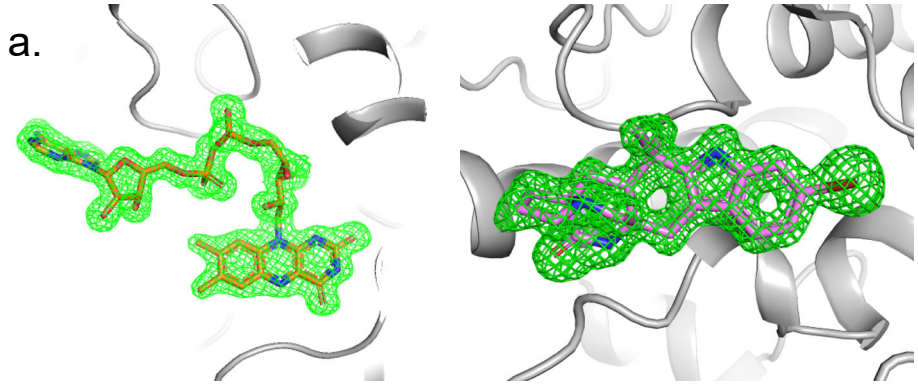

Figure S51. Omit map contoured at 3σ for FAD (a) and malbrancheamide C (**22**) (b) in PhqK cocrystal structure.

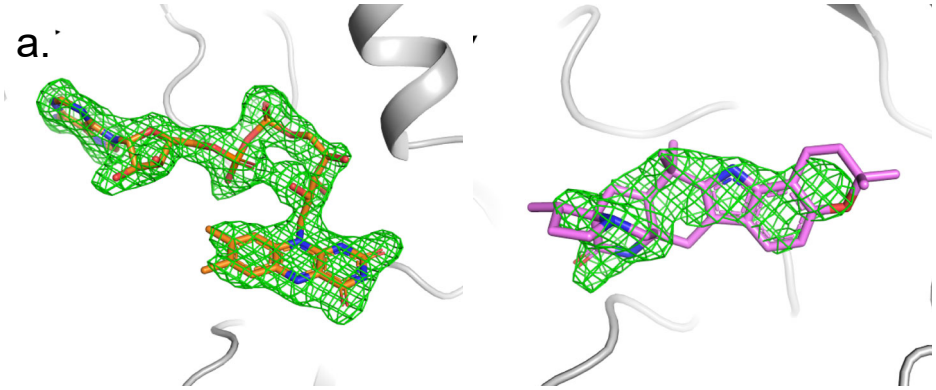

Figure S52. Omit map contoured at 3σ for FAD (a) and paraherquamide K (**14**) (b) in PhqK cocrystal structure.

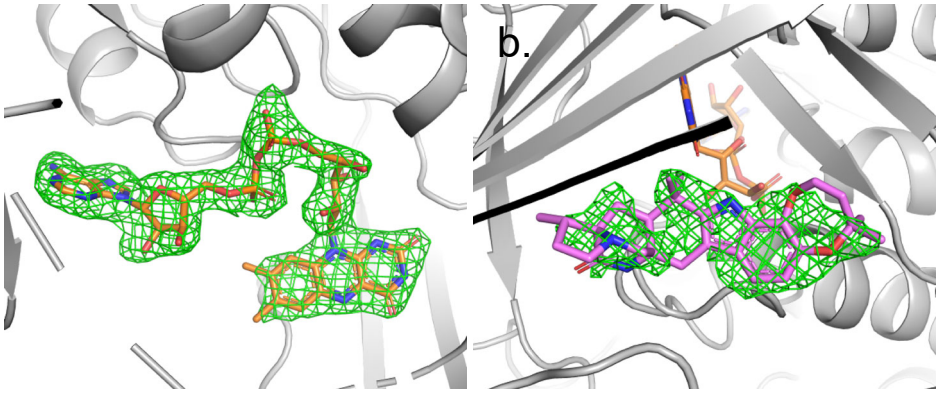

Figure S53. Omit map contoured at 3σ for FAD (a) and paraherquamide L (**15**) (b) in PhqK cocrystal structure.

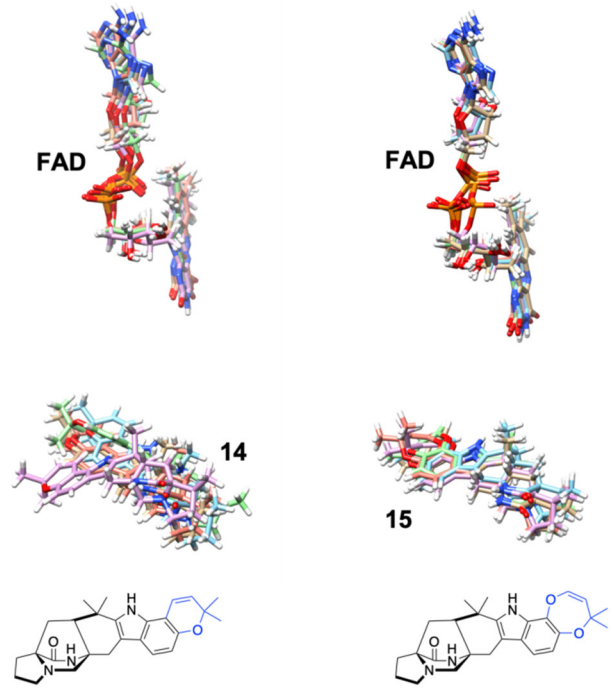

Figure S54. Overlay of the top five clusters in 1.5 μs MD simulations of **14** (left) and **15** (right).

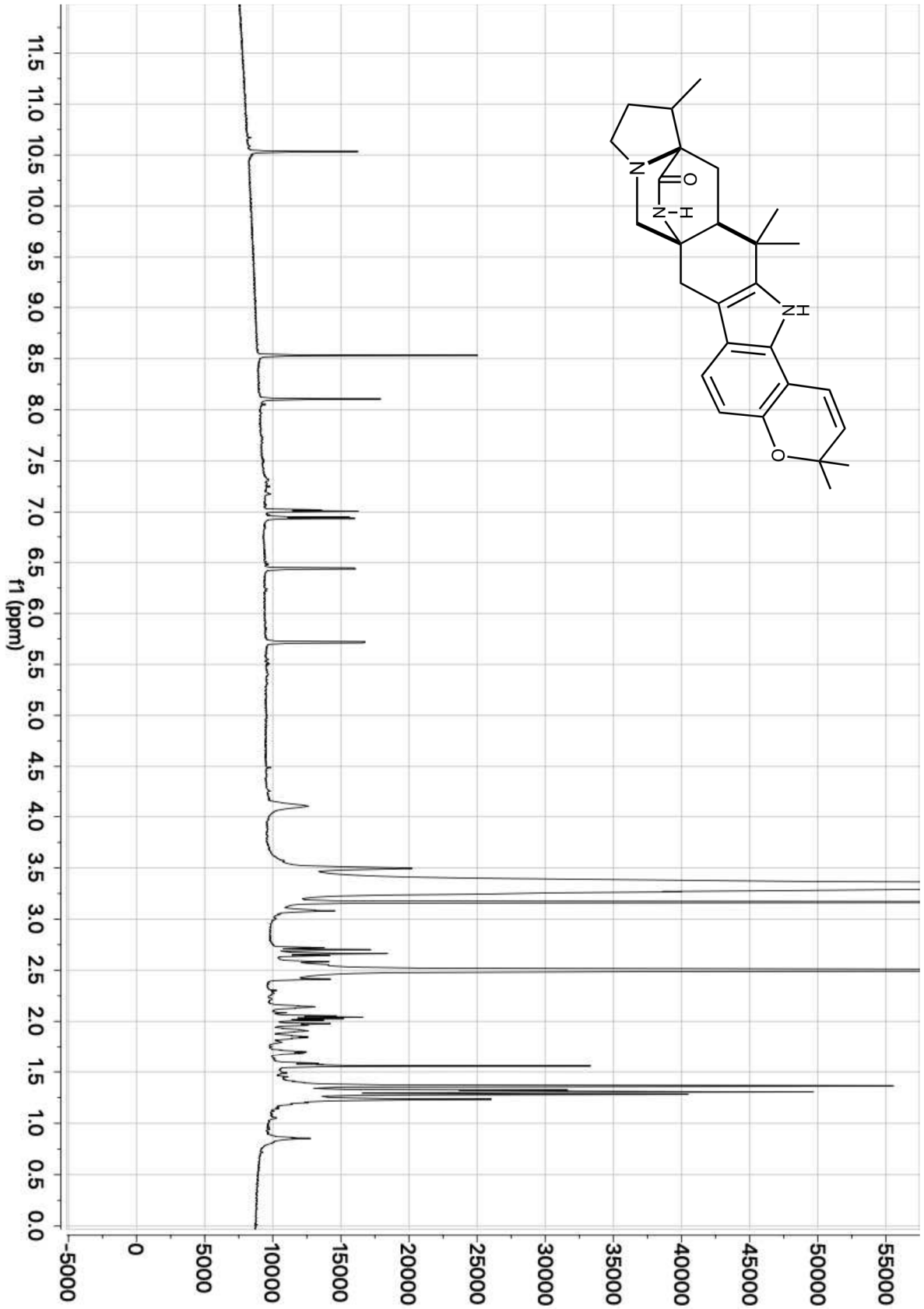

Figure S55. ^{1}H-NMR of paraherquamide K (**14**) (800 MHz, $(CD_3)_2SO$-d_6).

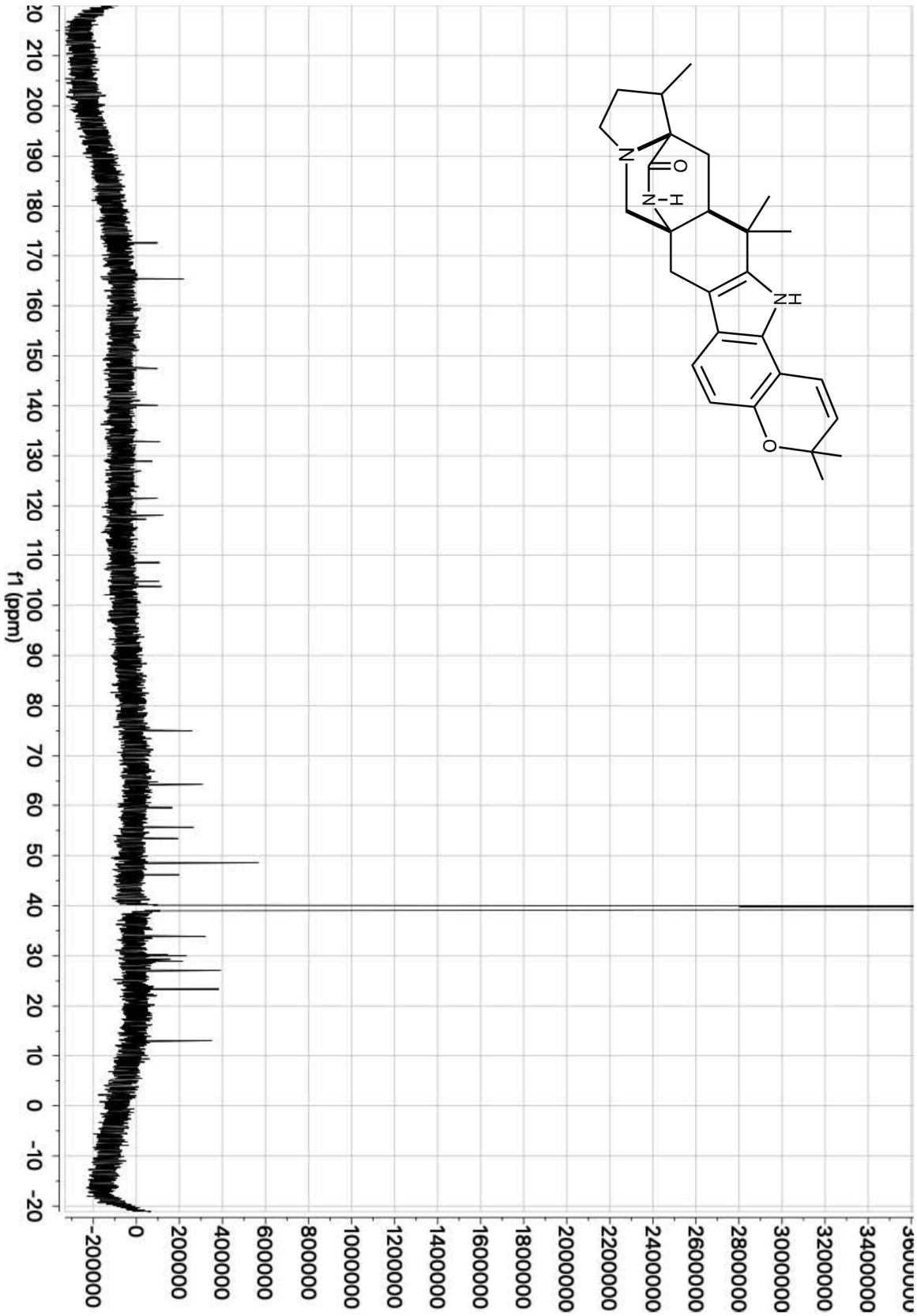

Figure S56. ^{13}C-NMR of paraherquamide K (**14**) (201 MHz, $(CD_3)_2SO$-d_6).

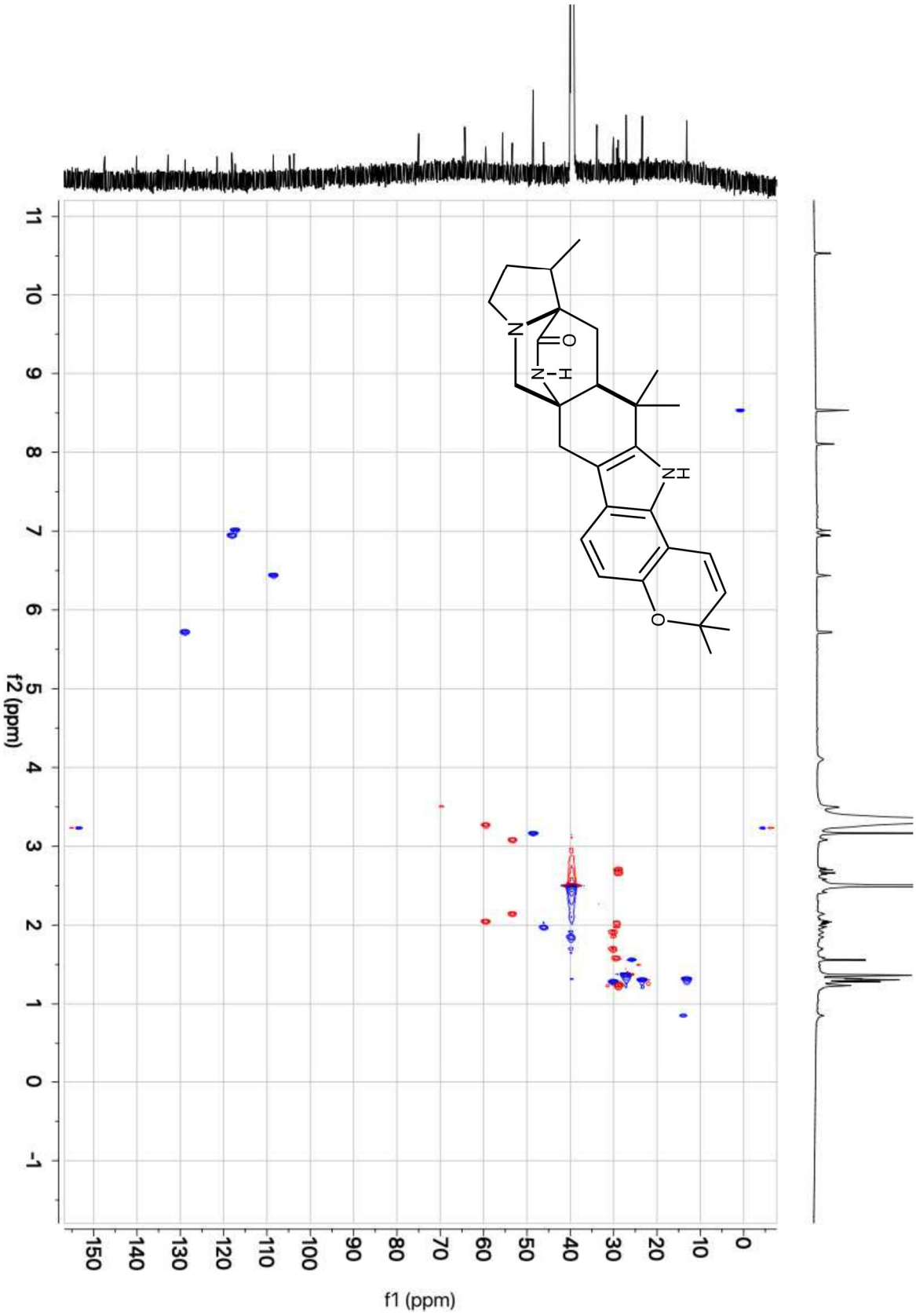

Figure S57. gHSQCAD correlations of paraherquamide K (**14**) (800 MHz, $(CD_3)_2SO$-d_6).

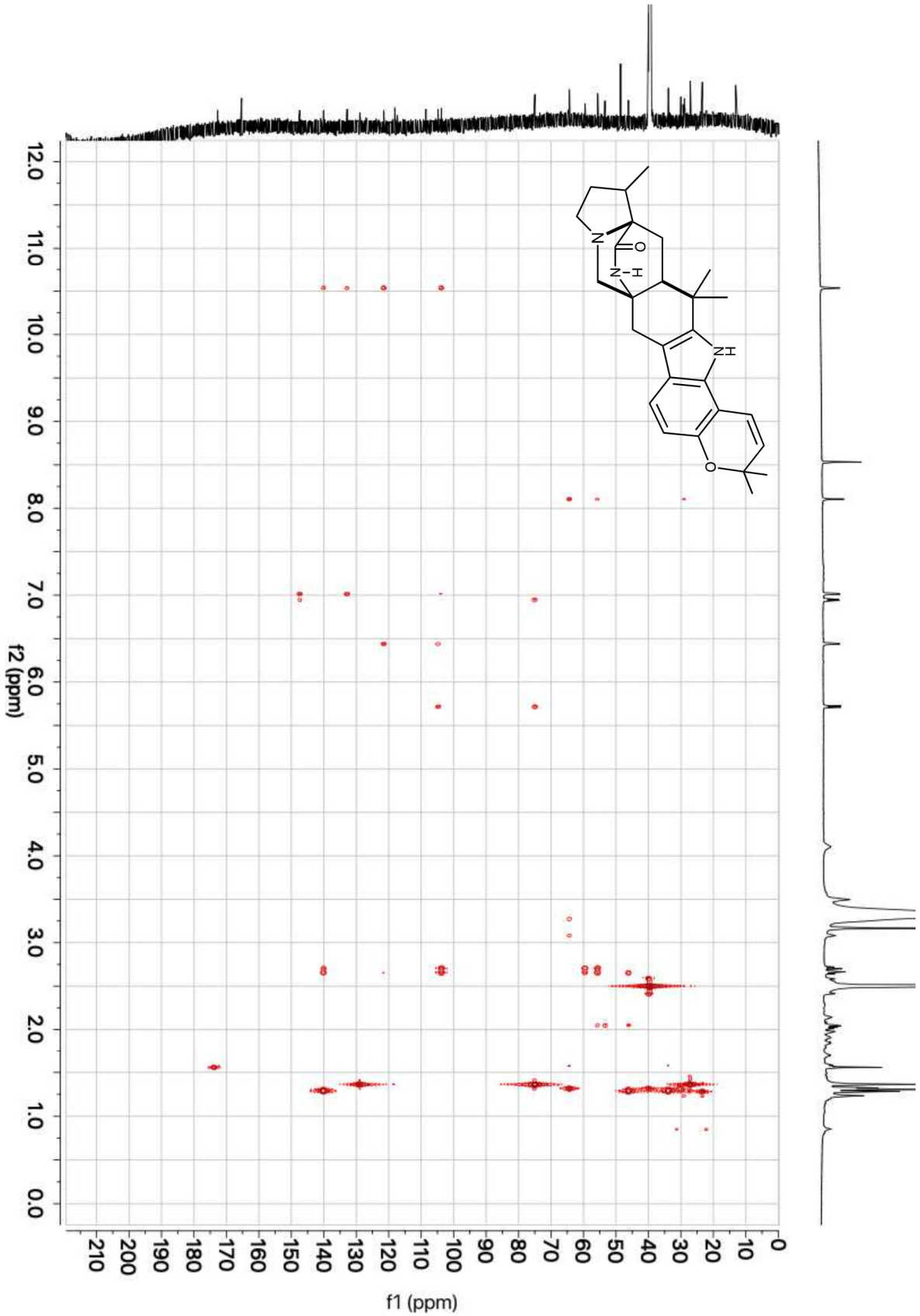

Figure S58. gHMBCAD correlations of paraherquamide K (**14**) (800 MHz, $(CD_3)_2SO$-d_6).

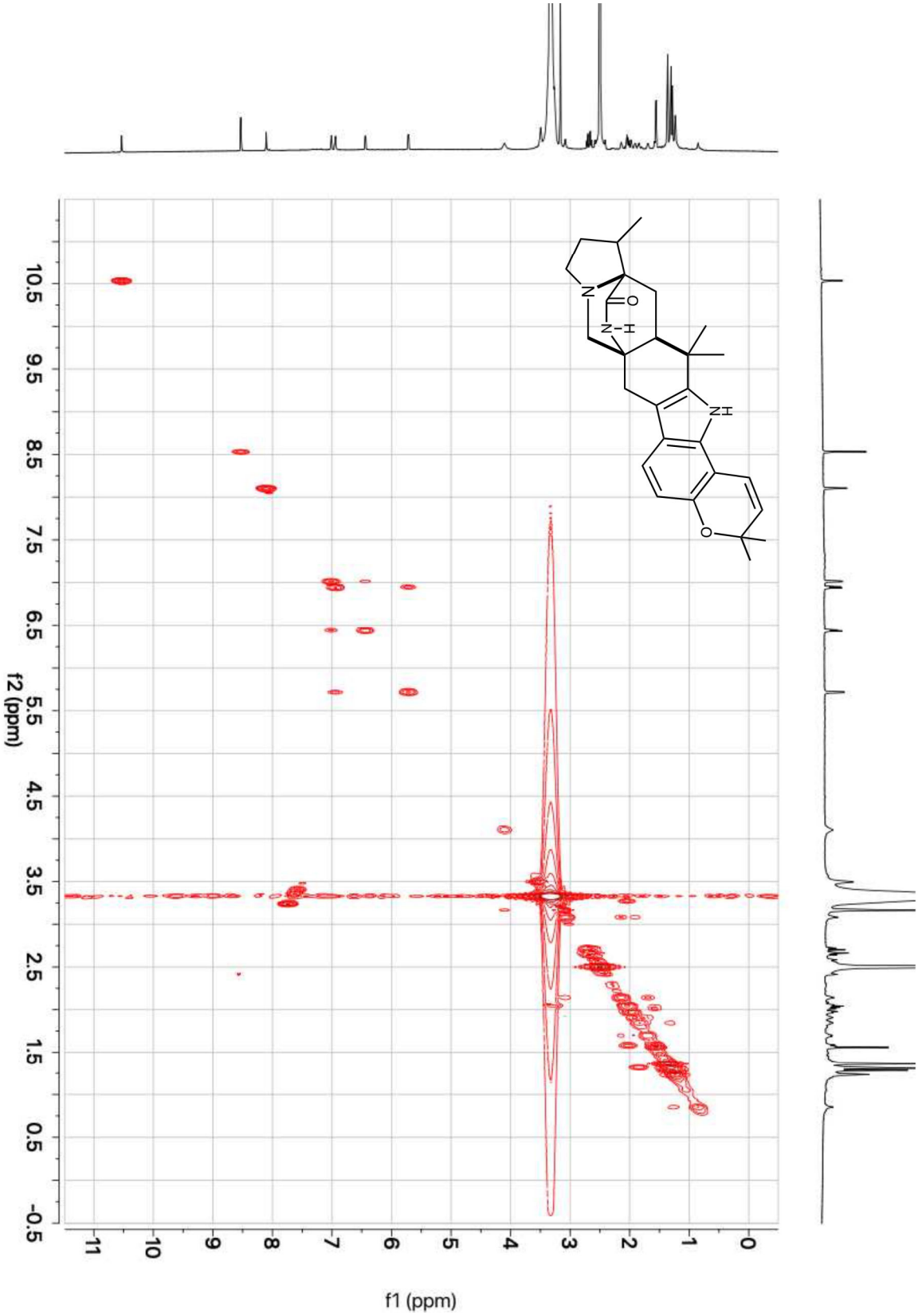

Figure S59. gCOSY correlations of paraherquamide K (**14**) (800 MHz, $(CD_3)_2SO$-d_6).

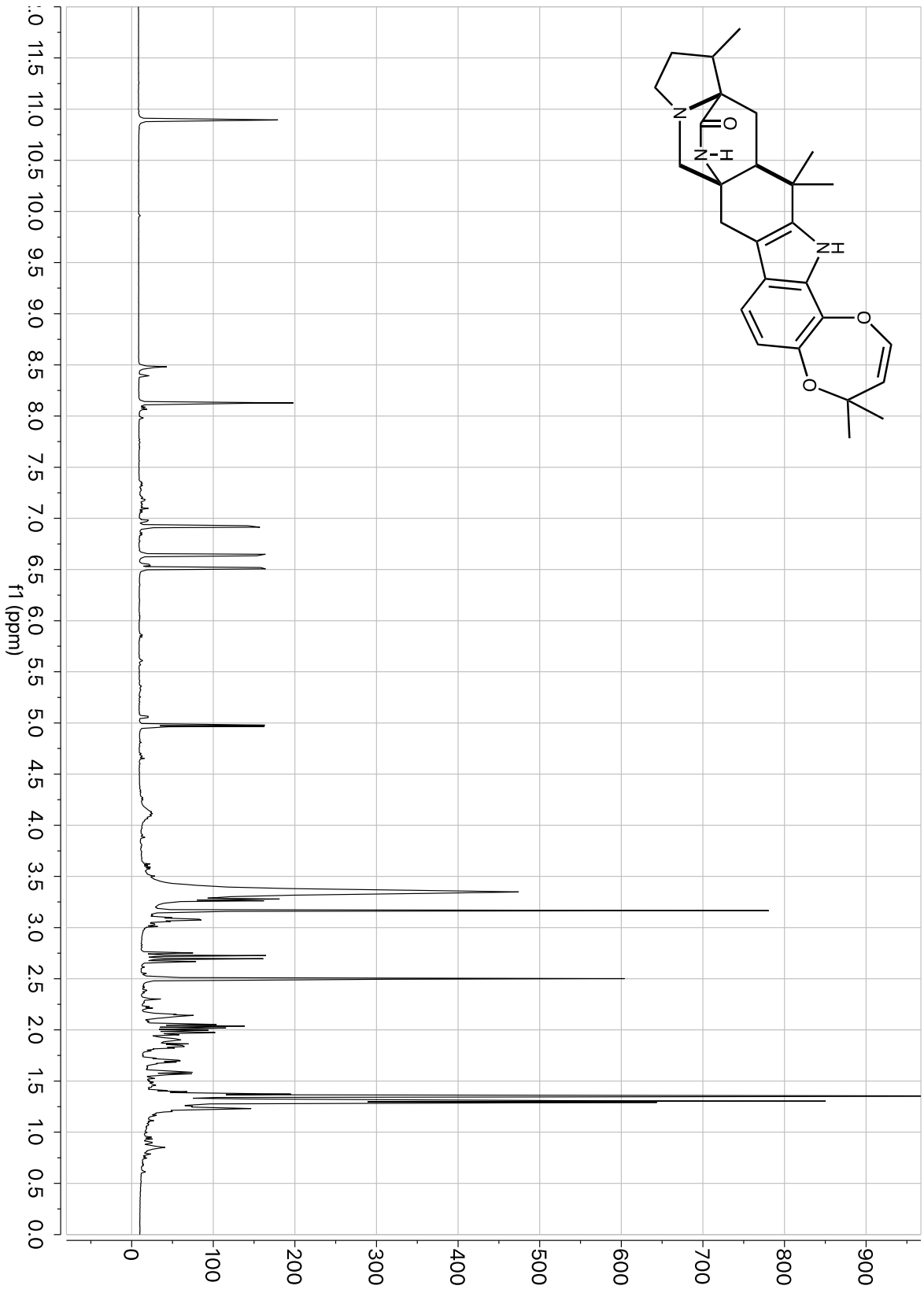

Figure S60. ^{1}H-NMR of paraherquamide L (**15**) (600 MHz, $(CD_3)_2SO$-d_6).

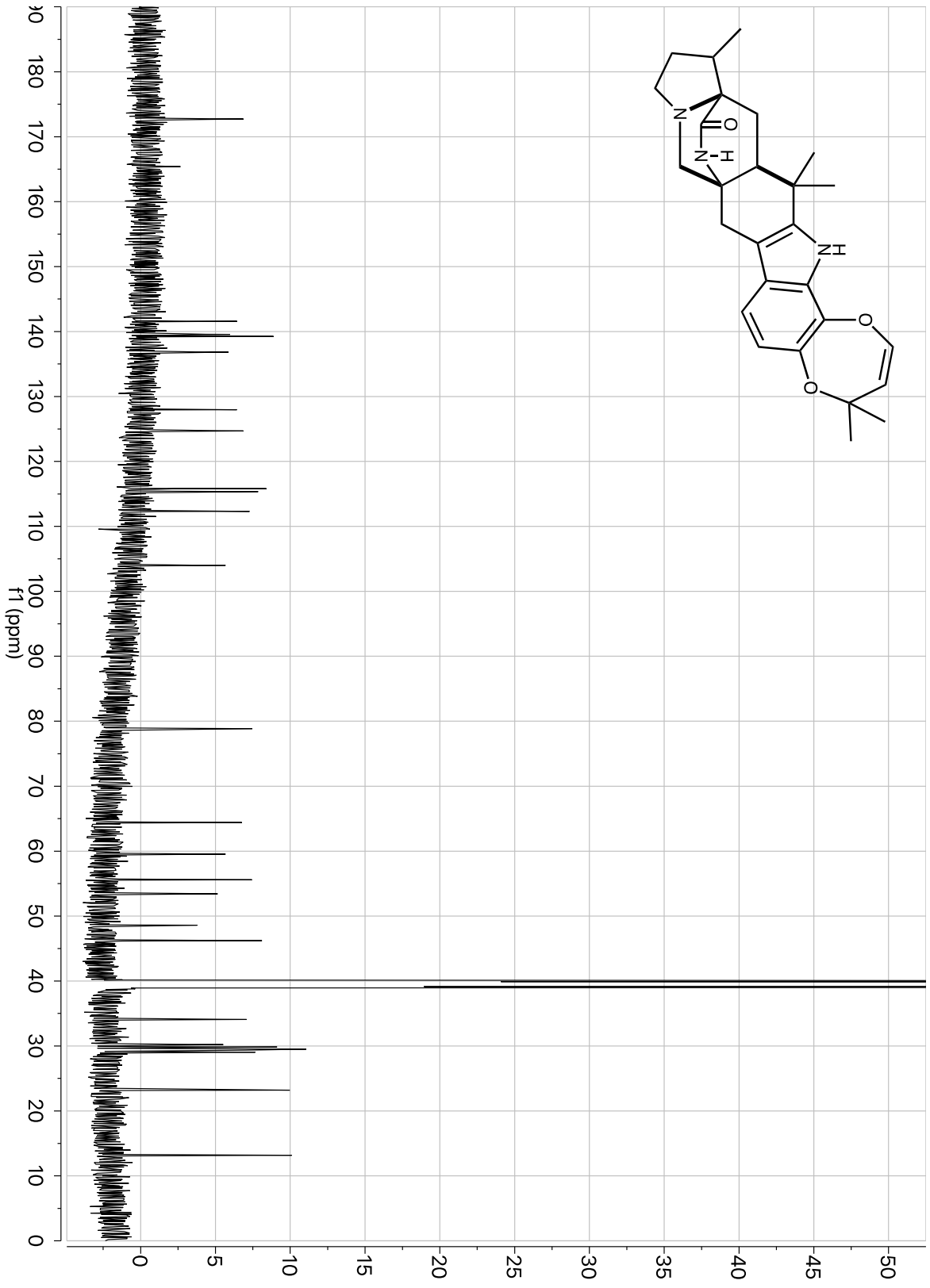

Figure S61. ^{13}C-NMR of paraherquamide L (**15**) (150 MHz, $(CD_3)_2SO$-d_6).

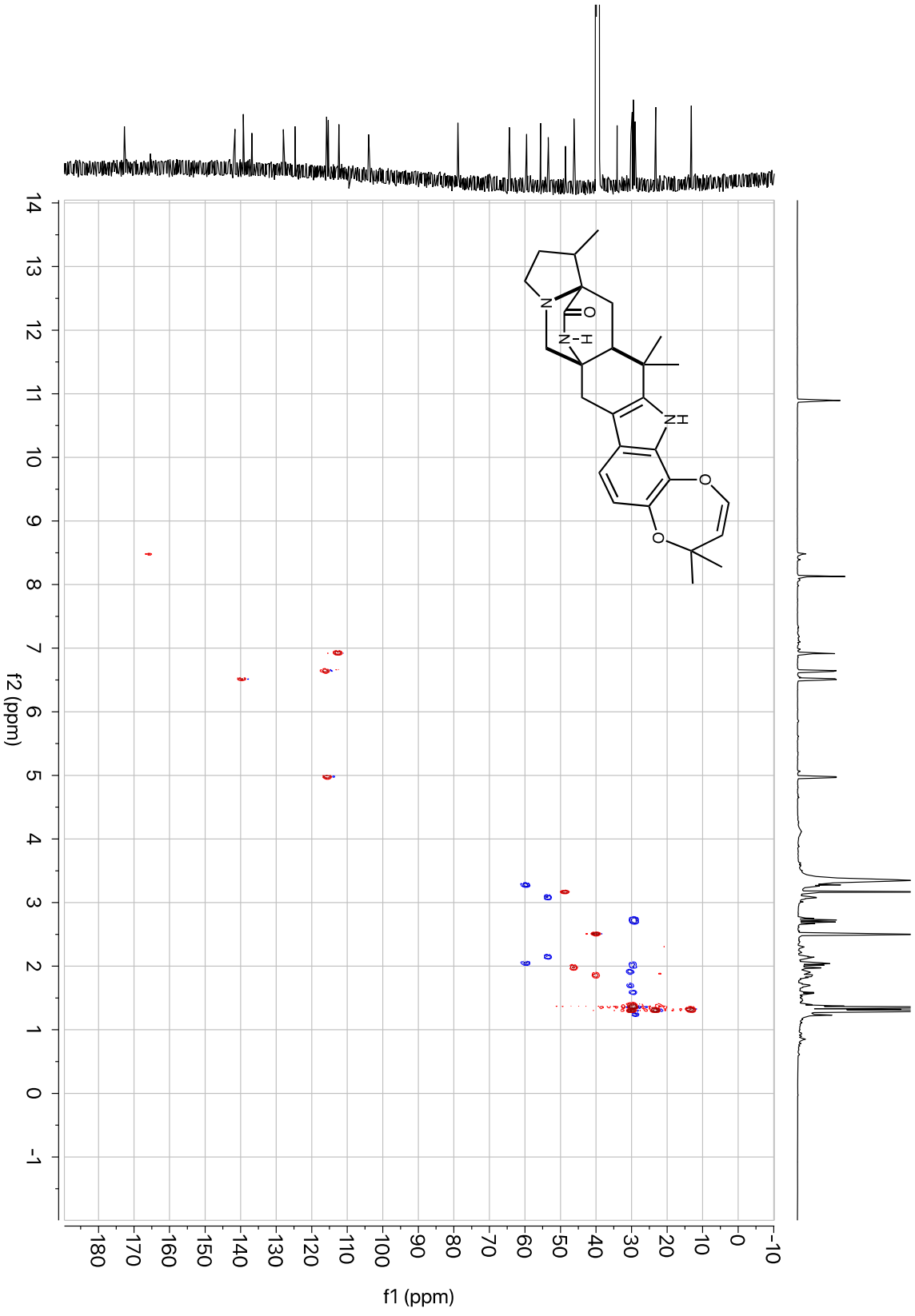

Figure S62. gHSQCAD correlations of paraherquamide L (**15**) (600 MHz, $(CD_3)_2SO$-d_6).

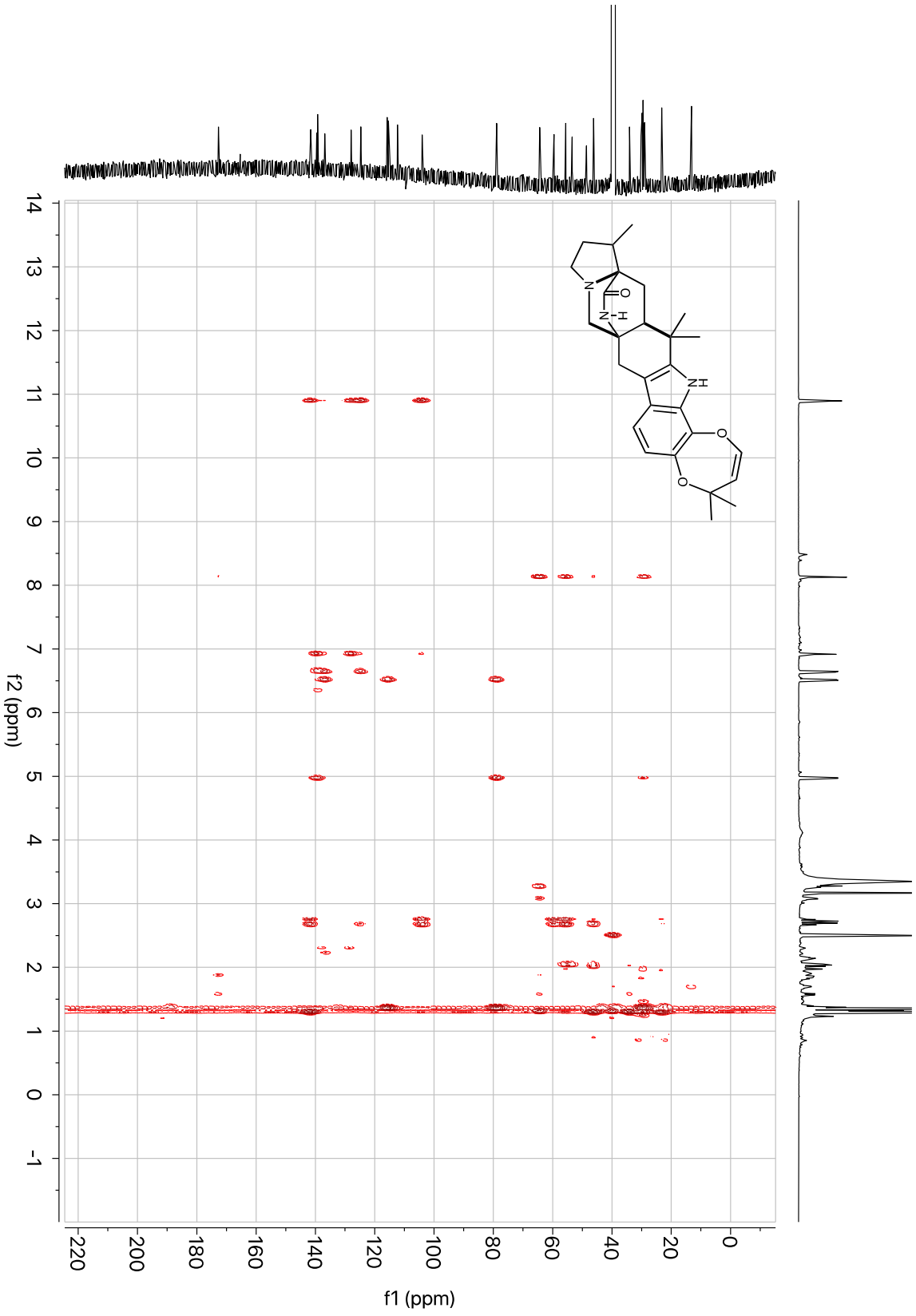

Figure S63. gHMBCAD correlations of paraherquamide L (**15**) (600 MHz, $(CD_3)_2SO$-d_6).

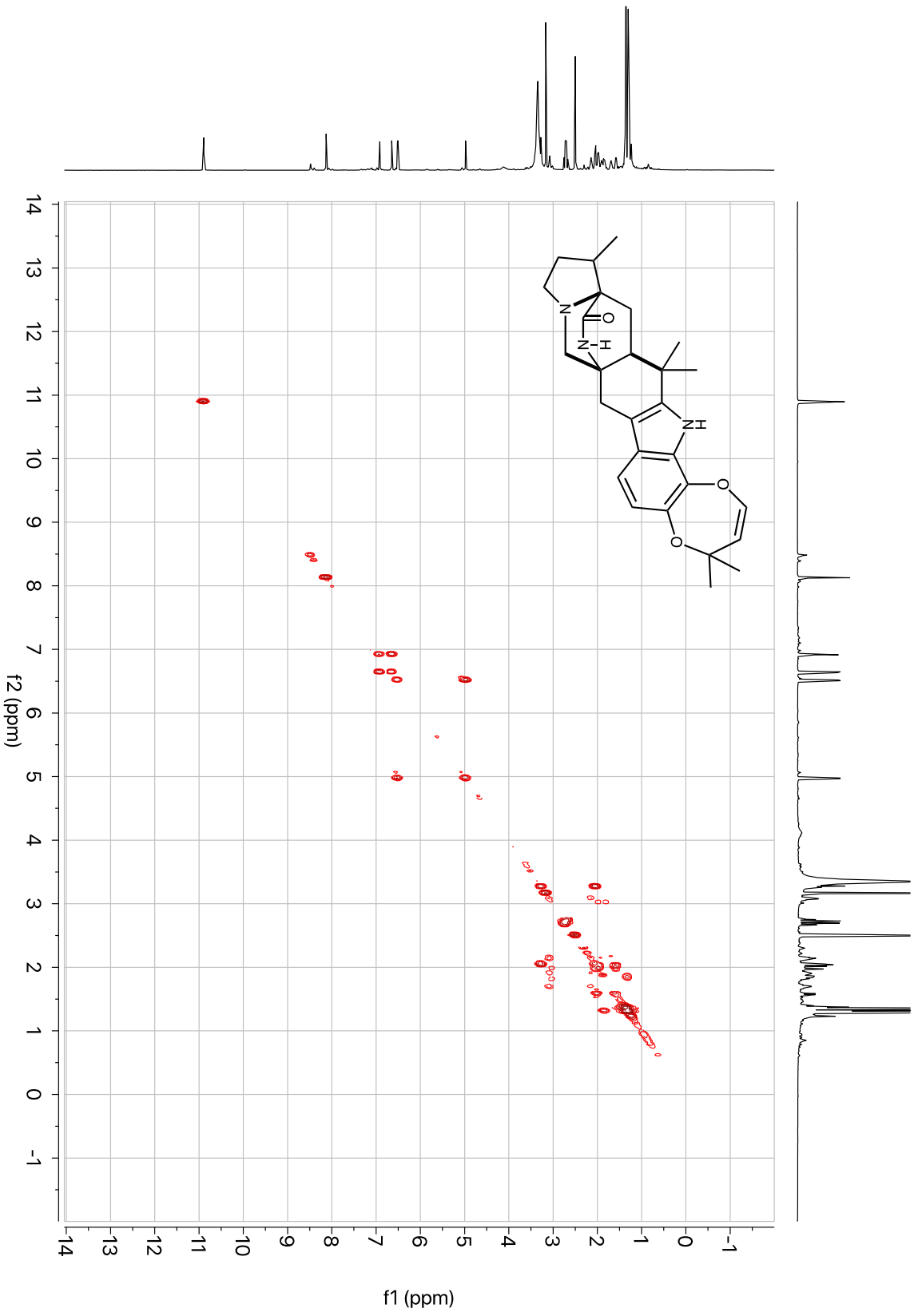

Figure S64. gCOSY correlations of paraherquamide L (**15**) (600 MHz, $(CD_3)_2SO$-d_6).

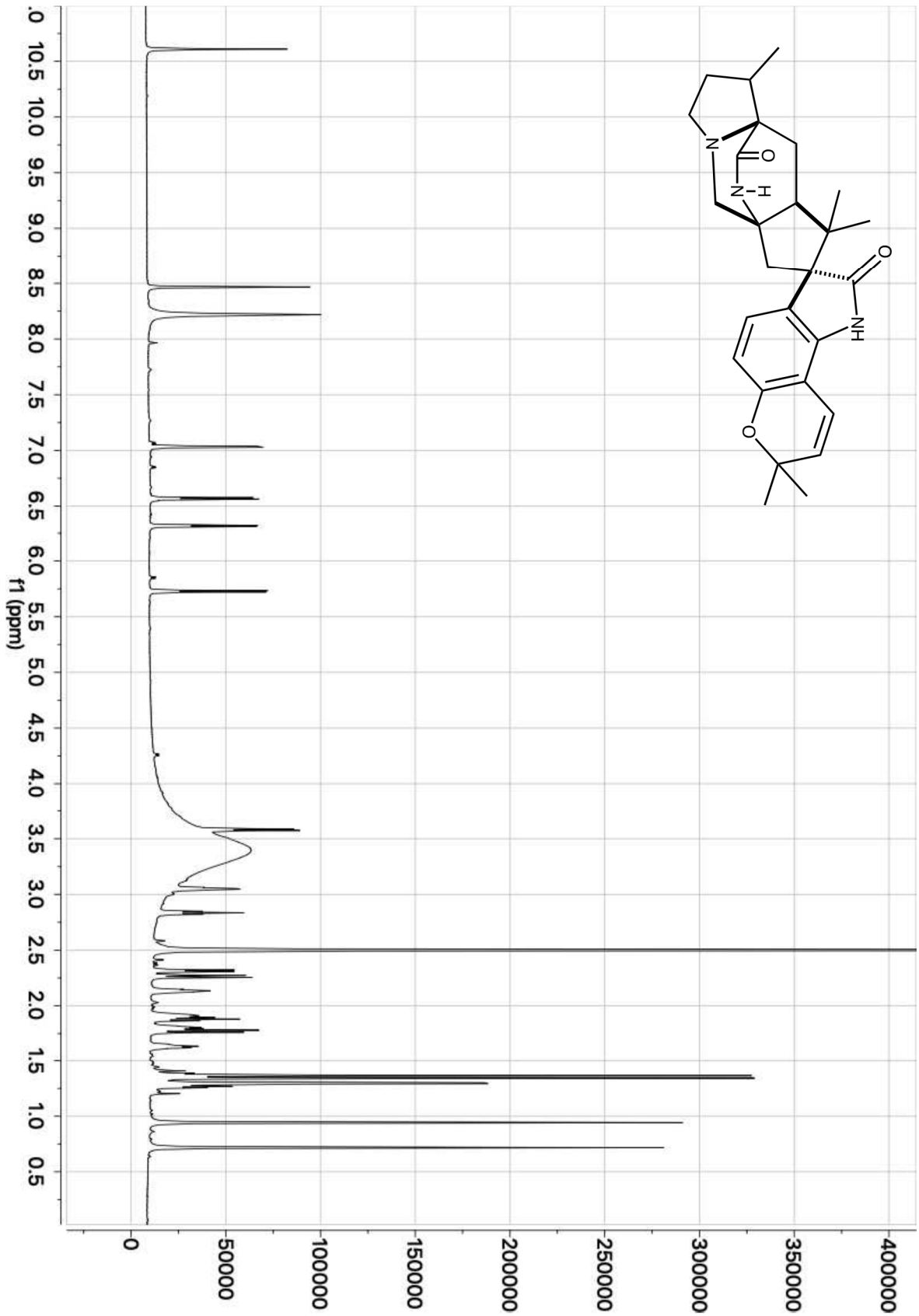

Figure S65. ^{1}H-NMR of paraherquamide M (**16**) (800 MHz, $(CD_3)_2SO$-d_6).

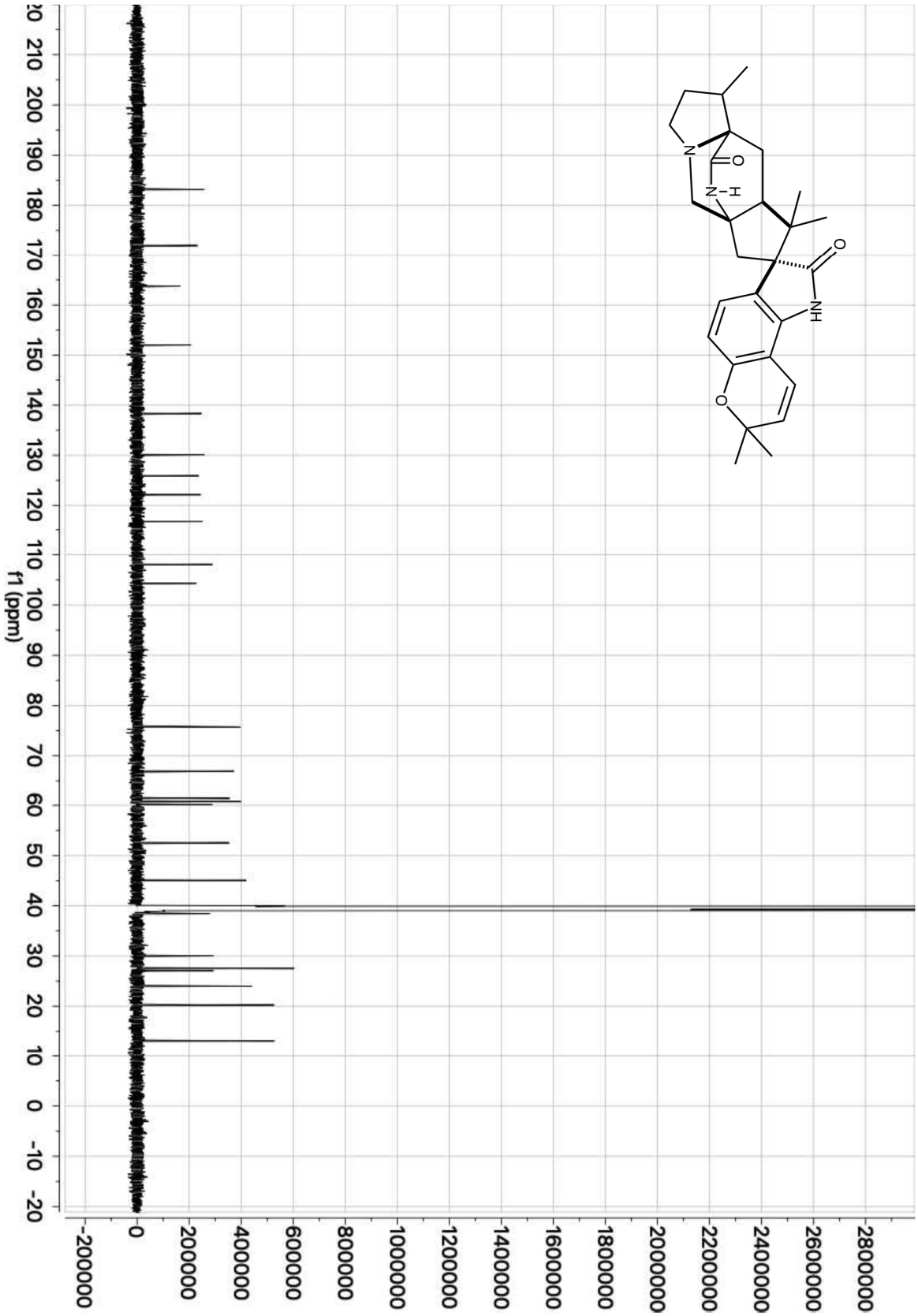

Figure S66. ^{13}C-NMR of paraherquamide M (**16**) (201 MHz, $(CD_3)_2SO$-d_6).

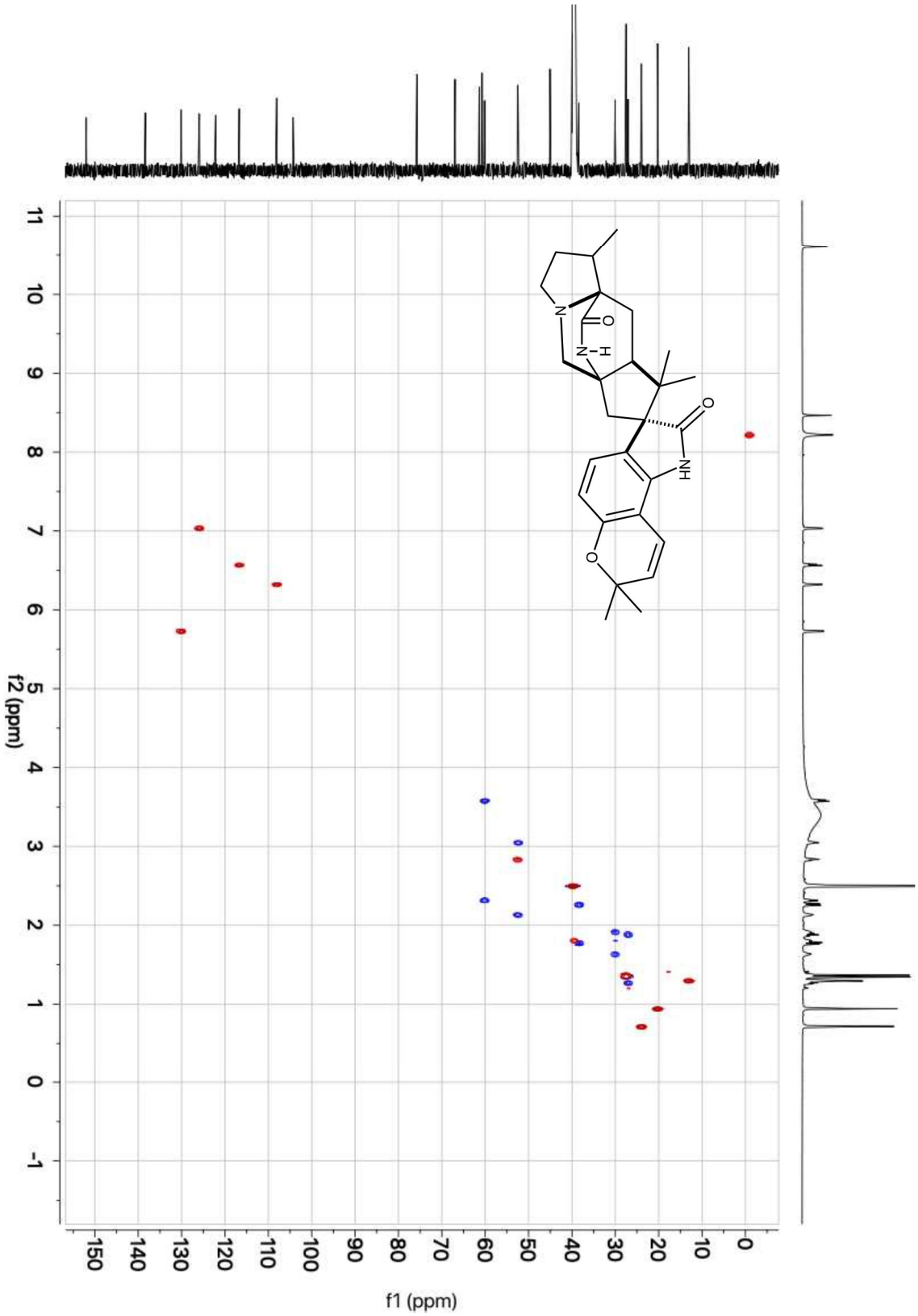

Figure S67. gHSQCAD correlations of paraherquamide M (**16**) (800 MHz, $(CD_3)_2SO$-d_6).

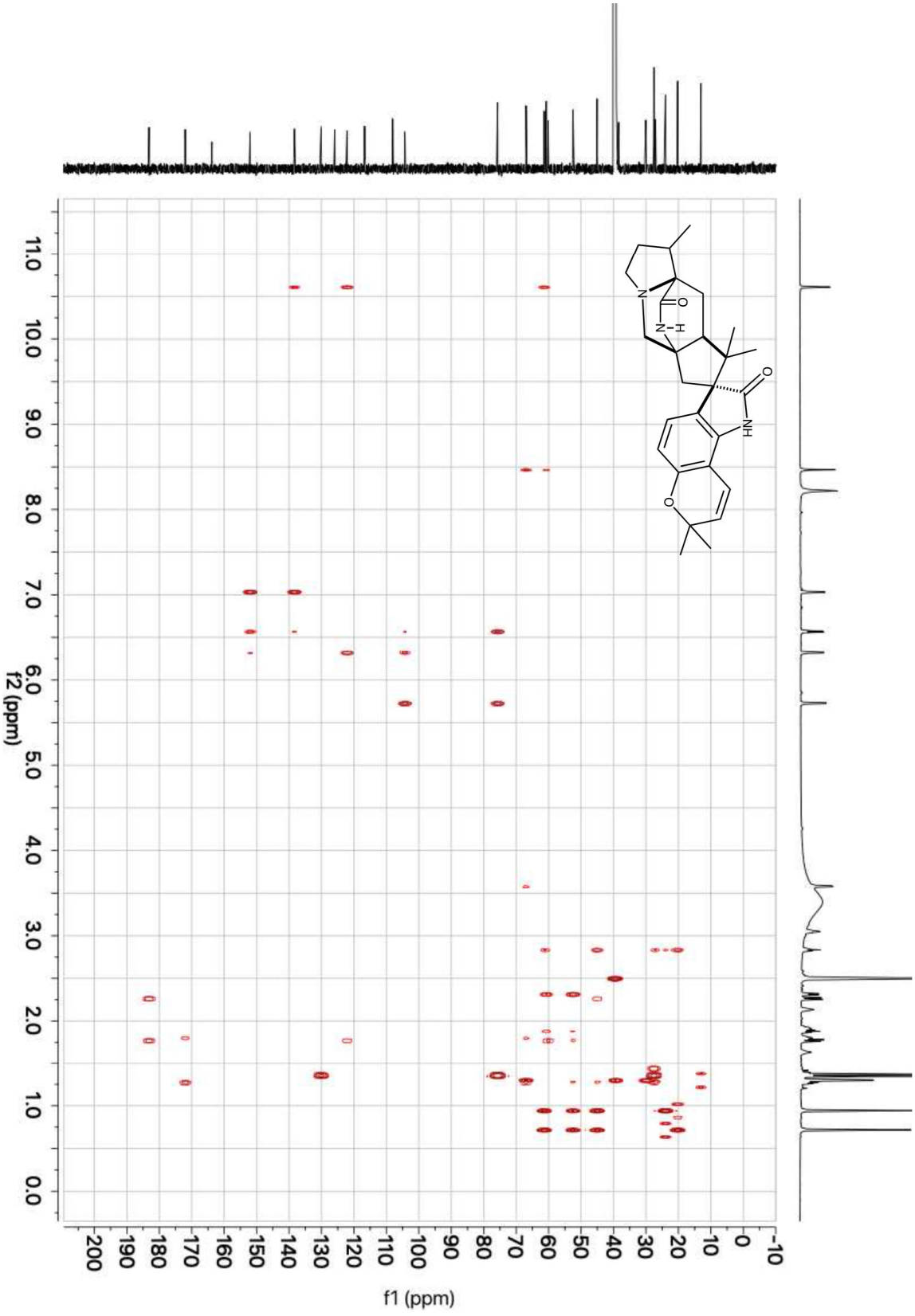

Figure S68. gHMBCAD correlations of paraherquamide M (**16**) (800 MHz, $(CD_3)_2SO$-d_6).

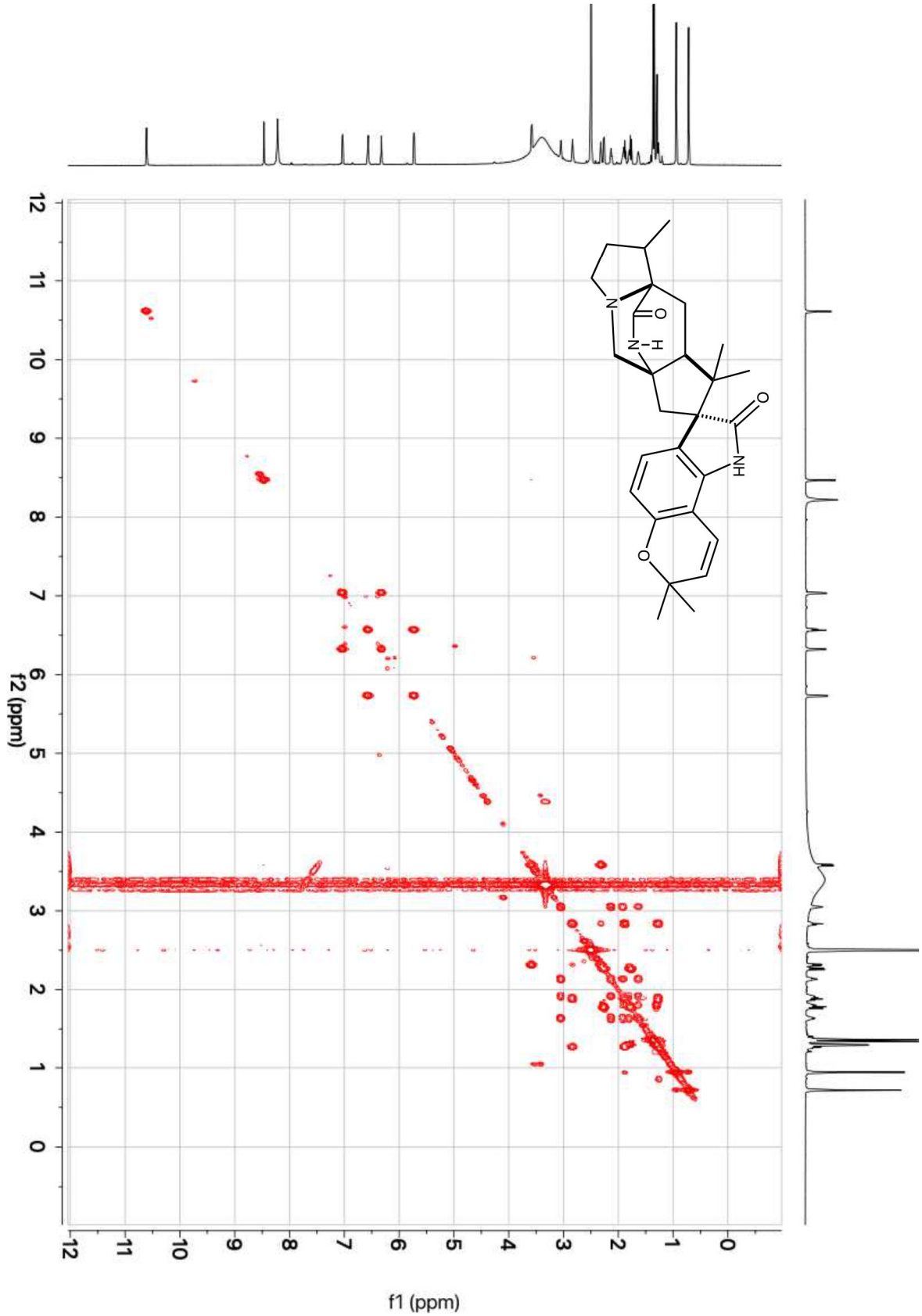

Figure S69. gCOSY correlations of paraherquamide M (**16**) (600 MHz, $(CD_3)_2SO$-d_6).

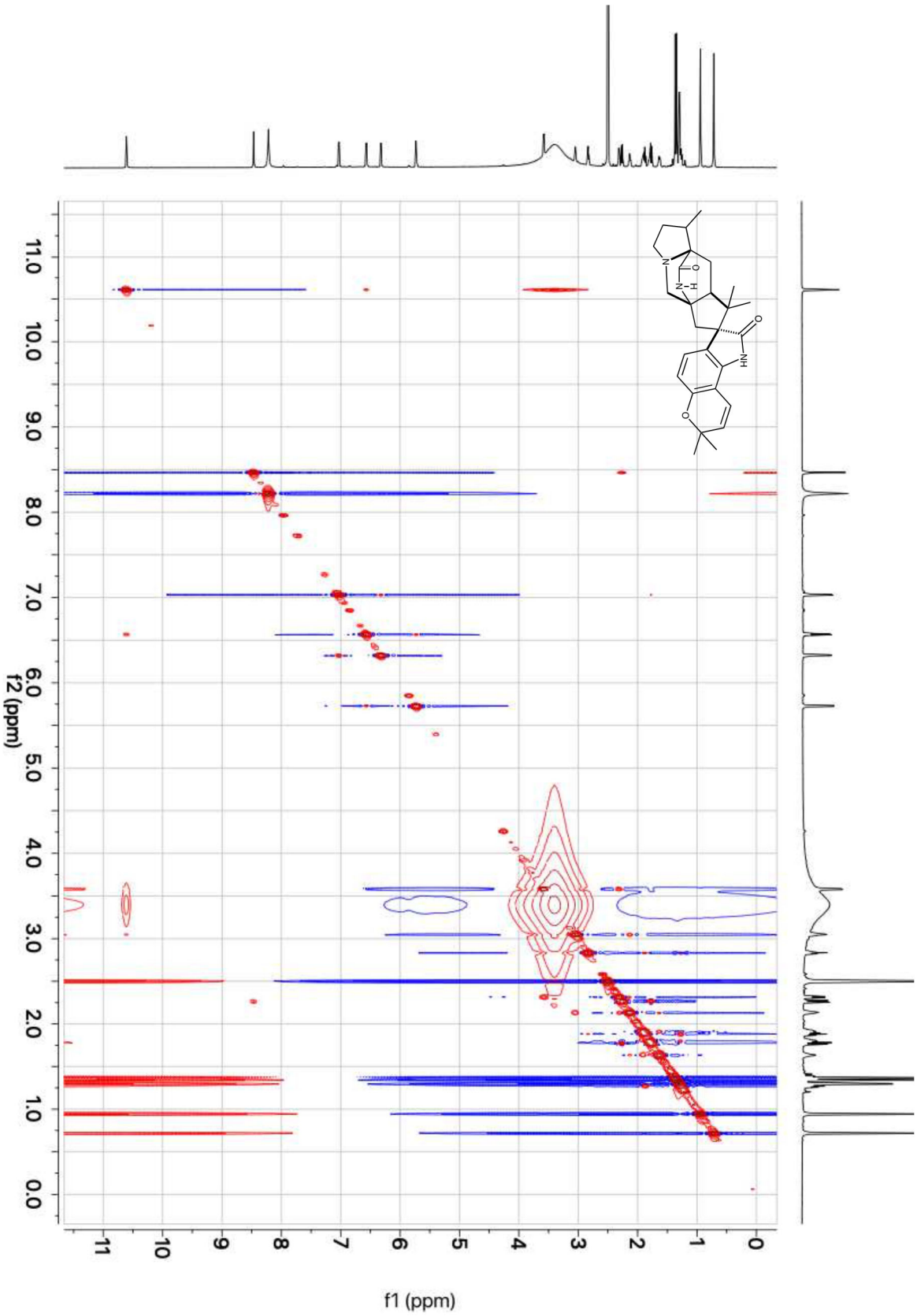

Figure S70. NOE correlations of paraherquamide M (**16**) (800 MHz, $(CD_3)_2SO$-d_6).

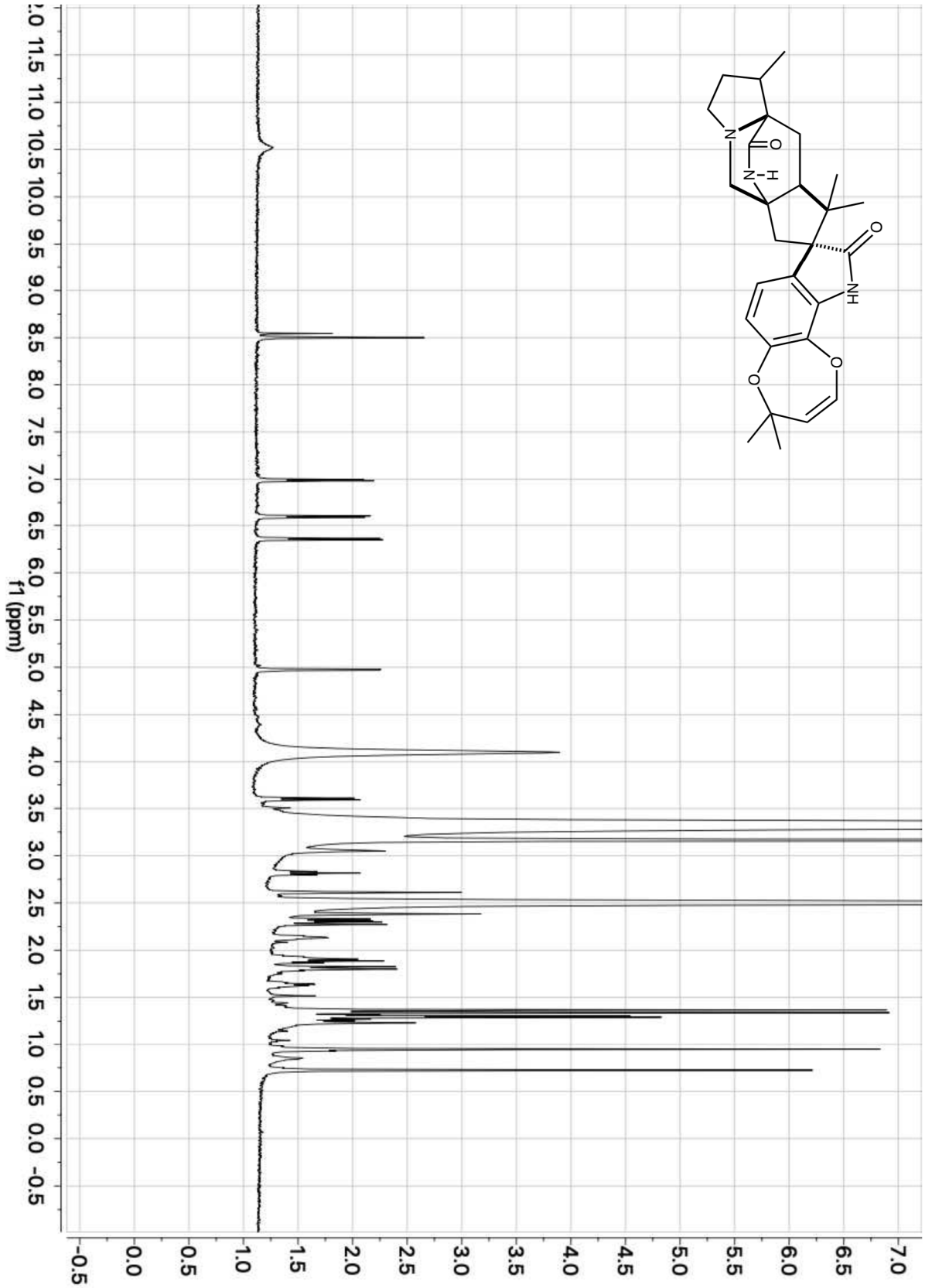

Figure S71. ^{1}H-NMR of paraherquamide N (**17**) (600 MHz, $(CD_3)_2SO$-d_6).

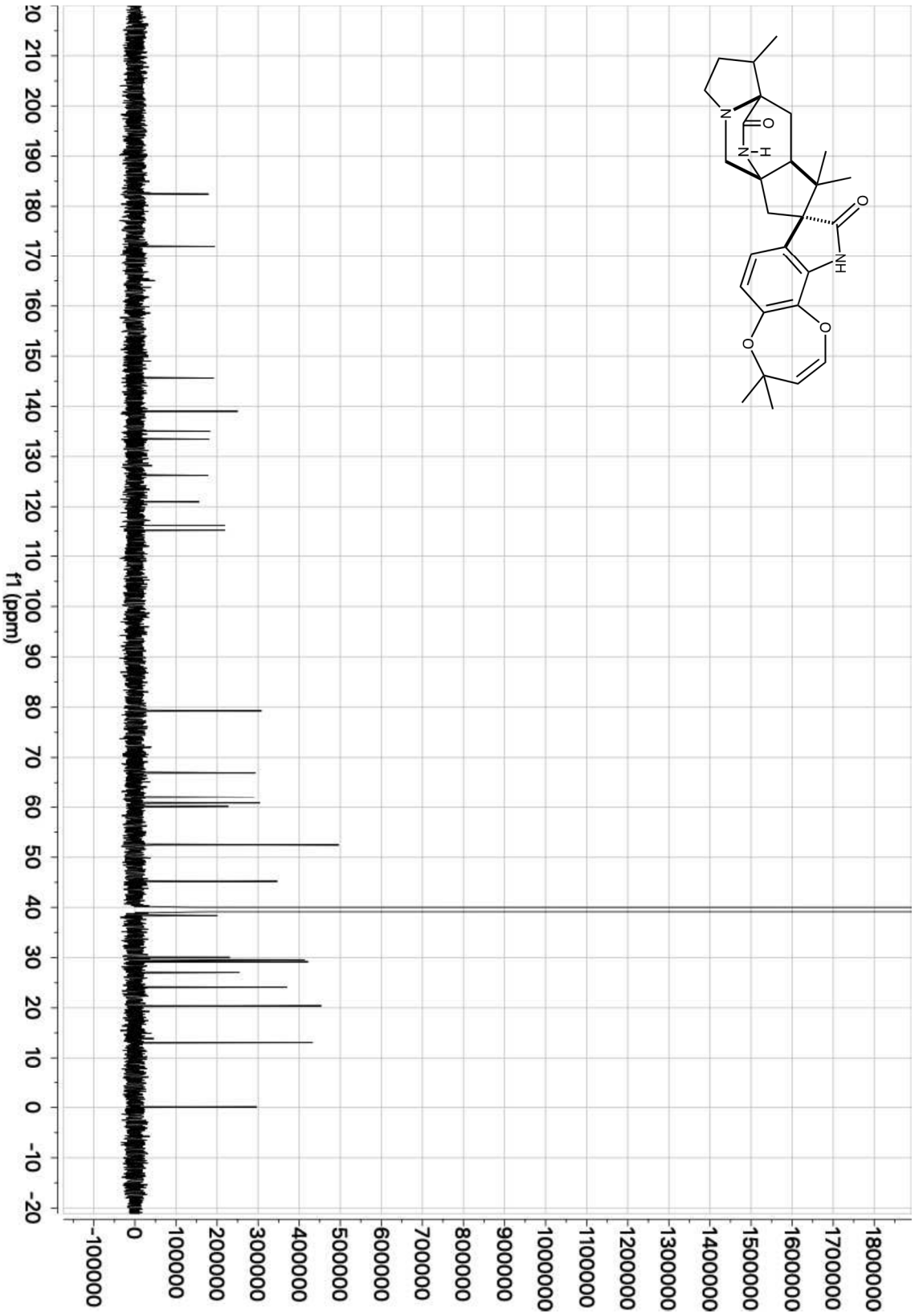

Figure S72. ^{13}C-NMR of paraherquamide N (**17**) (201 MHz, $(CD_3)_2SO$-d_6).

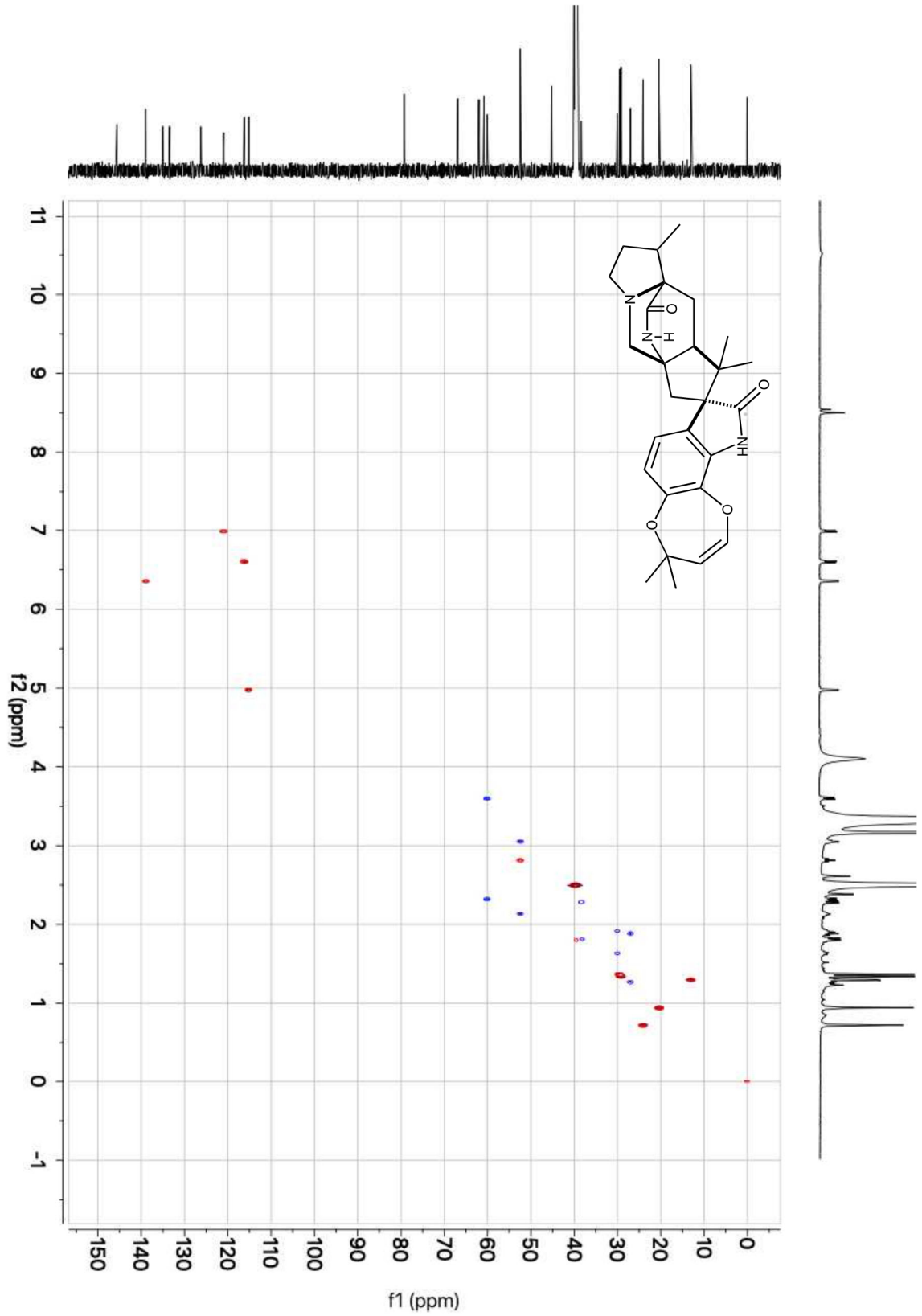

Figure S73. gHSQCAD correlations of paraherquamide N (**17**) (800 MHz, $(CD_3)_2SO$-d_6).

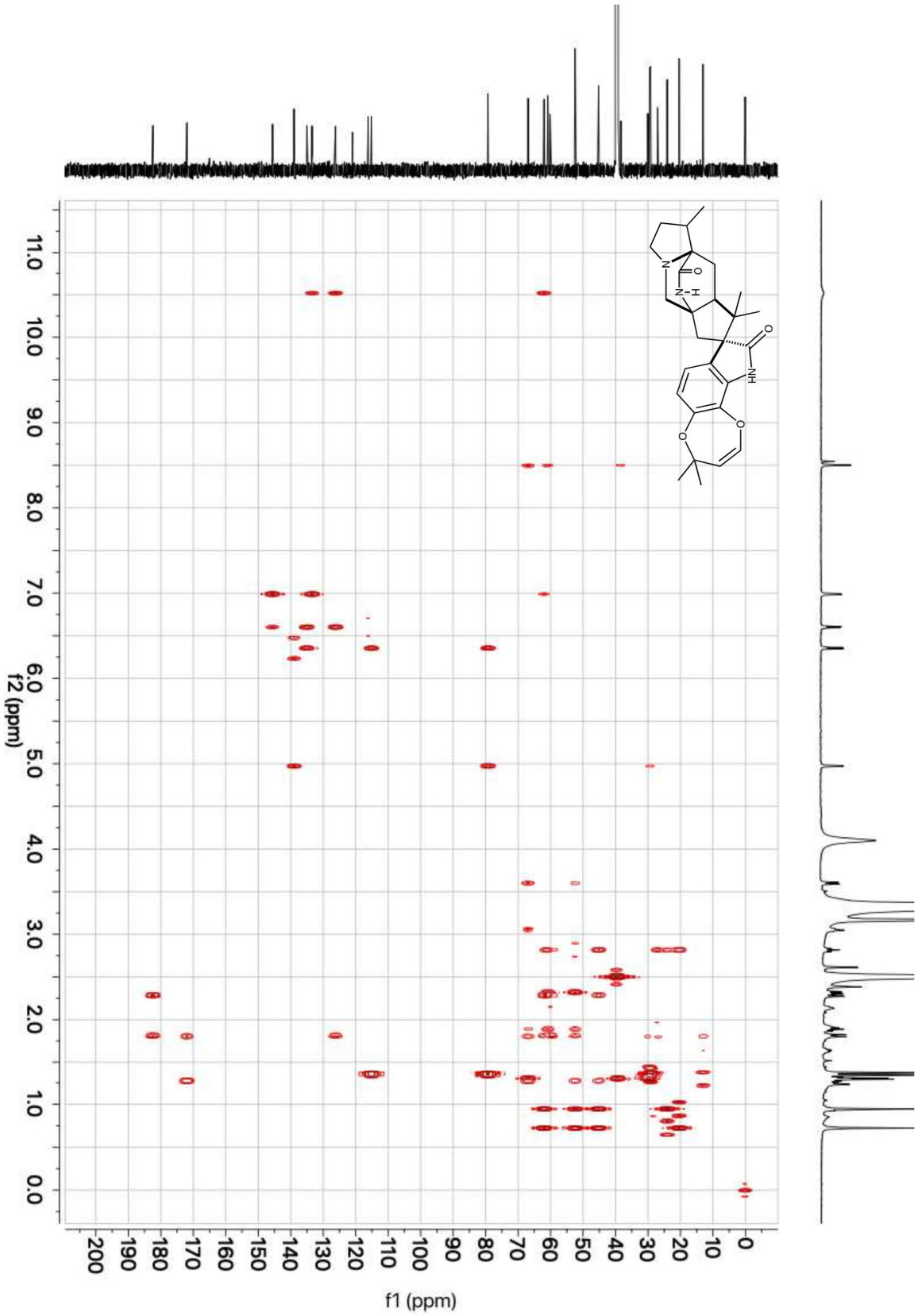

Figure S74. gHMBCAD correlations of paraherquamide N (**17**) (800 MHz, $(CD_3)_2SO$-d_6).

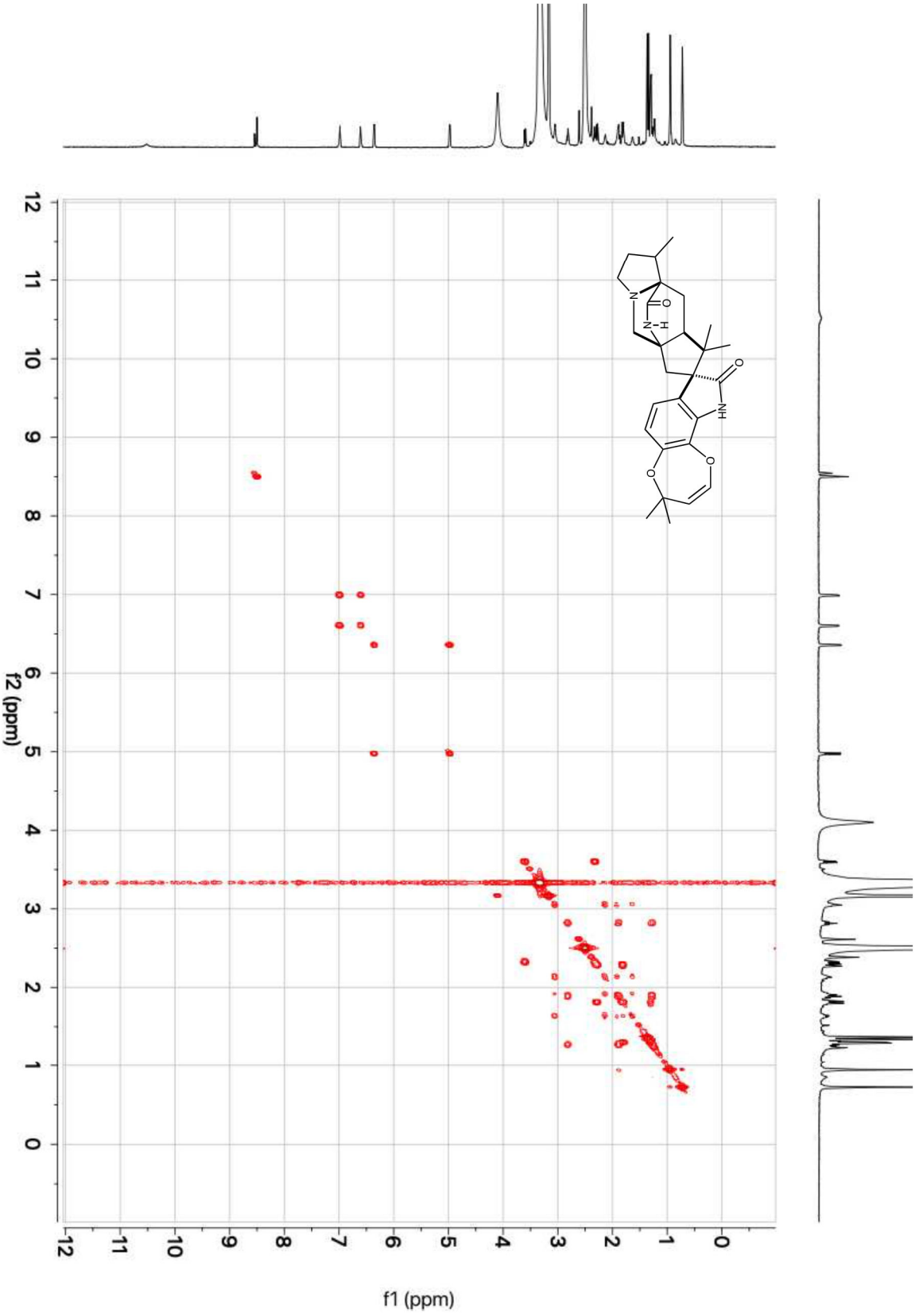

Figure S75. gCOSY correlations of paraherquamide N (**17**) (600 MHz, $(CD_3)_2SO$-d_6).

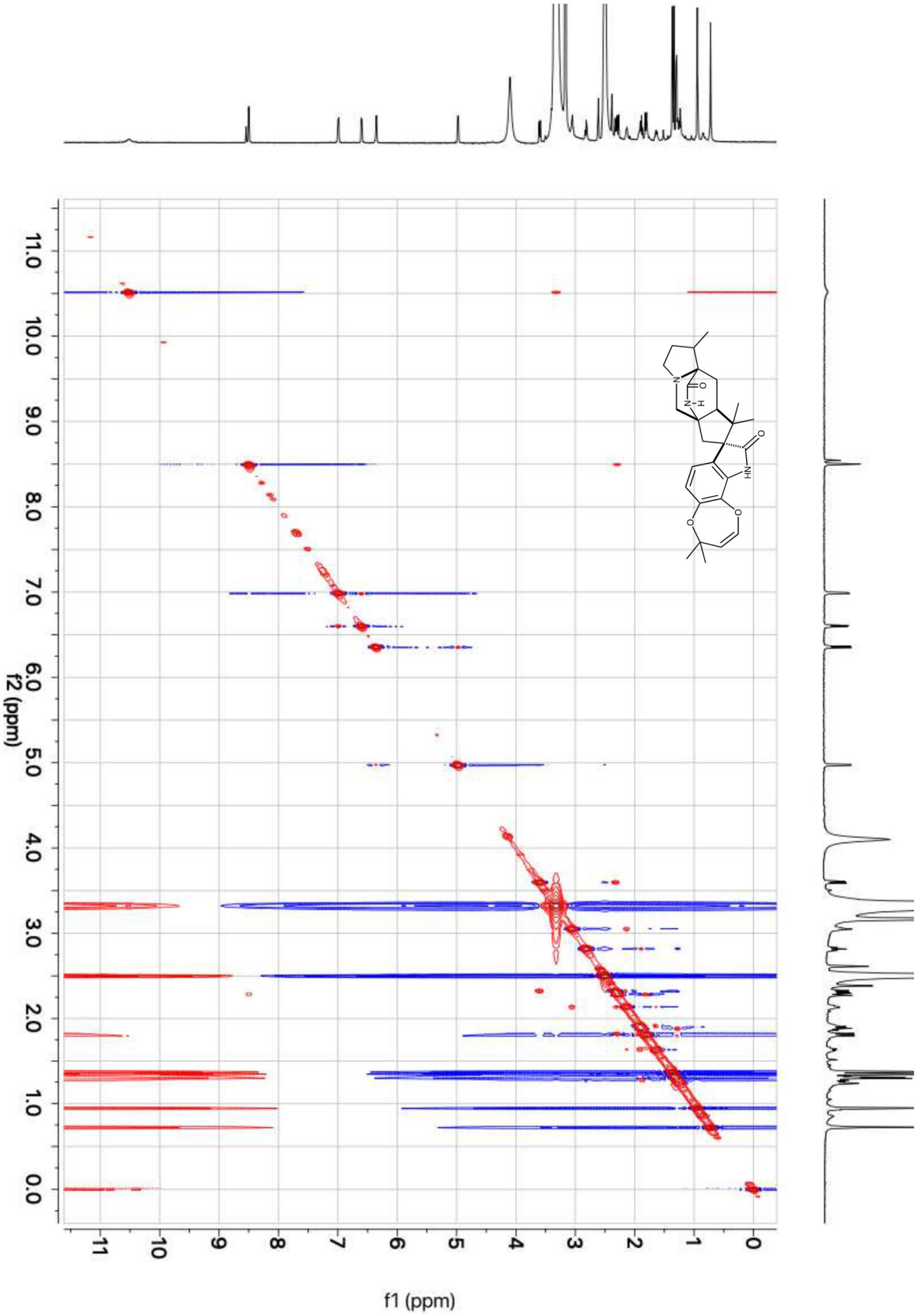

Figure S76. NOE correlations of paraherquamide N (**17**) (800 MHz, $(CD_3)_2SO$-d_6).

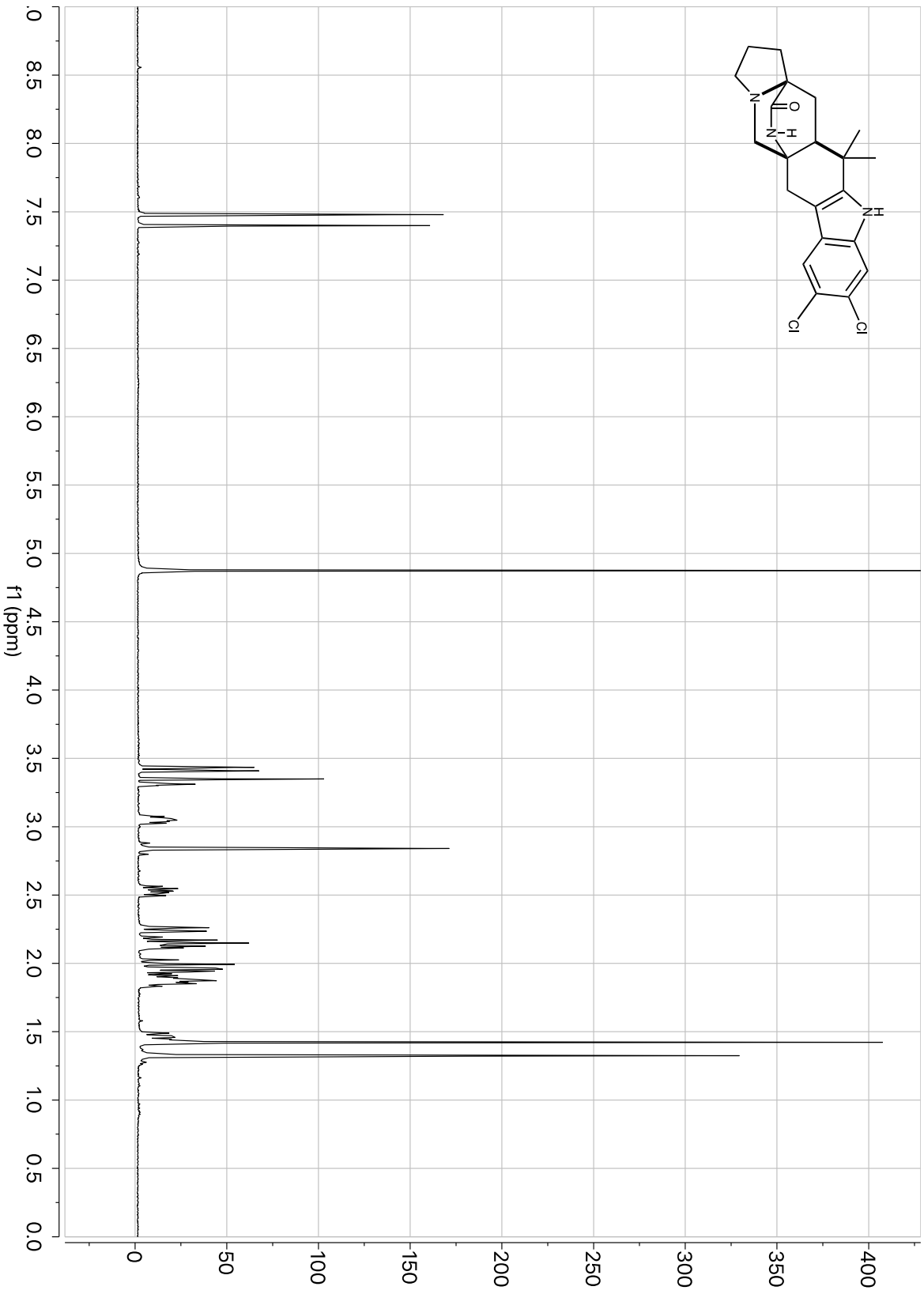

Figure S77. ^{1}H-NMR of fungal malbrancheamide (**19**) (600 MHz, CD_3OD).

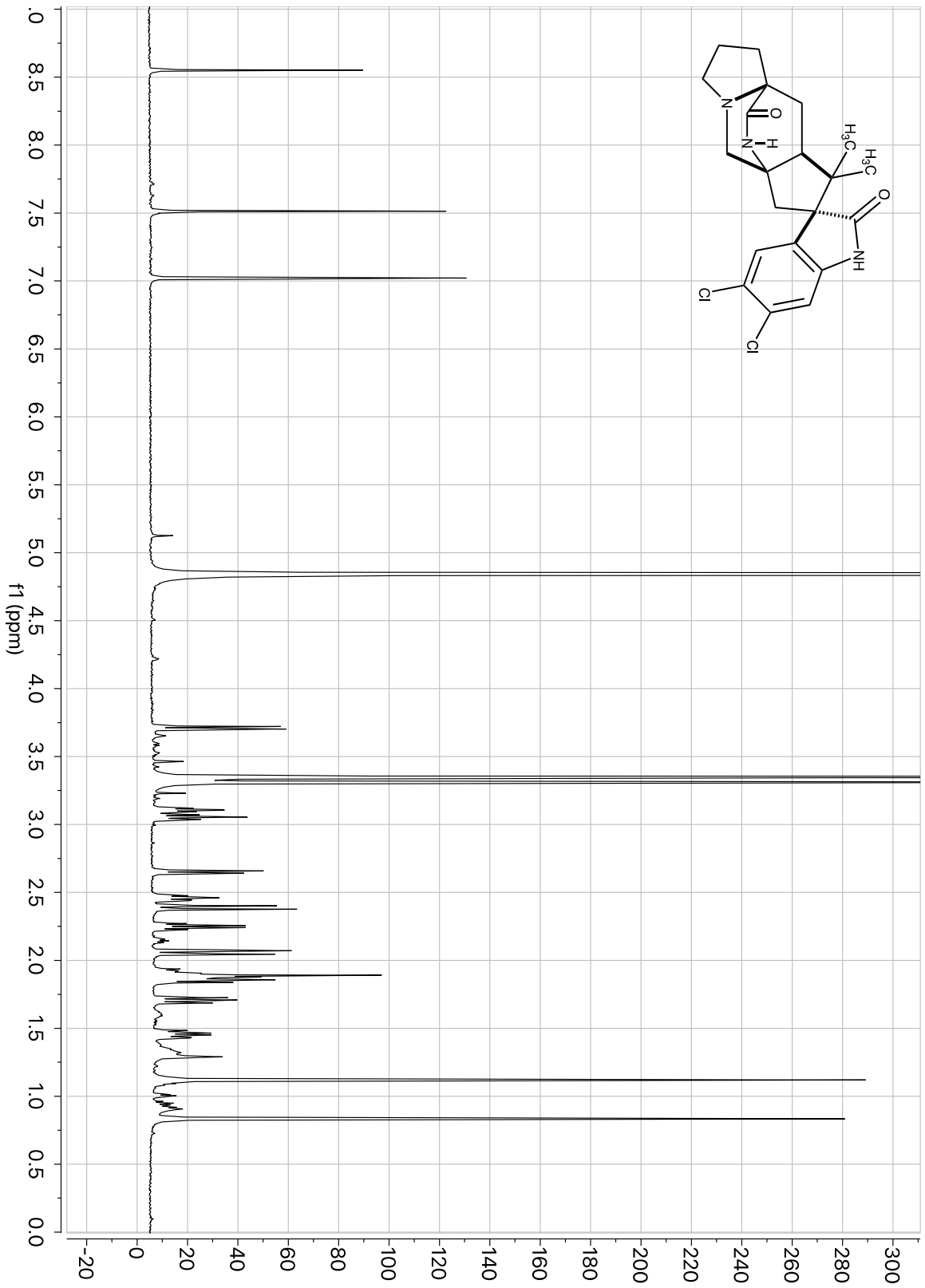

Figure S78. ^{1}H-NMR of spiromalbramide (**20**) (600 MHz, CD_3OD).

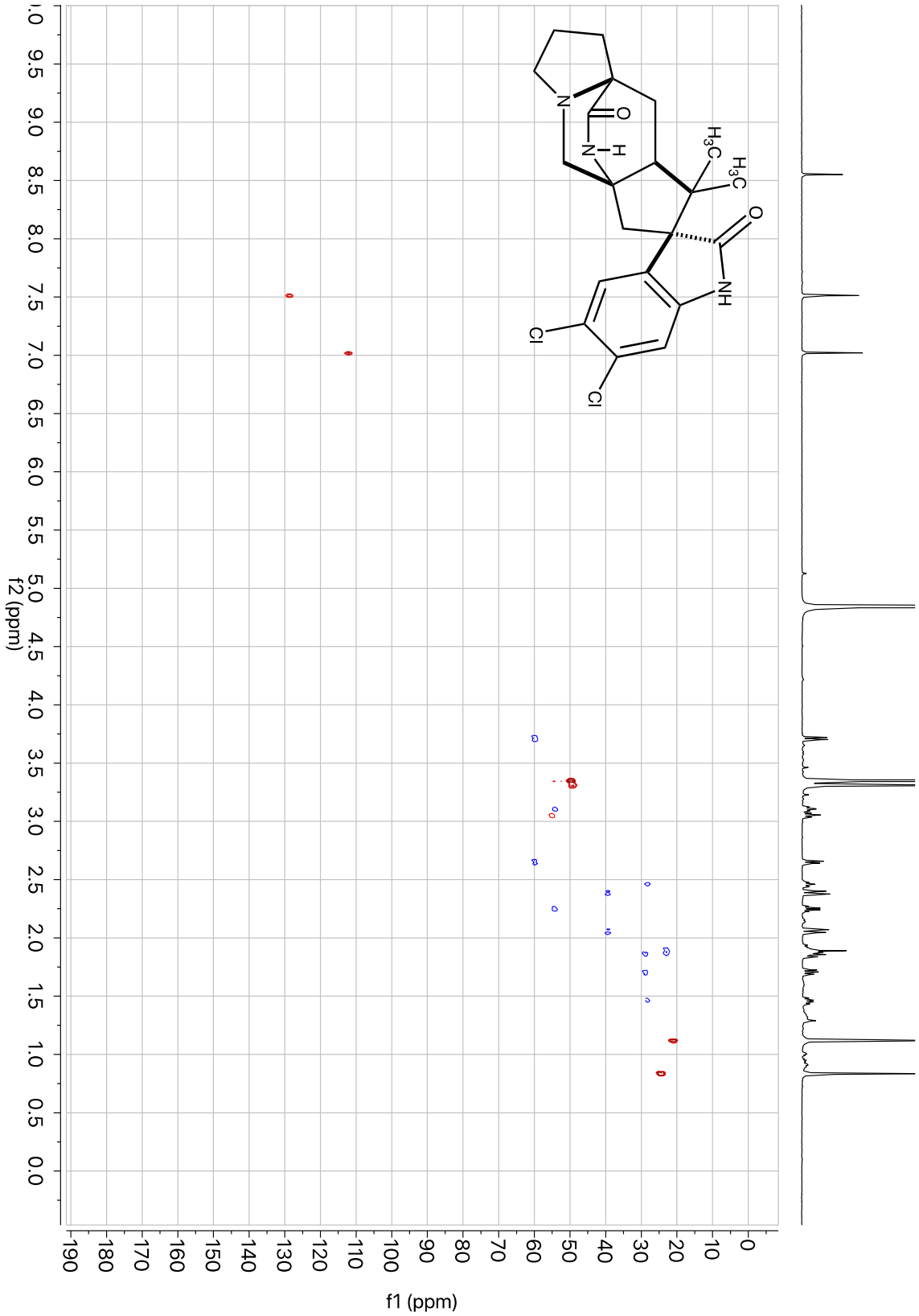

Figure S79. gHSQCAD correlations of spiromalbramide (**20**) (600 MHz, CD_3OD).

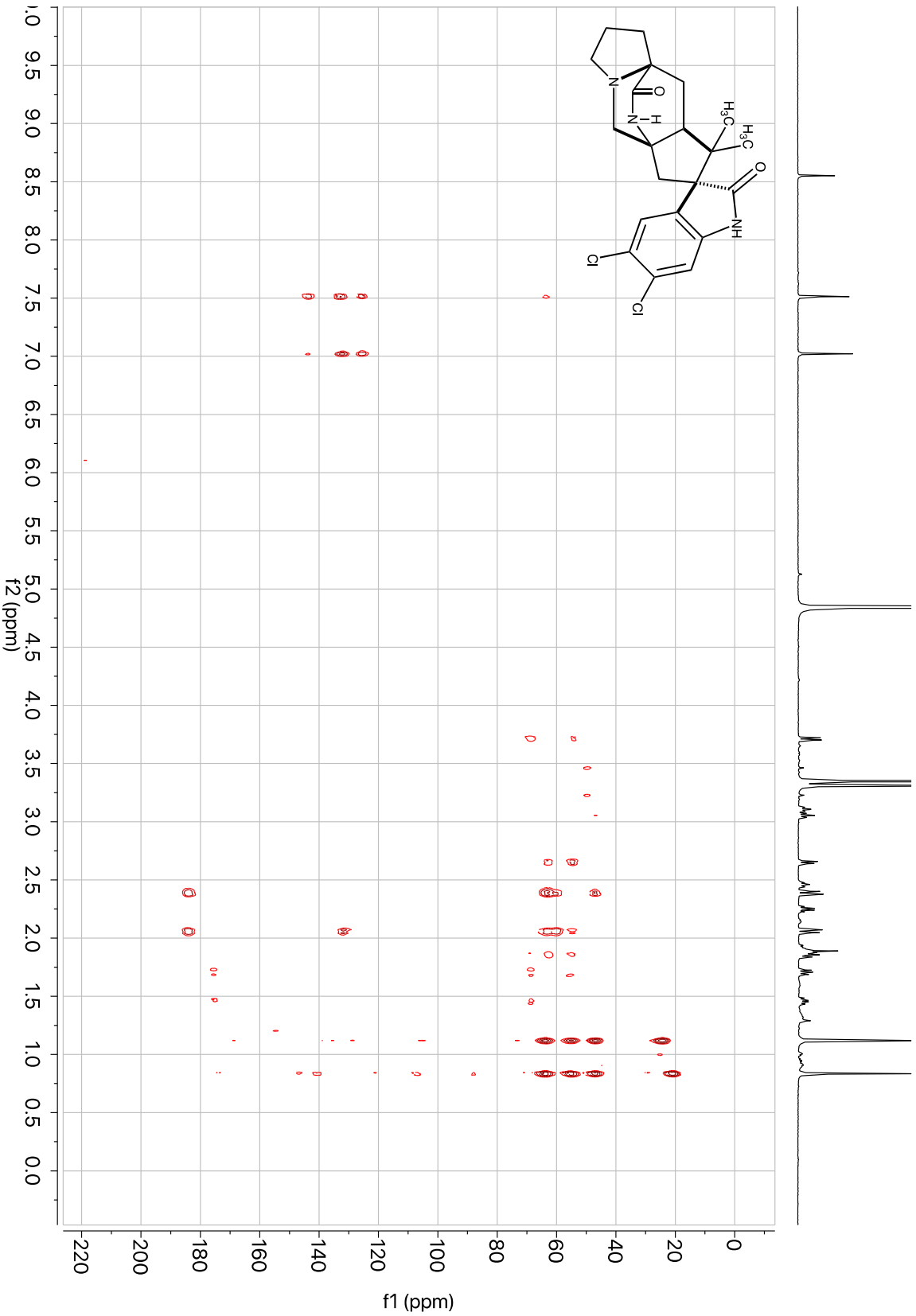

Figure S80. gHMBCAD correlations of spiromalbramide (**20**) (600 MHz, CD_3OD).

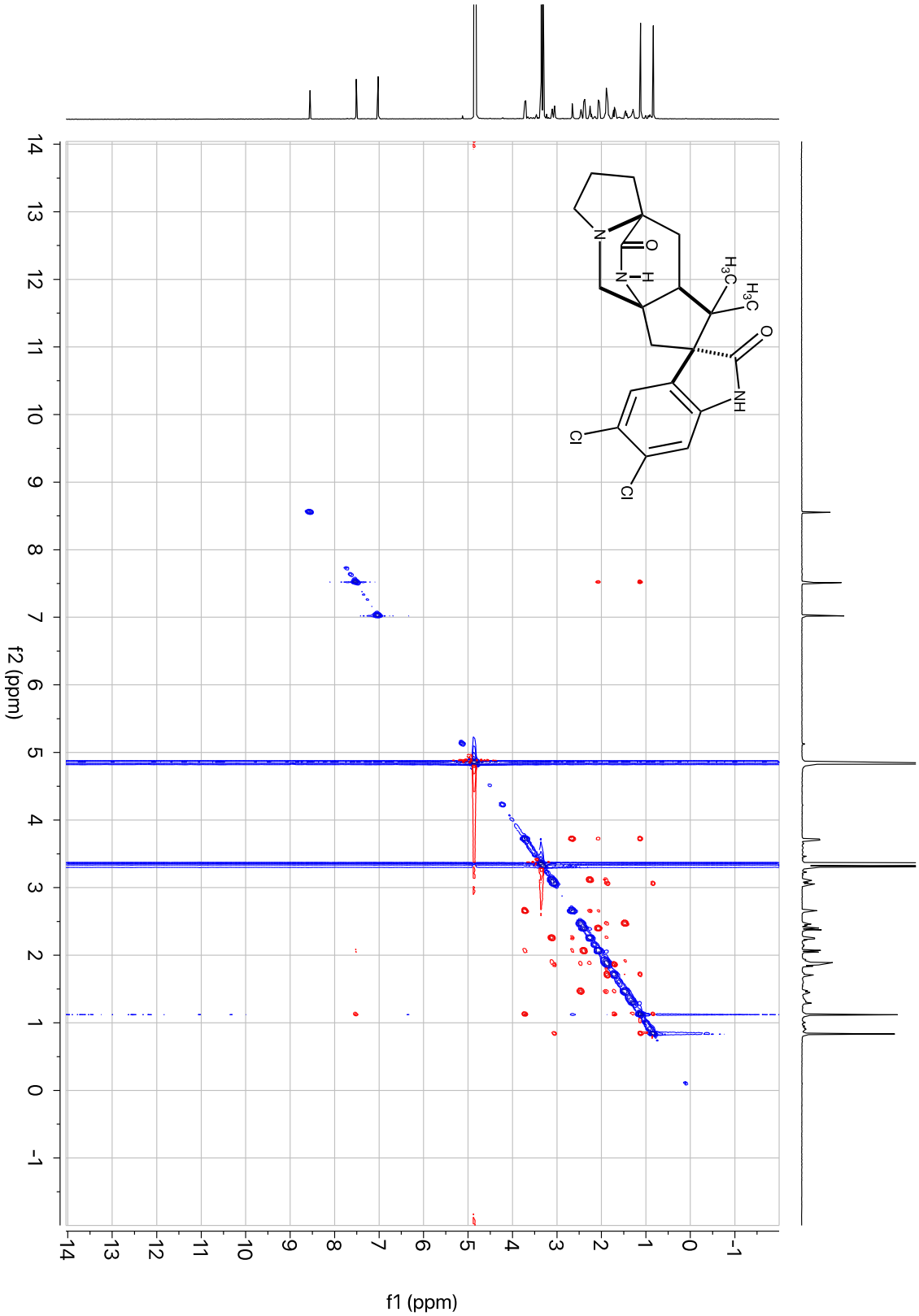

Figure S81. NOE correlations of spiromalbramide (**20**) (600 MHz, CD_3OD).

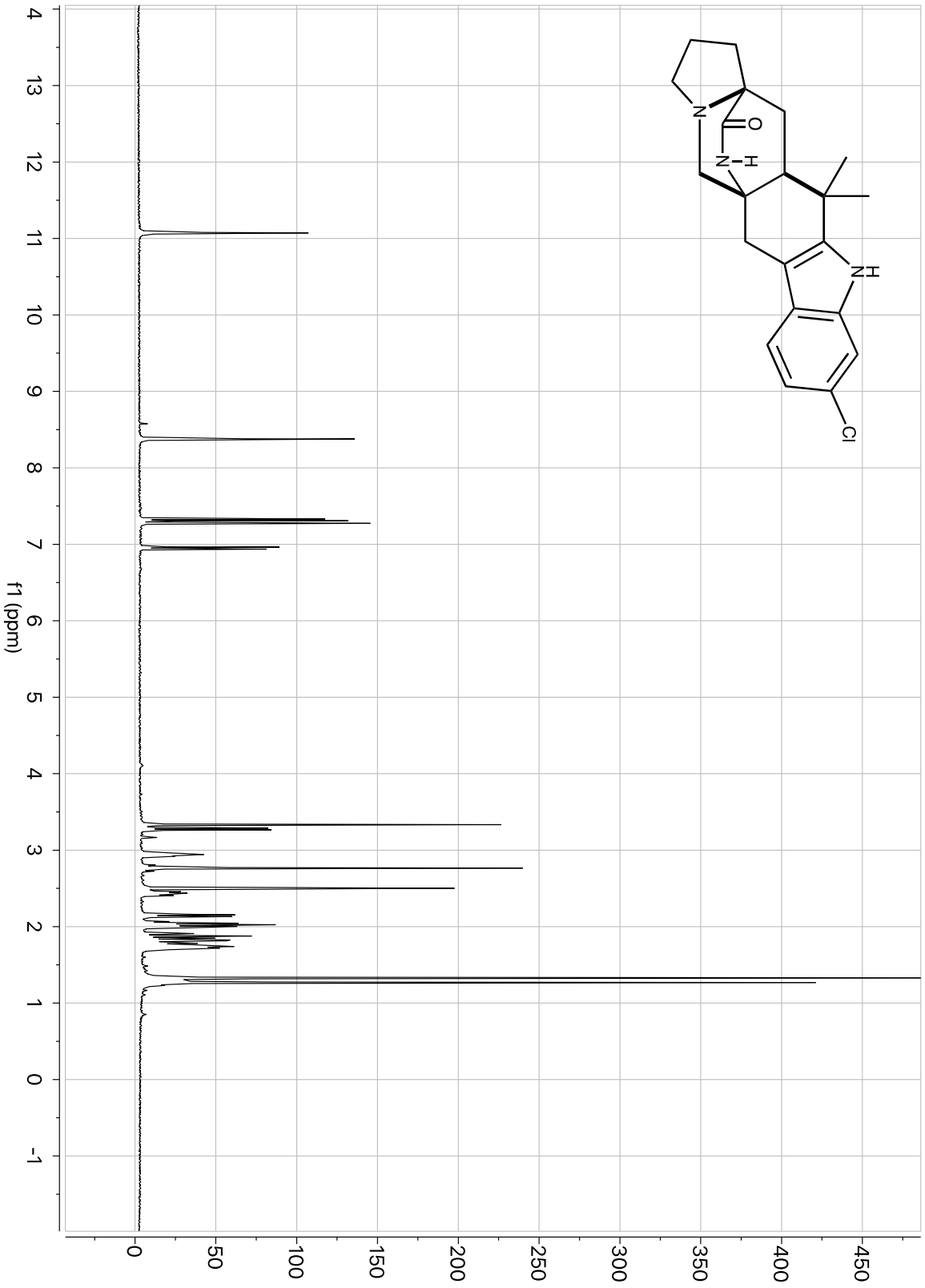

Figure S82. ^{1}H-NMR of malbrancheamide B (**21**) (600 MHz, $(CD_3)_2SO$-d_6).

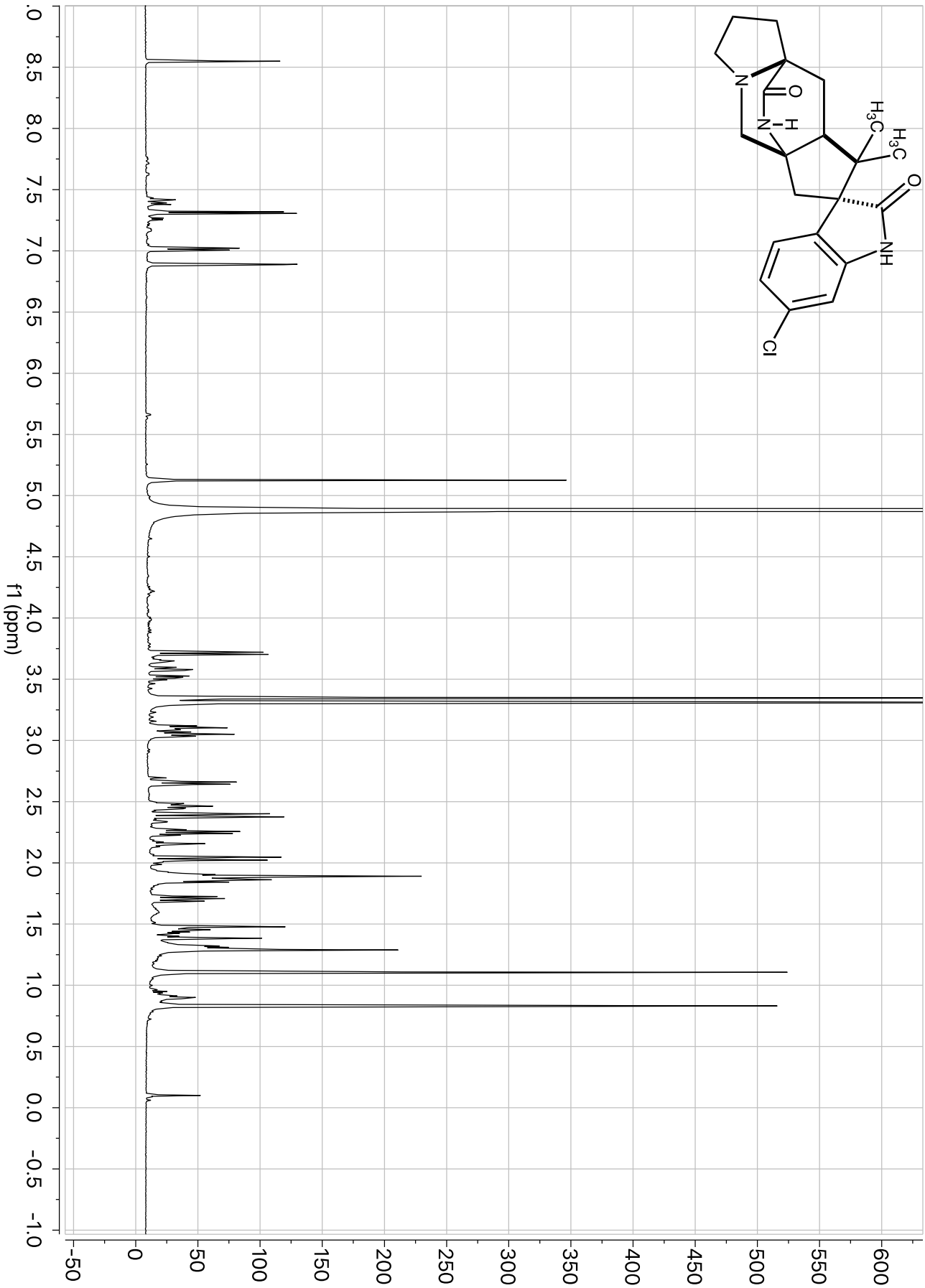

Figure S83. ^{1}H-NMR of spiromalbrancheamide B (**25**) (600 MHz, CD_3OD).

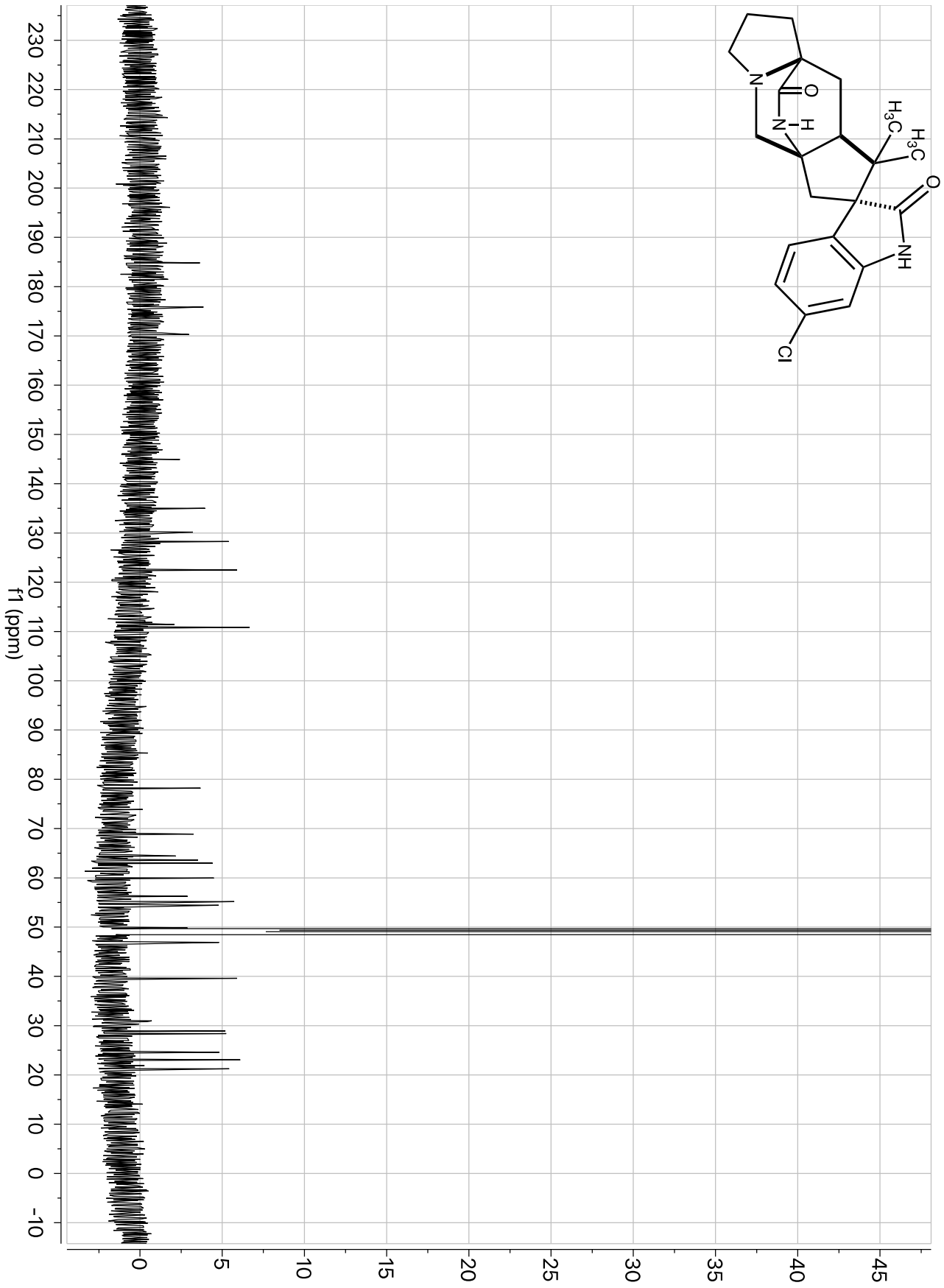

Figure S84. ^{13}C-NMR of spiromalbrancheamide B (**25**) (150 MHz, CD_3OD).

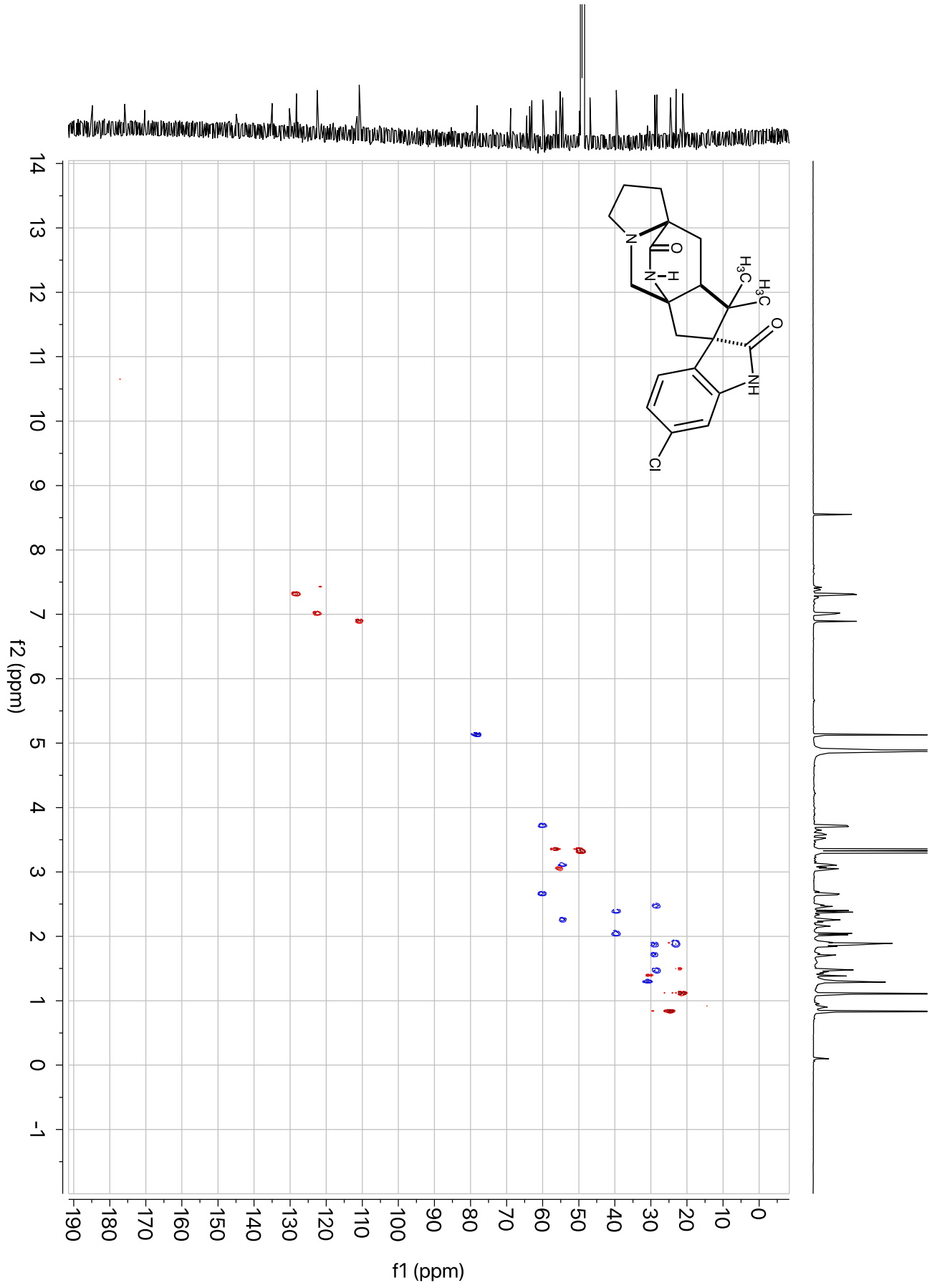

Figure S85. gHSQCAD correlations of spiromalbrancheamide B (**25**) (600 MHz, CD_3OD).

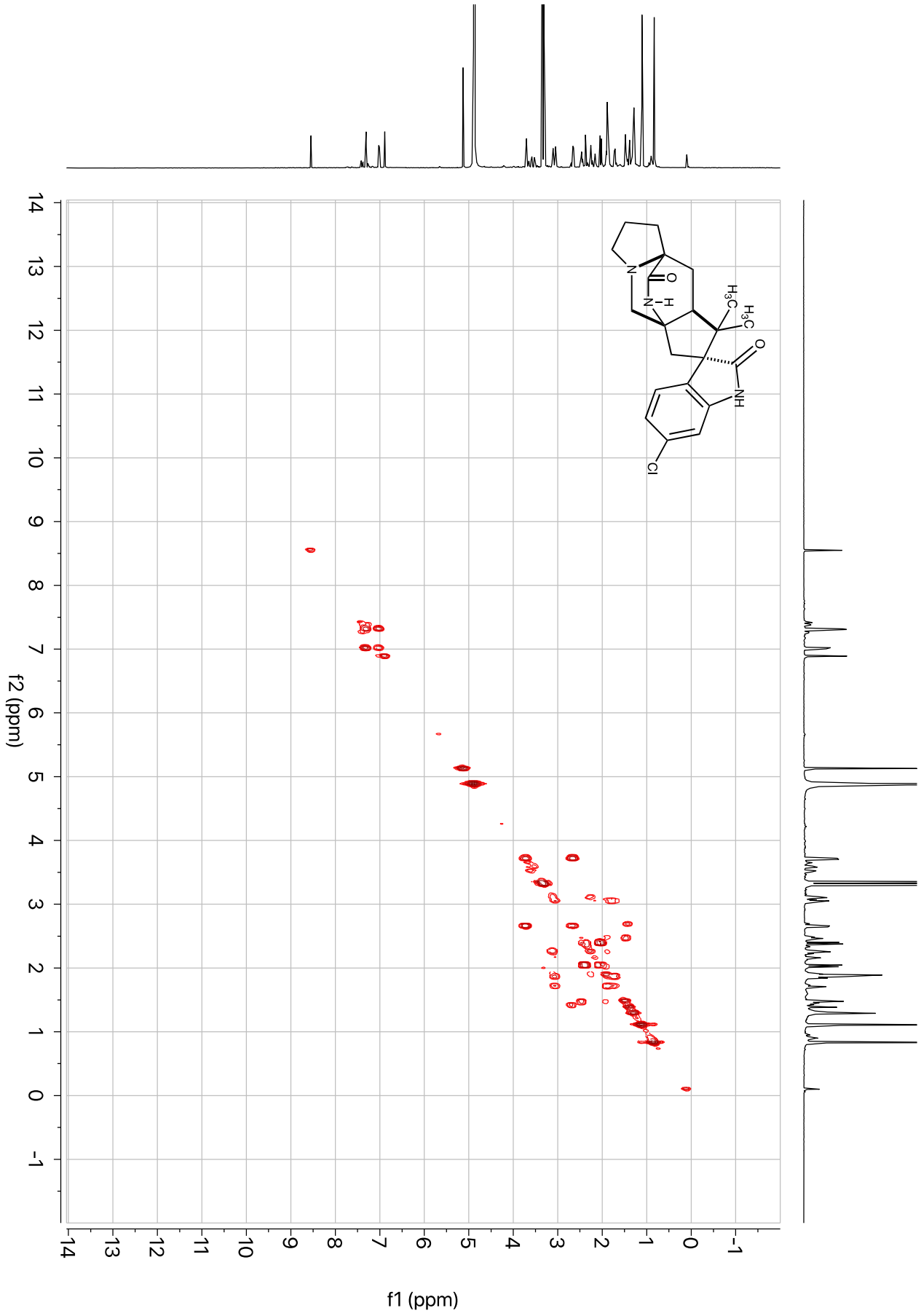

Figure S86. gCOSY correlations of spiromalbrancheamide B (**25**) (600 MHz, CD_3OD).

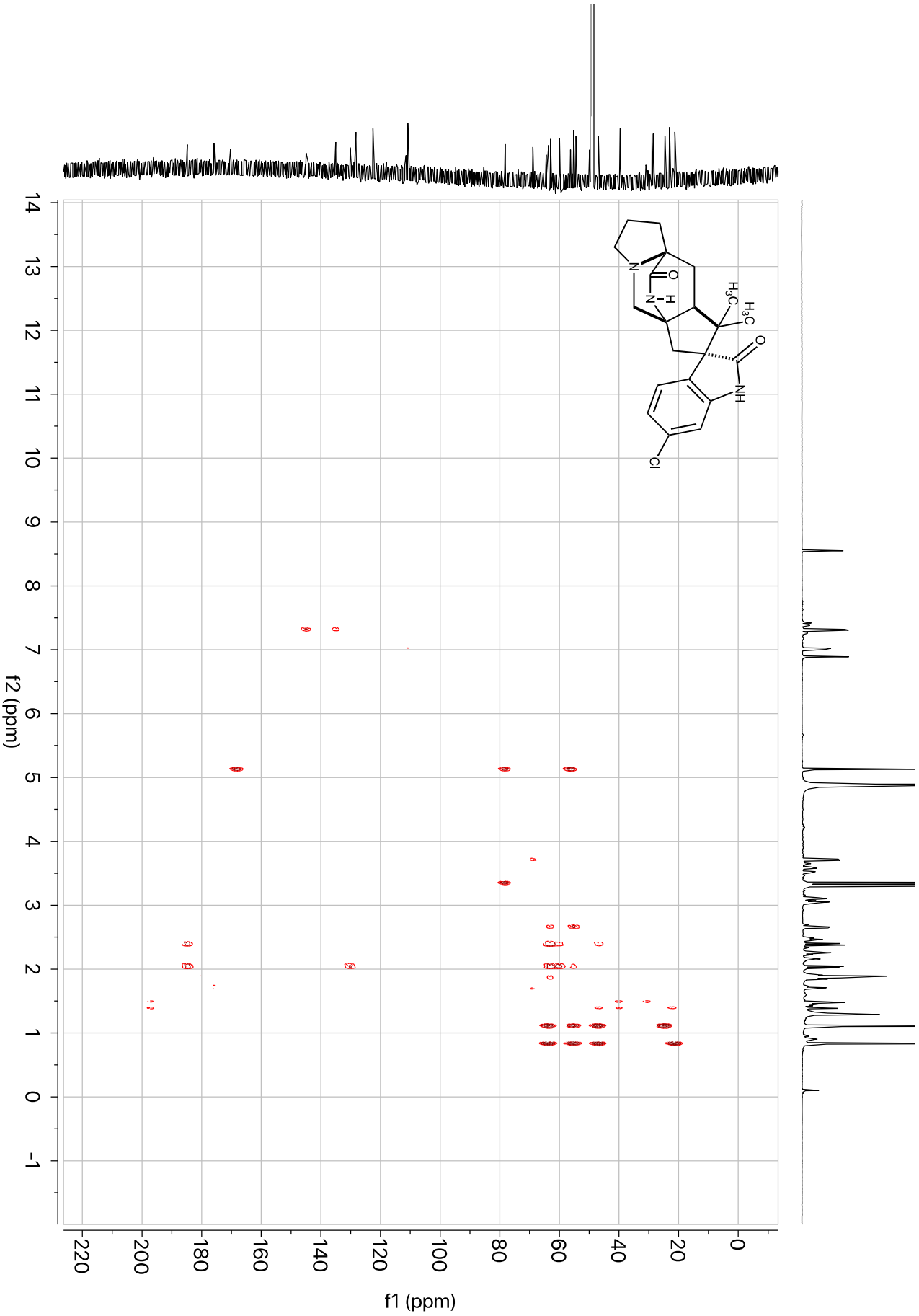

Figure S87. gHMBCAD correlations of spiromalbrancheamide B (**25**) (600 MHz, CD_3OD).

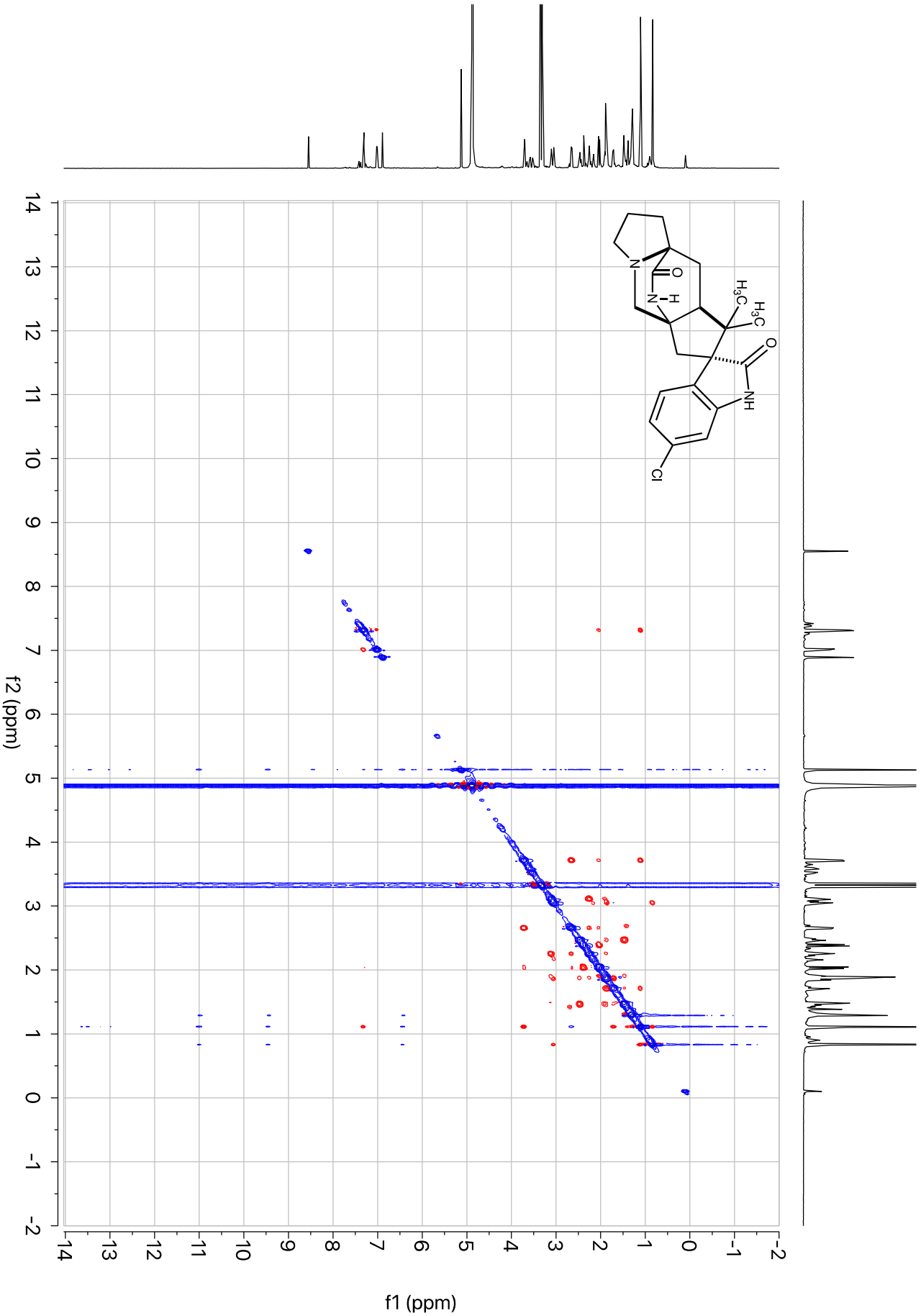

Figure S88. NOESY correlations of spiromalbrancheamide B (**25**) (600 MHz, CD_3OD).

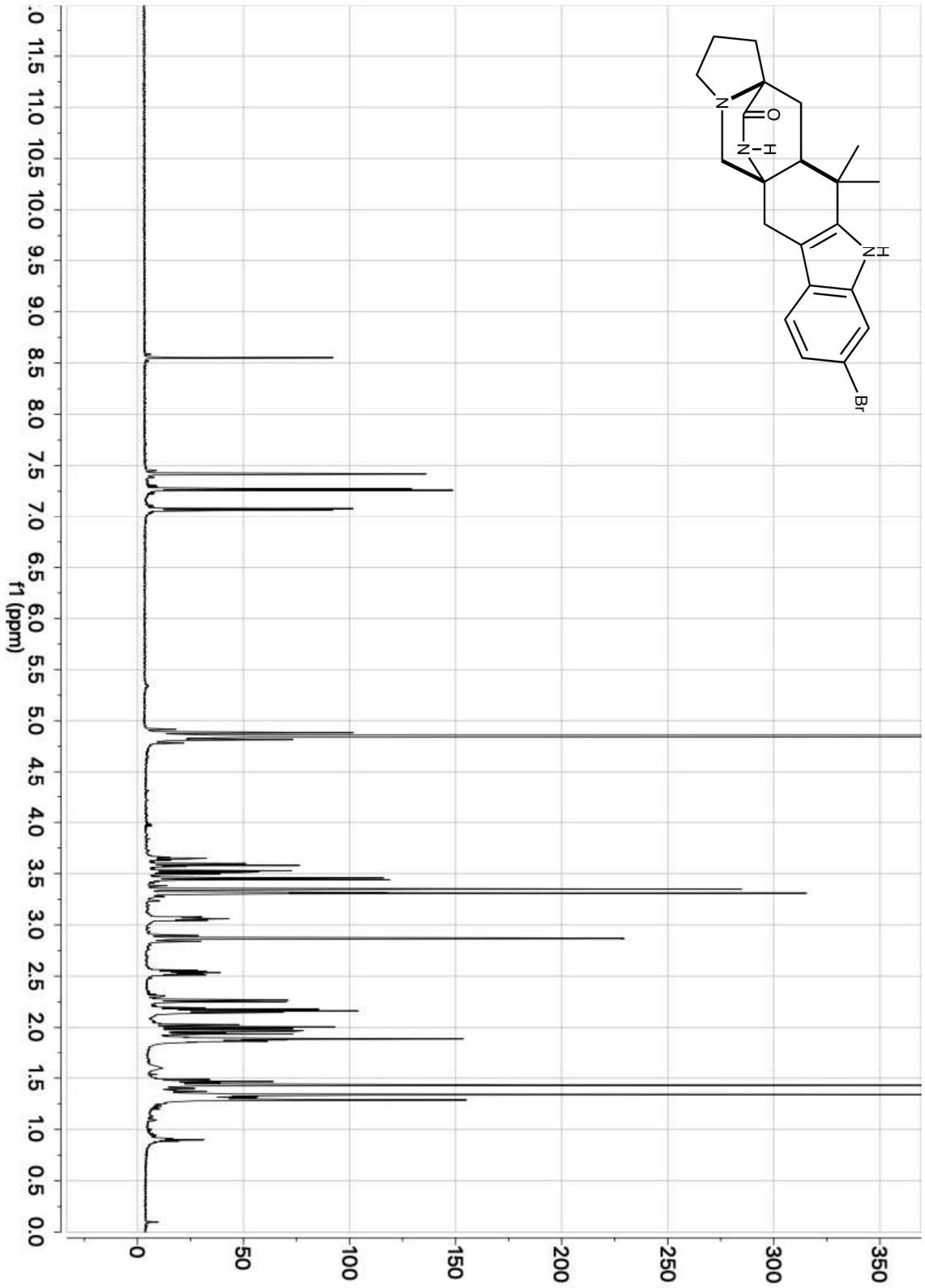

Figure S89. ^{1}H-NMR of malbrancheamide C (**22**) isolated from *in vitro* reaction with MalA (700 MHz, CD_3OD).

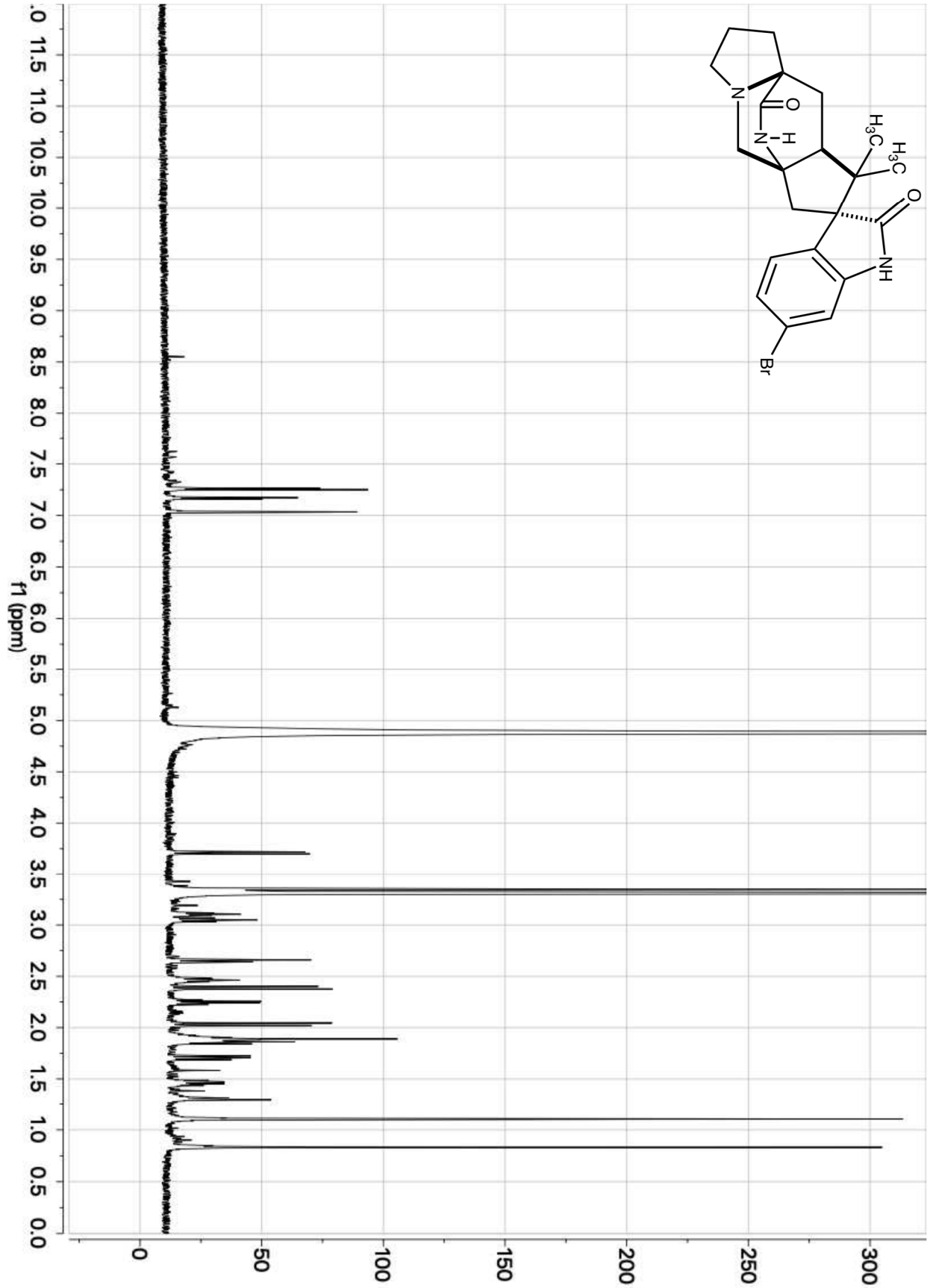

Figure S90. ^{1}H-NMR of spiromalbrancheamide C (**26**) isolated from *in vitro* reaction with MalA (800 MHz, CD_3OD).

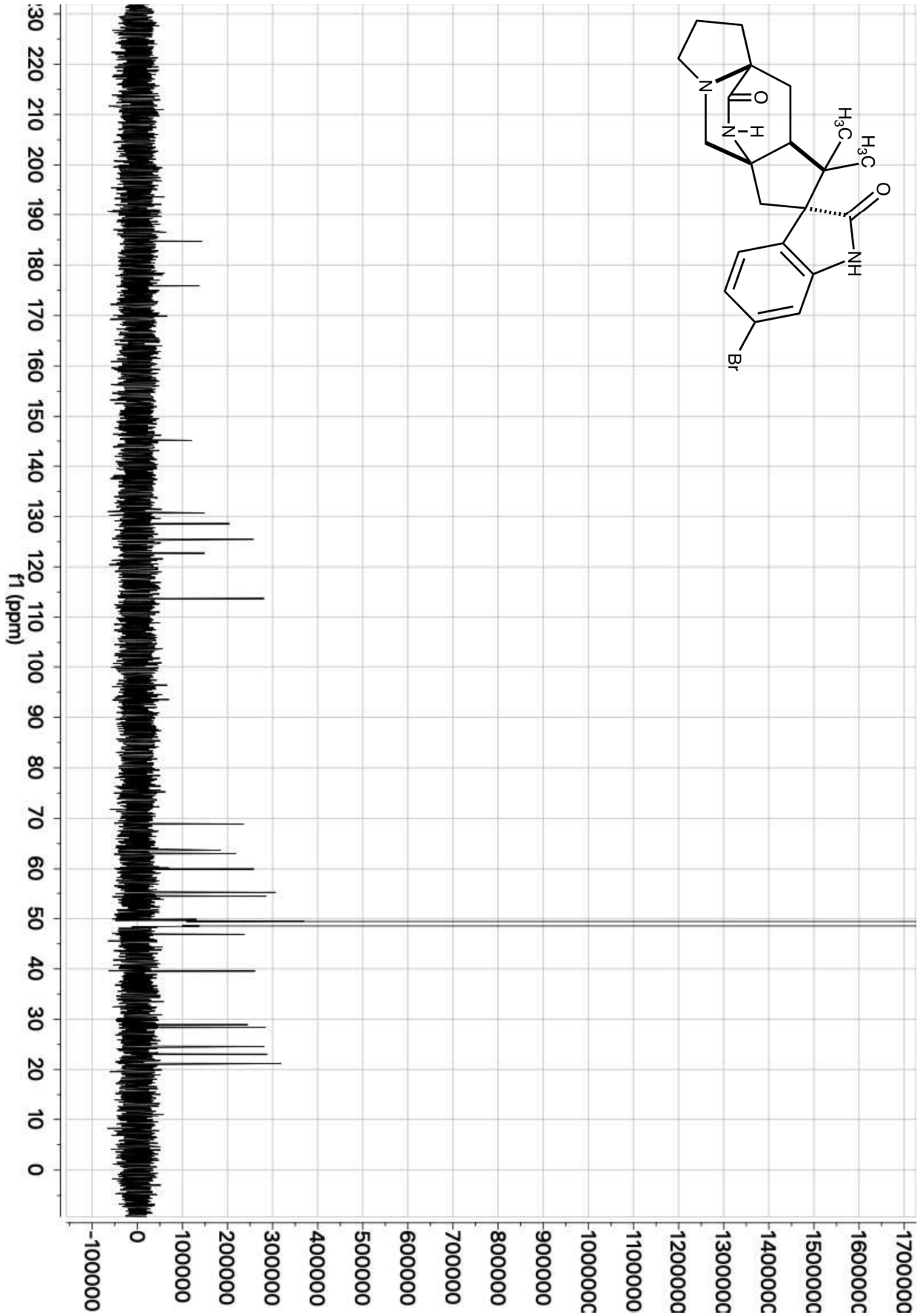

Figure S91. ^{13}C-NMR of spiromalbrancheamide C (**26**) (201 MHz, CD_3OD).

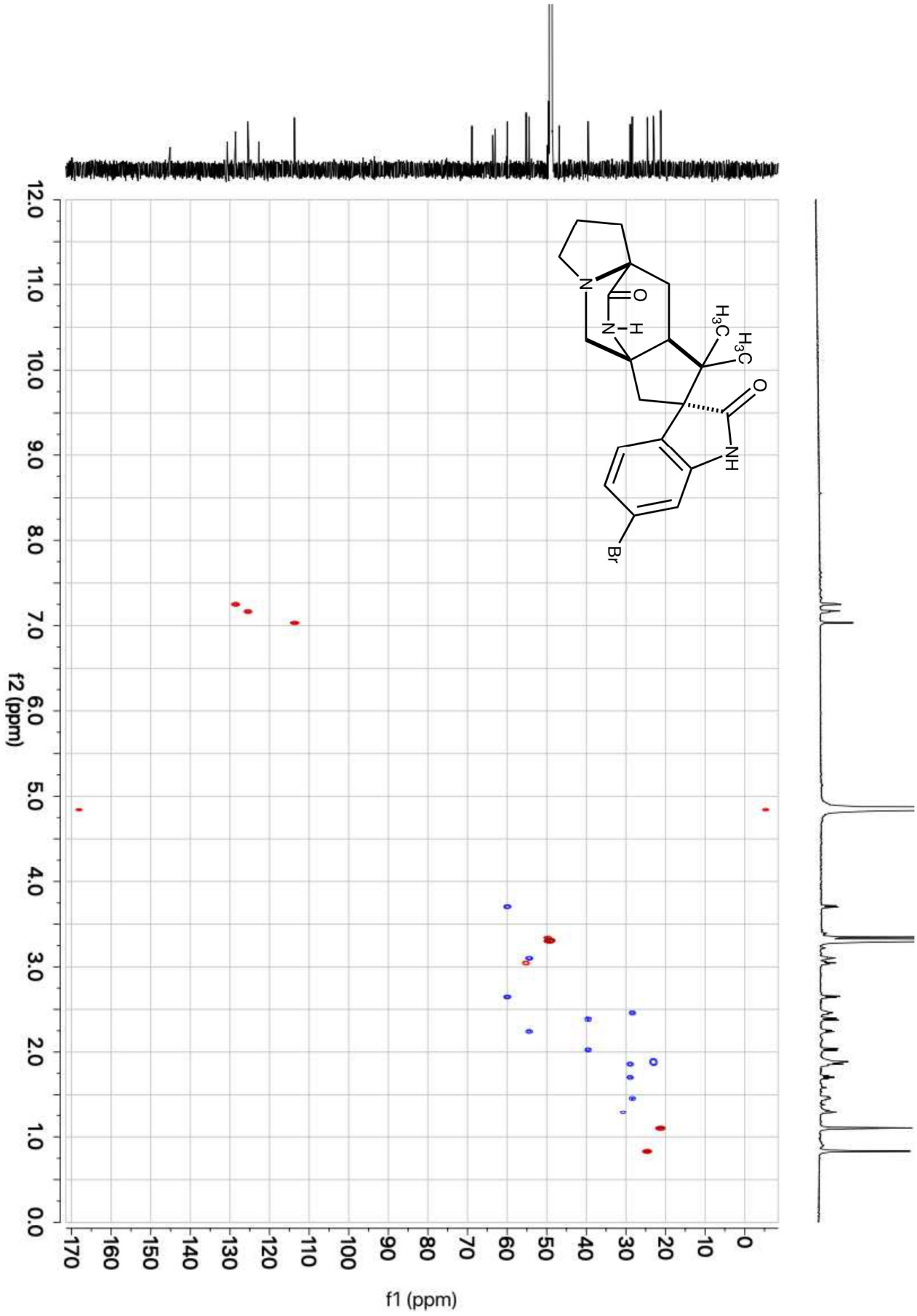

Figure S92. gHSQCAD correlations of spiromalbrancheamide C (**26**) (800 MHz, CD_3OD).

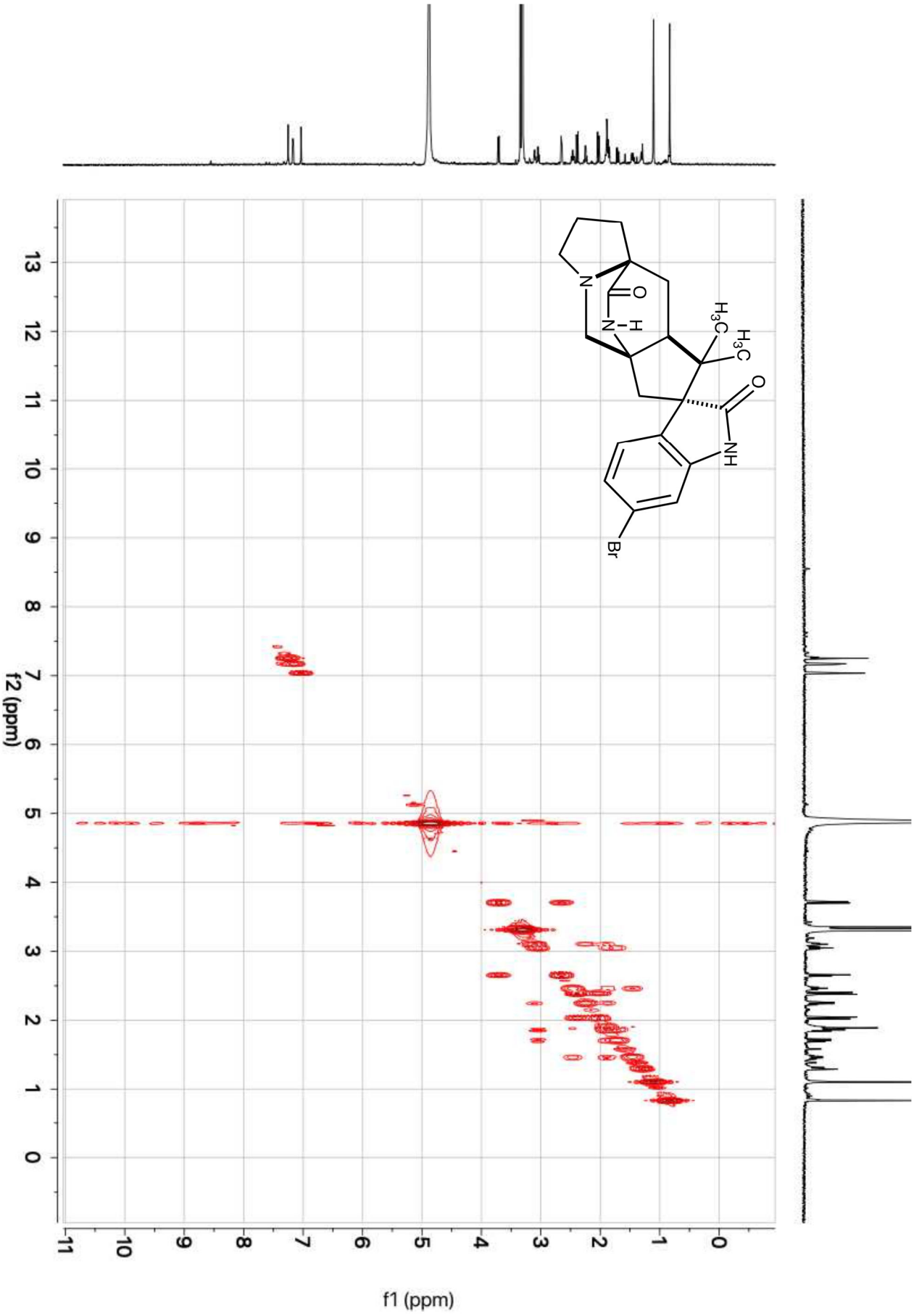

Figure S93. gCOSY correlations of spiromalbrancheamide C (**26**) (800 MHz, CD_3OD).

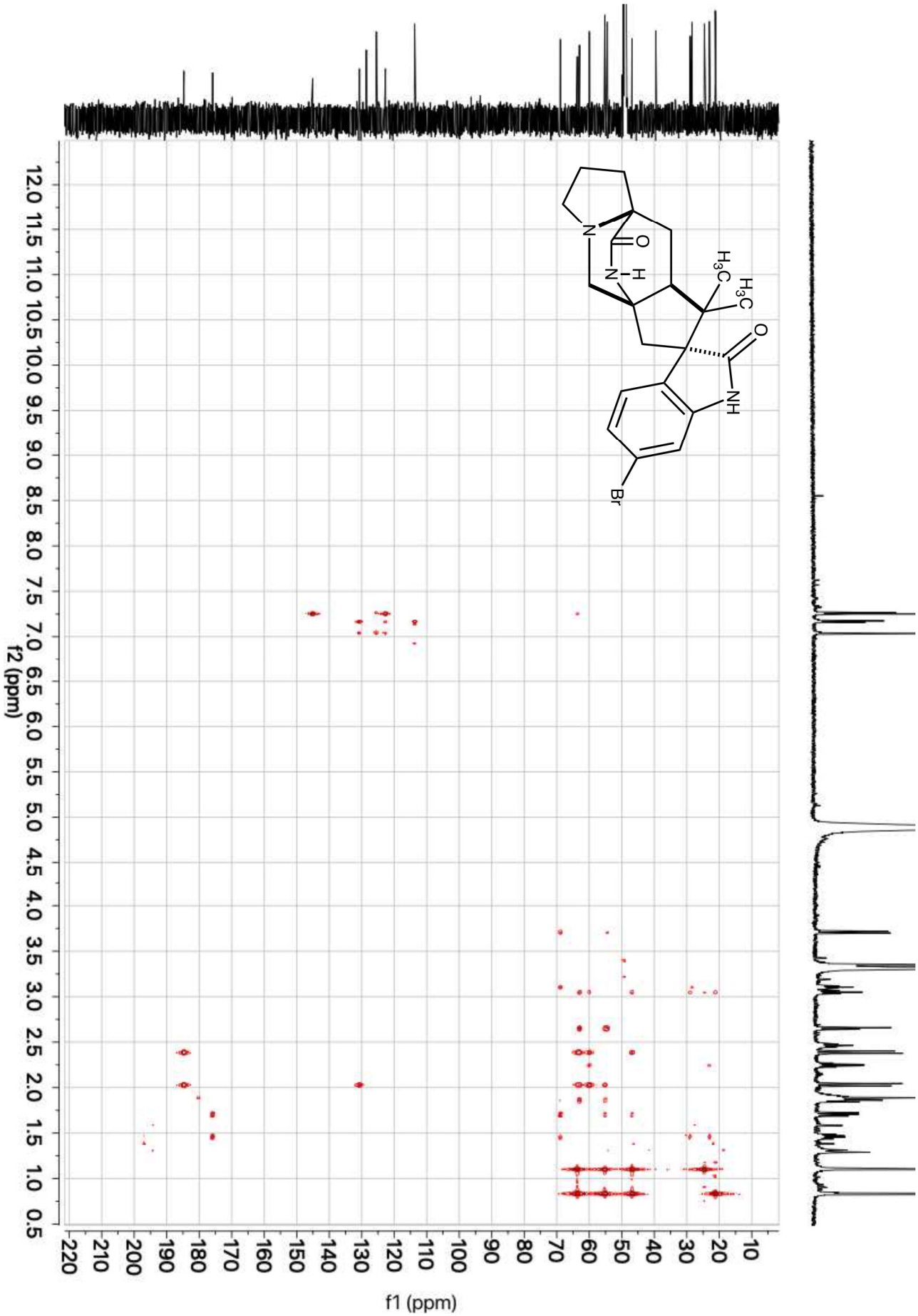

Figure S94. gHMBCAD correlations of spiromalbrancheamide C (**26**) (800 MHz, CD_3OD).

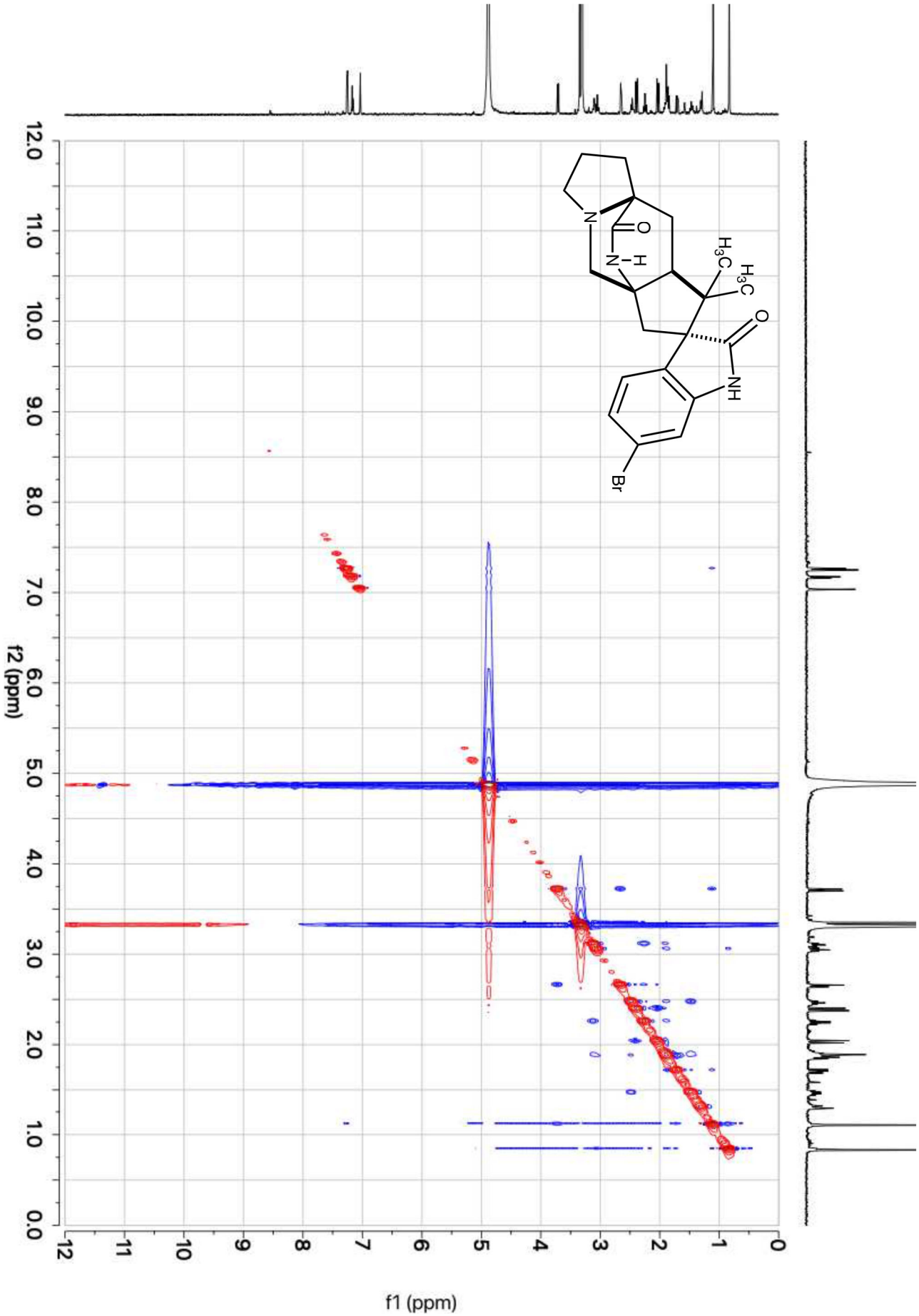

Figure S95. NOESY correlations of spiromalbrancheamide C (**26**) (800 MHz, CD_3OD).

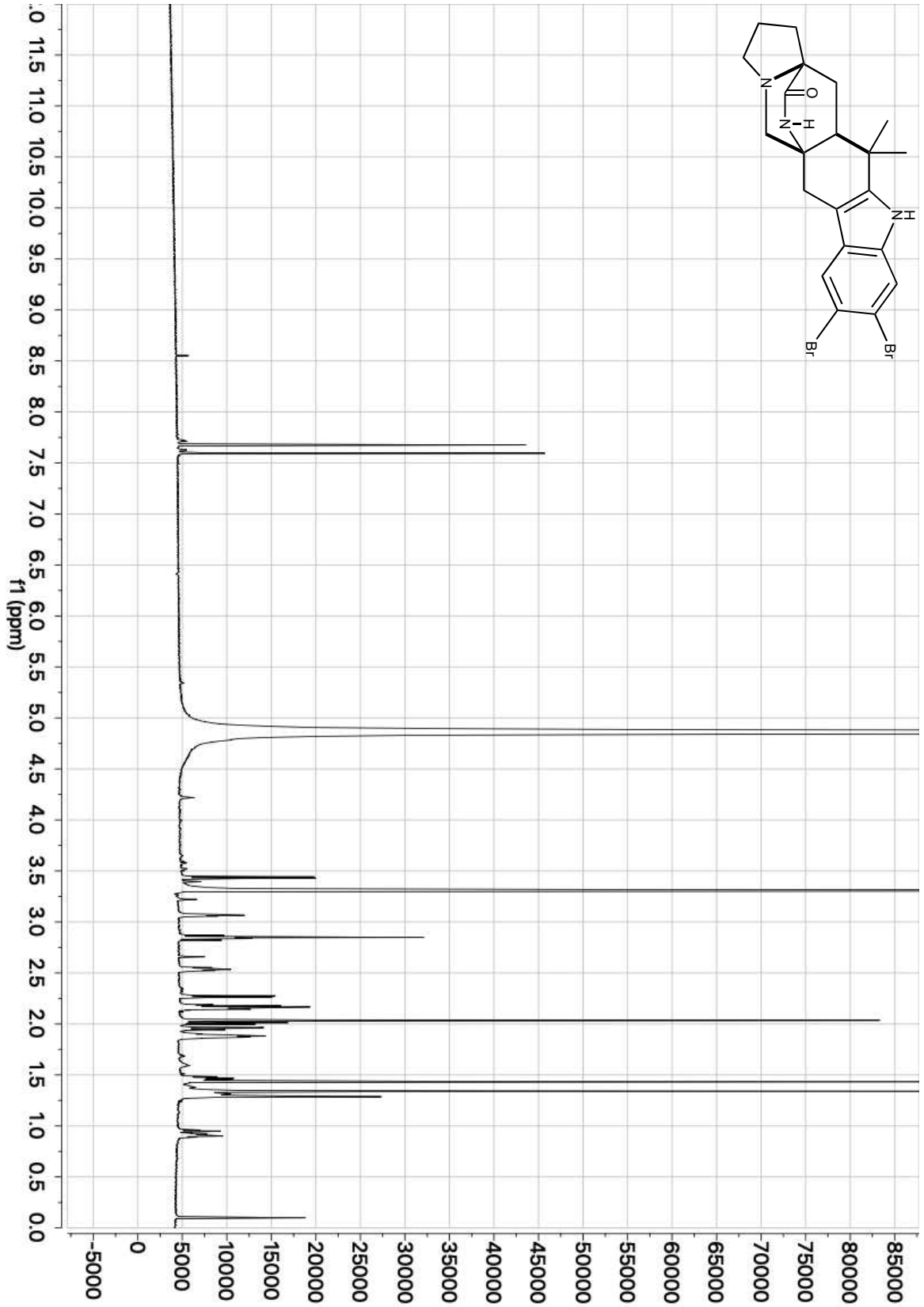

Figure S96. ^{1}H-NMR of malbrancheamide E (**23**) (800 MHz, CD_3OD).

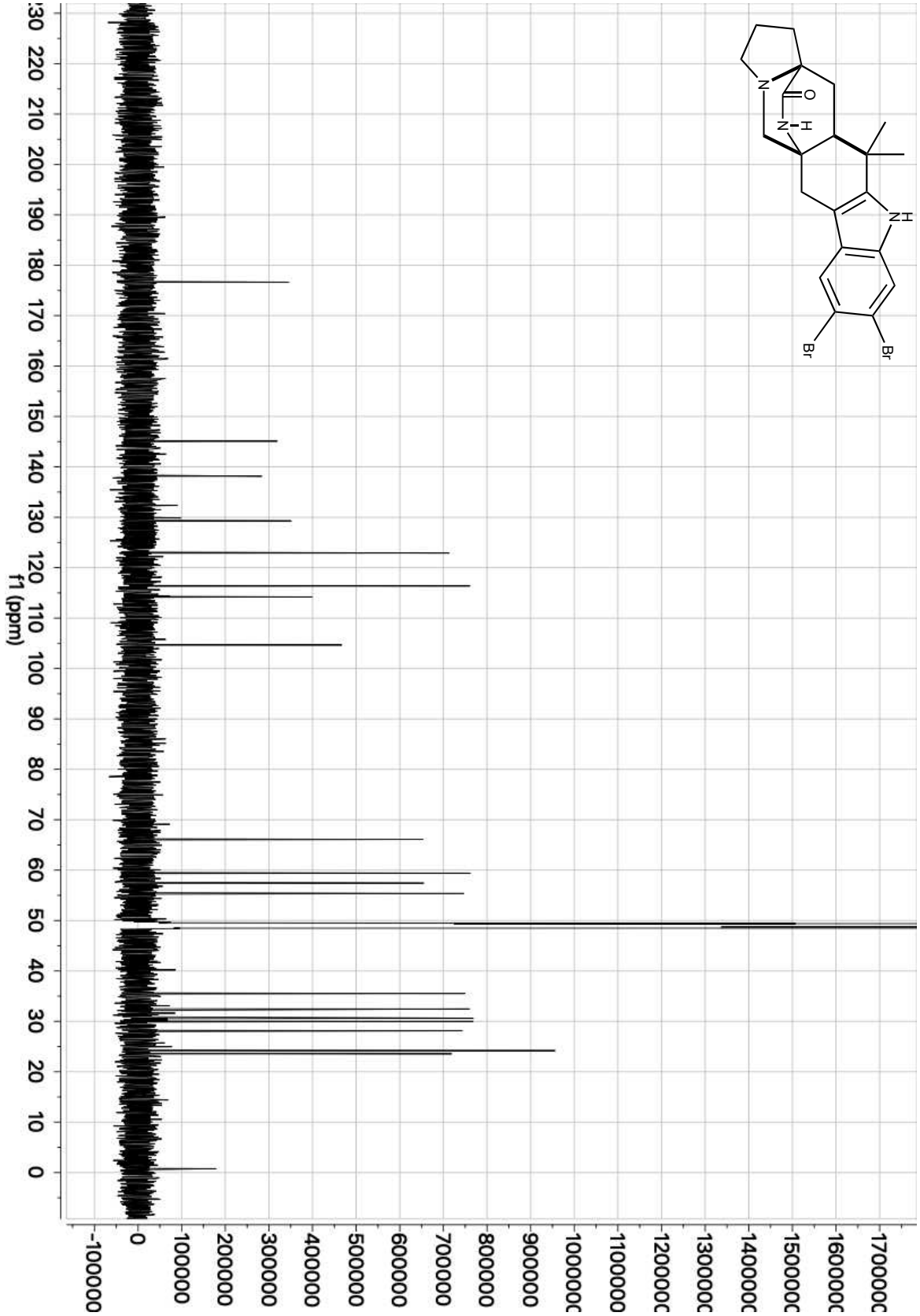

Figure S97. ^{13}C-NMR of malbrancheamide E (**23**) (201 MHz, CD_3OD).

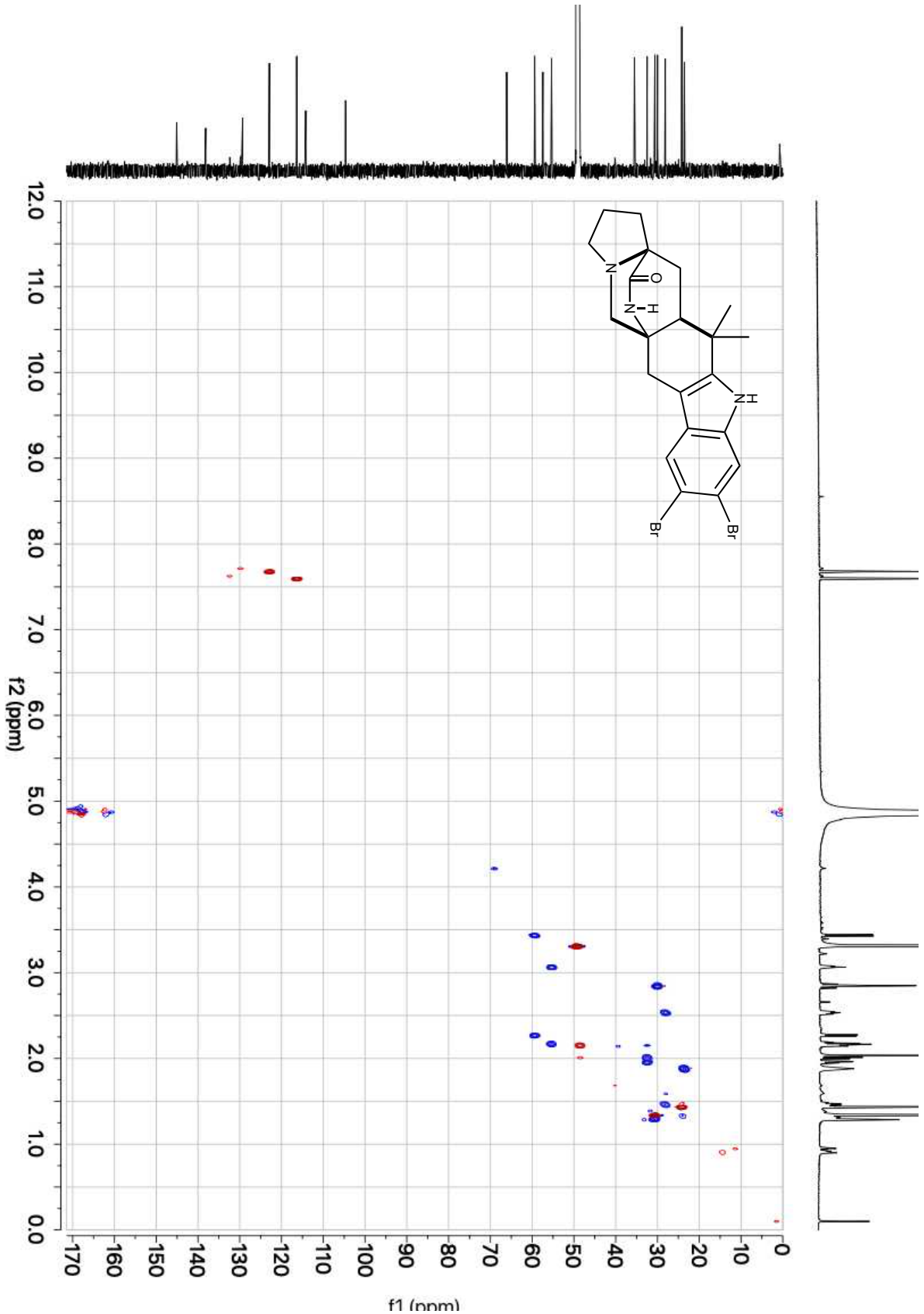

Figure S98. gHSQCAD correlations of malbrancheamide E (**23**) (800 MHz, CD_3OD).

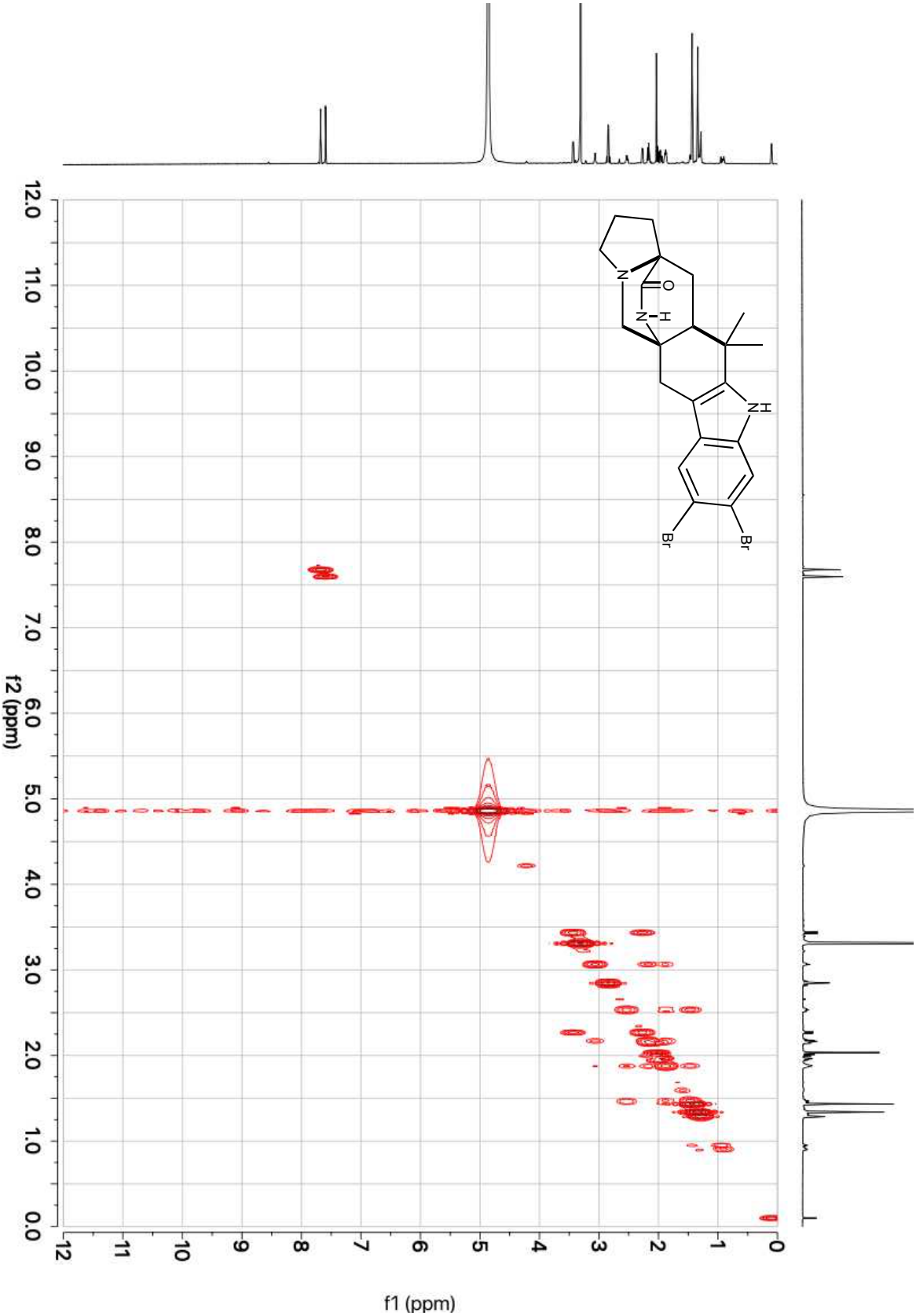

Figure S99. gCOSY correlations of malbrancheamide E (**23**) (800 MHz, CD_3OD).

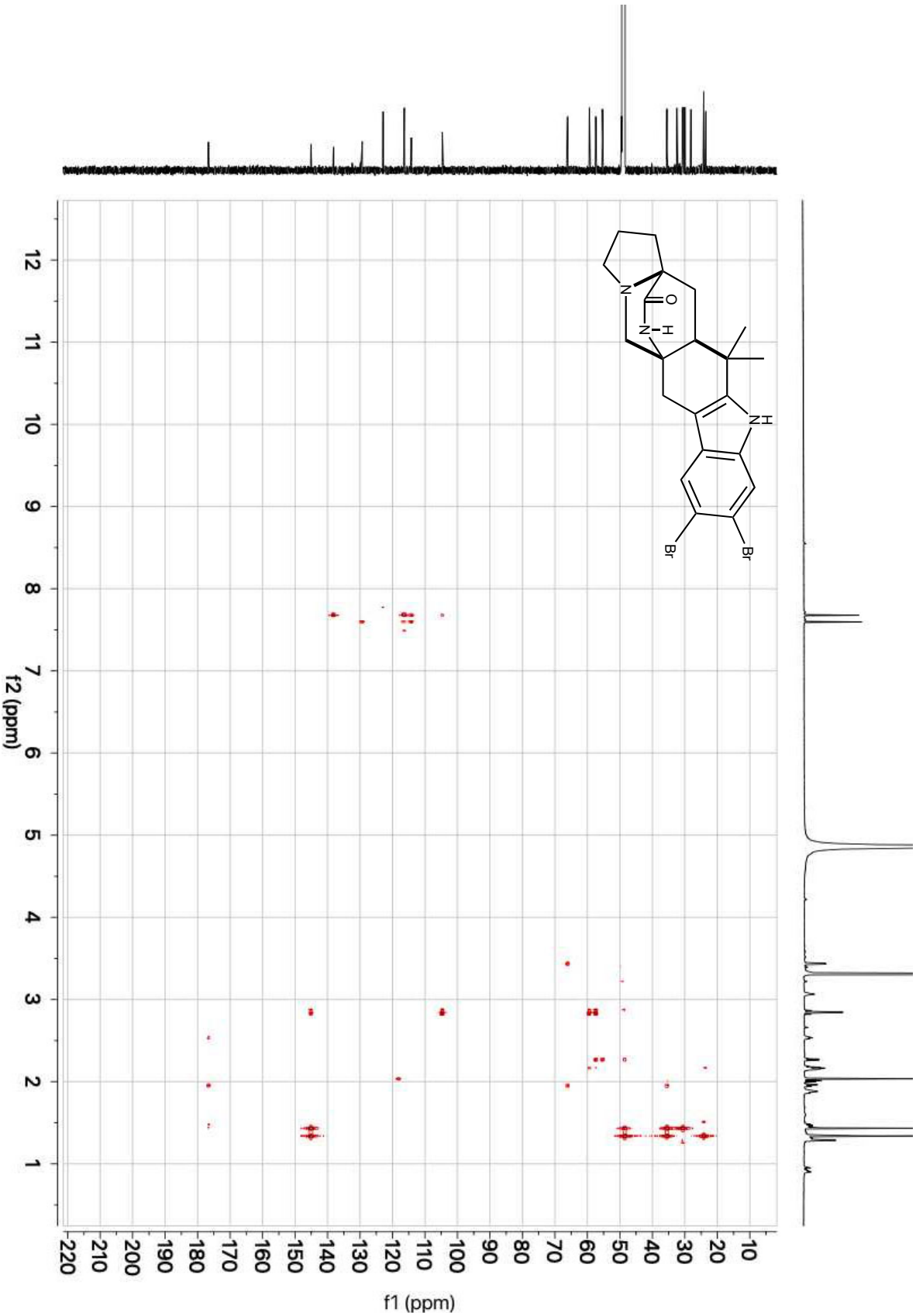

Figure S100. gHMBCAD correlations of malbrancheamide E (**23**) (800 MHz, CD_3OD).

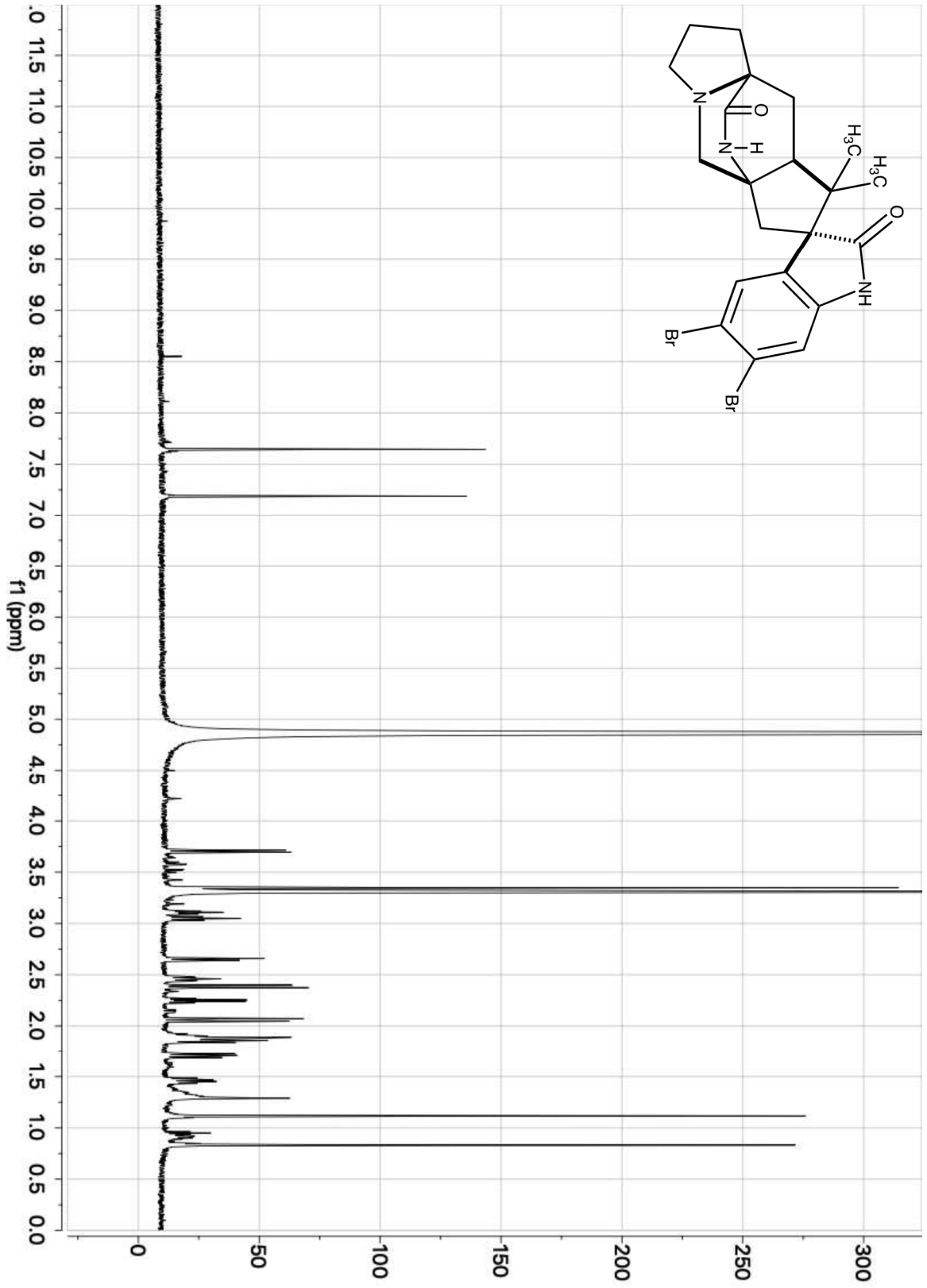

Figure S101. ^{1}H-NMR of spiromalbrancheamide E (**27**) (800 MHz, CD_3OD).

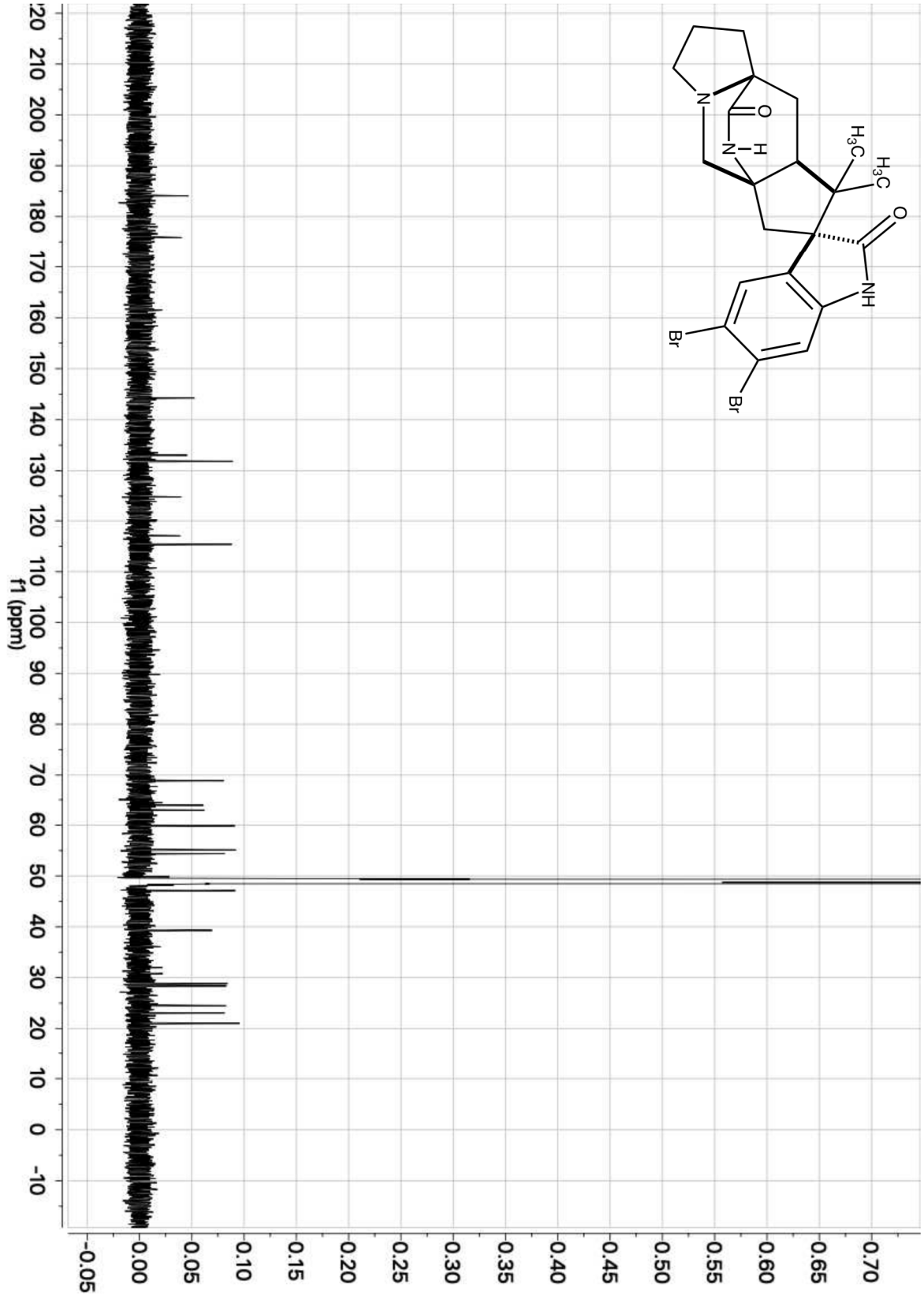

Figure S102. ^{13}C-NMR of spiromalbrancheamide E (**27**) (201 MHz, CD_3OD).

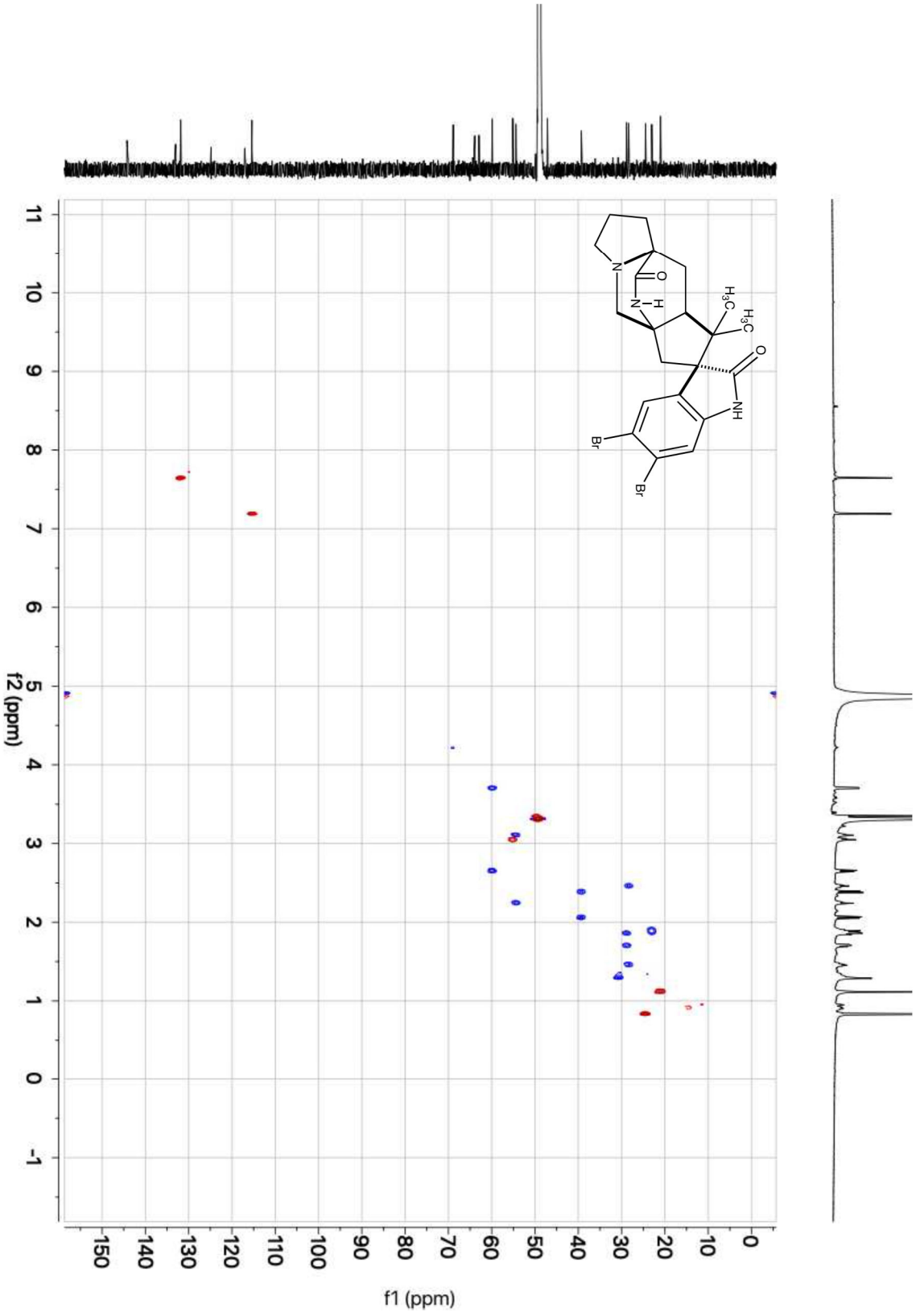

Figure S103. gHSQCAD correlations of spiromalbrancheamide E (**27**) (800 MHz, CD_3OD).

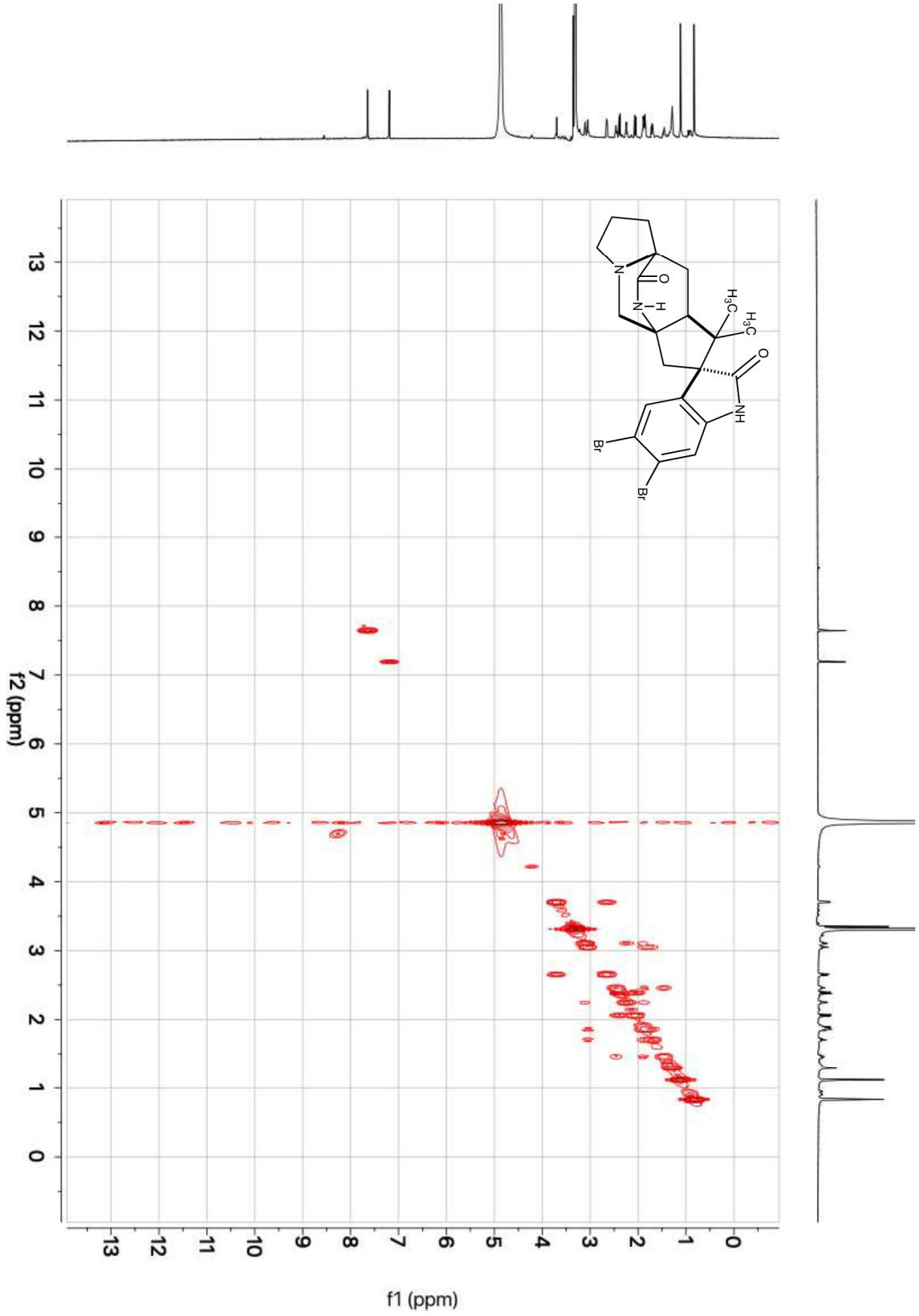

Figure S104. gCOSY correlations of spiromalbrancheamide E (**27**) (800 MHz, CD_3OD).

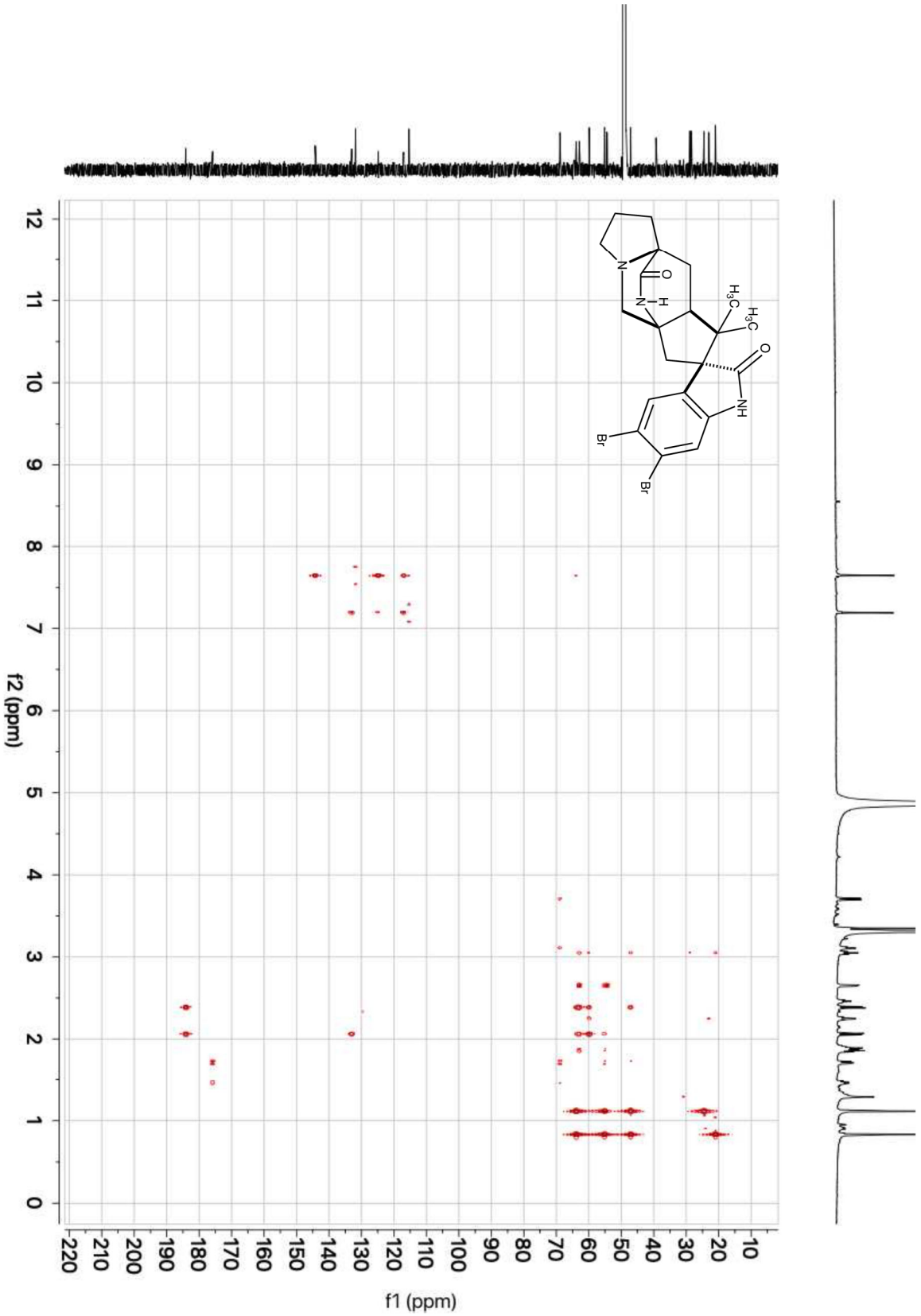

Figure S105. gHMBCAD correlations of spiromalbrancheamide E (**27**) (800 MHz, CD_3OD).

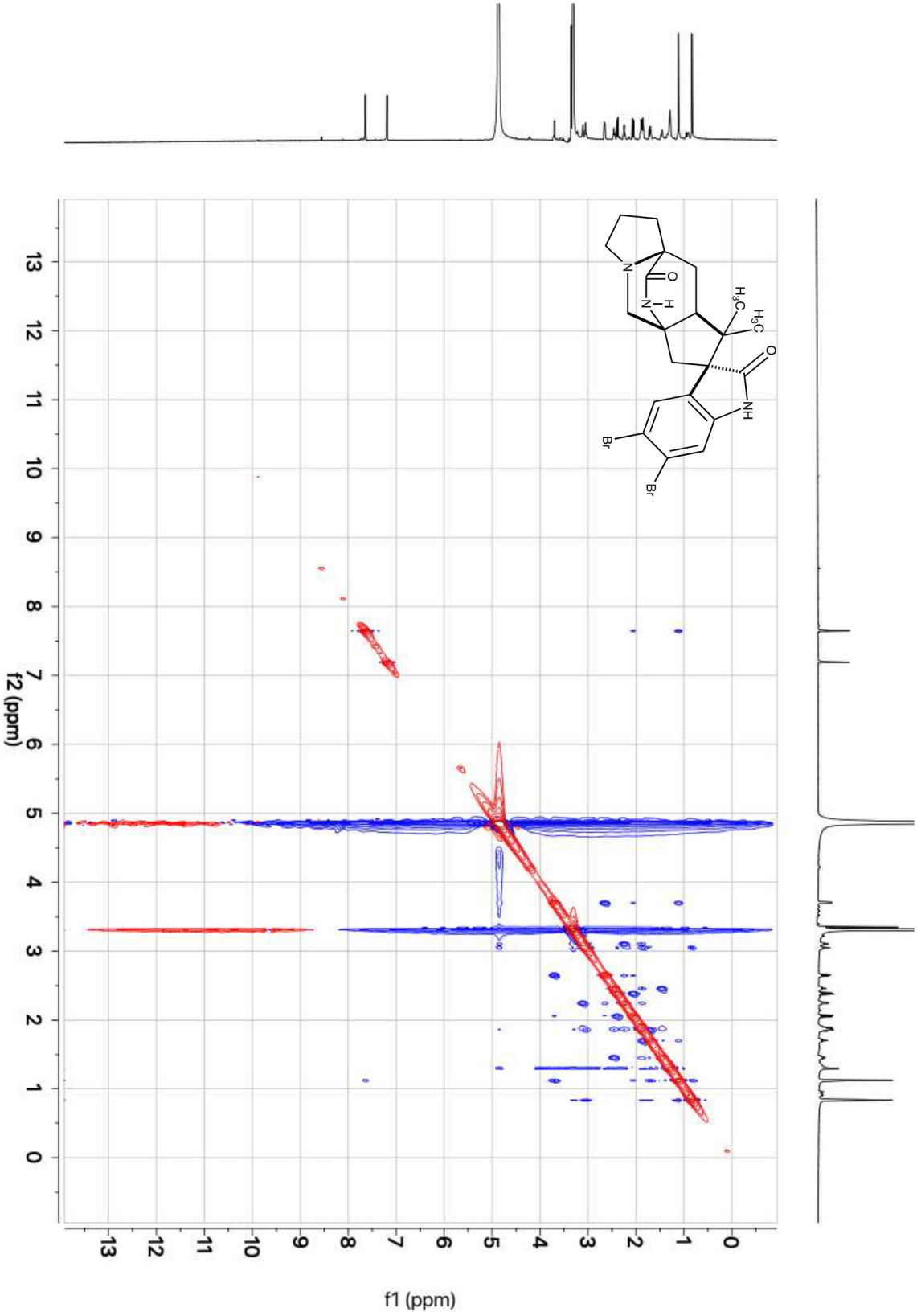

Figure S106. NOESY correlations of spiromalbrancheamide E (**27**) (800 MHz, CD_3OD).

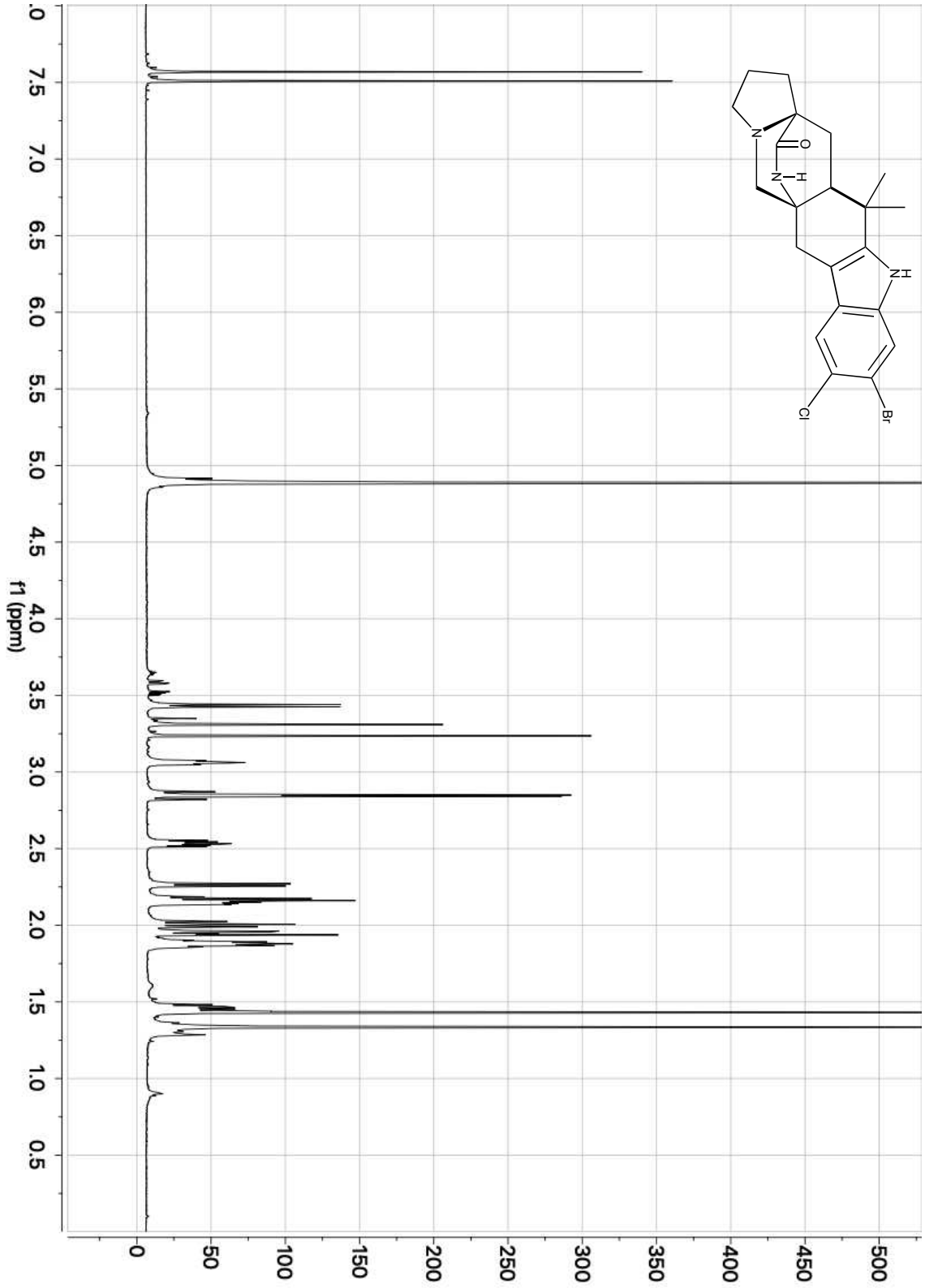

Figure S107. ^{1}H-NMR of isomalbrancheamide D (**24**) isolated from *in vitro* reaction with MalA (700 MHz, CD_3OD).

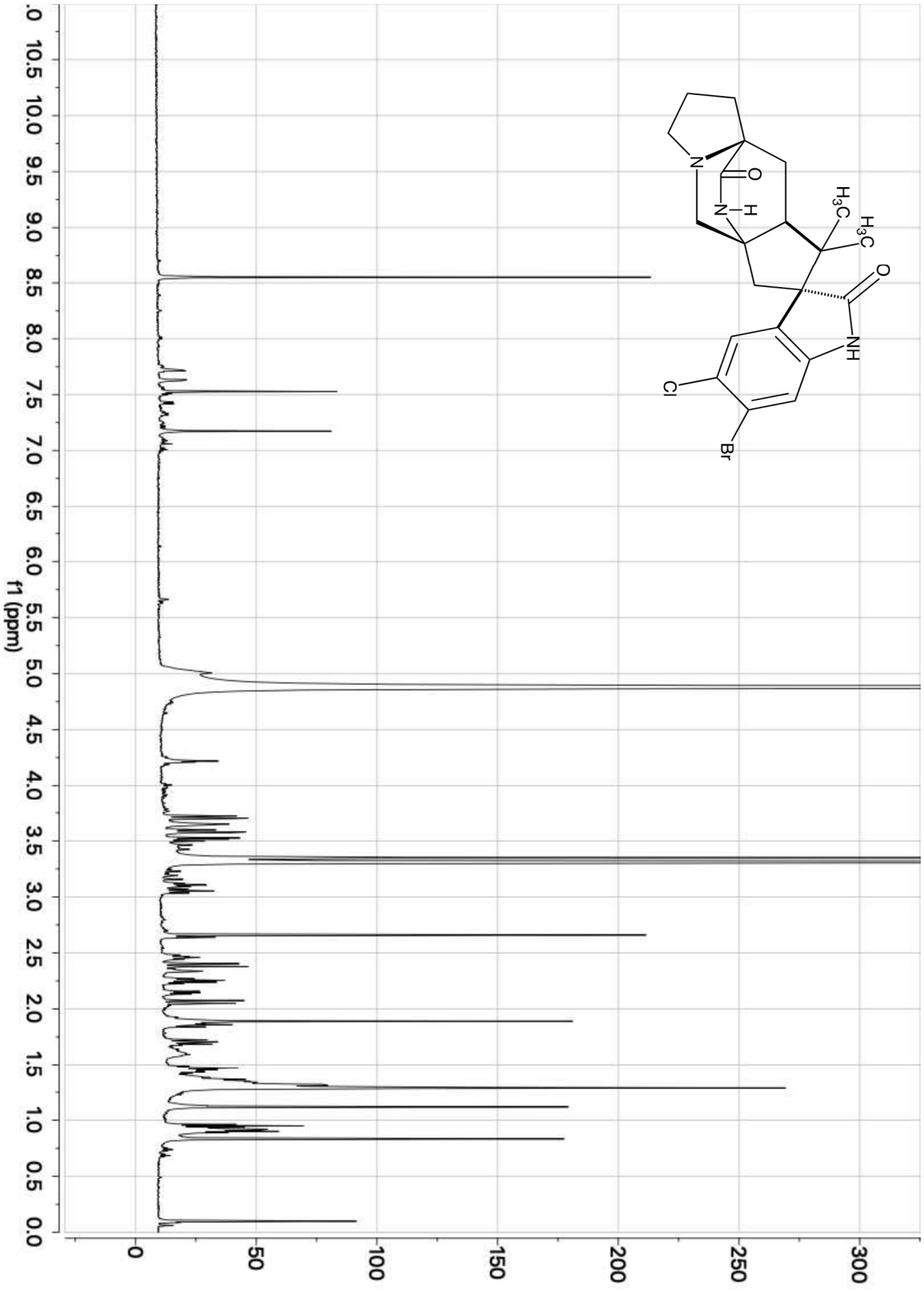

Figure S108. ^{1}H-NMR of spiroisomalbrancheamide D (**28**) (800 MHz, CD_3OD).

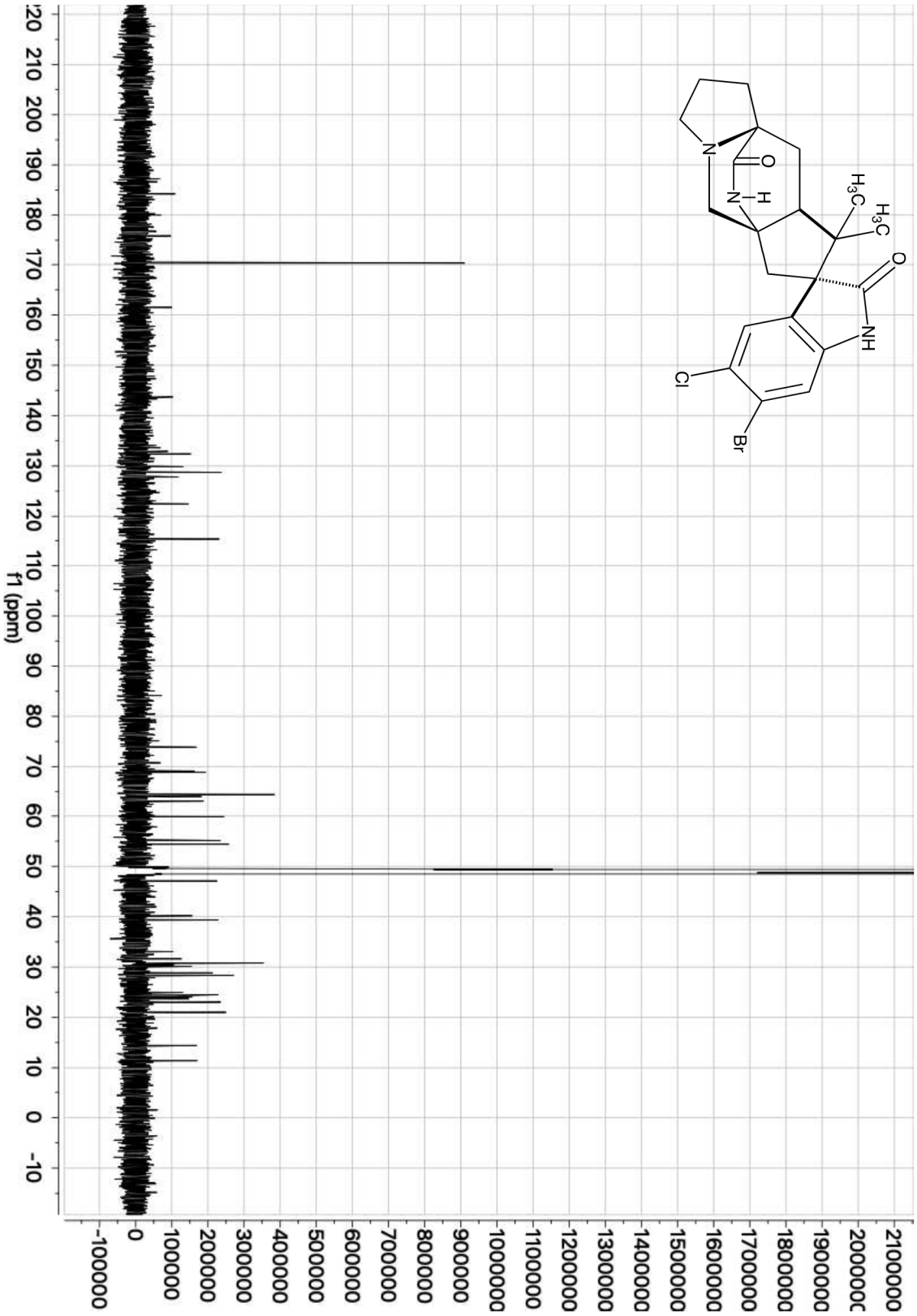

Figure S109. ^{13}C-NMR of spiroisomalbrancheamide D (**28**) (201 MHz, CD_3OD).

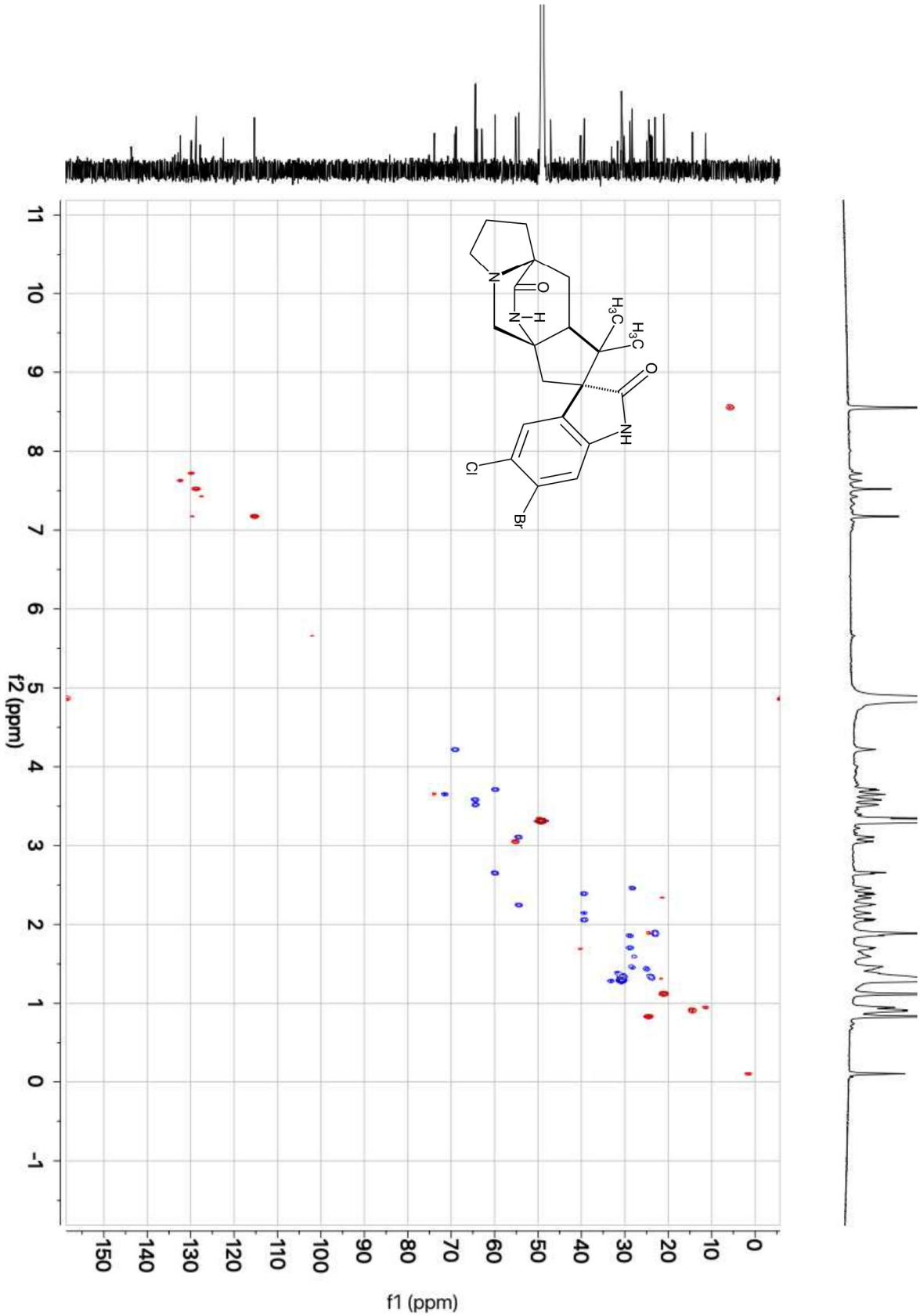

Figure S110. gHSQCAD correlations of spiroisomalbrancheamide D (**28**) (800 MHz, CD_3OD).

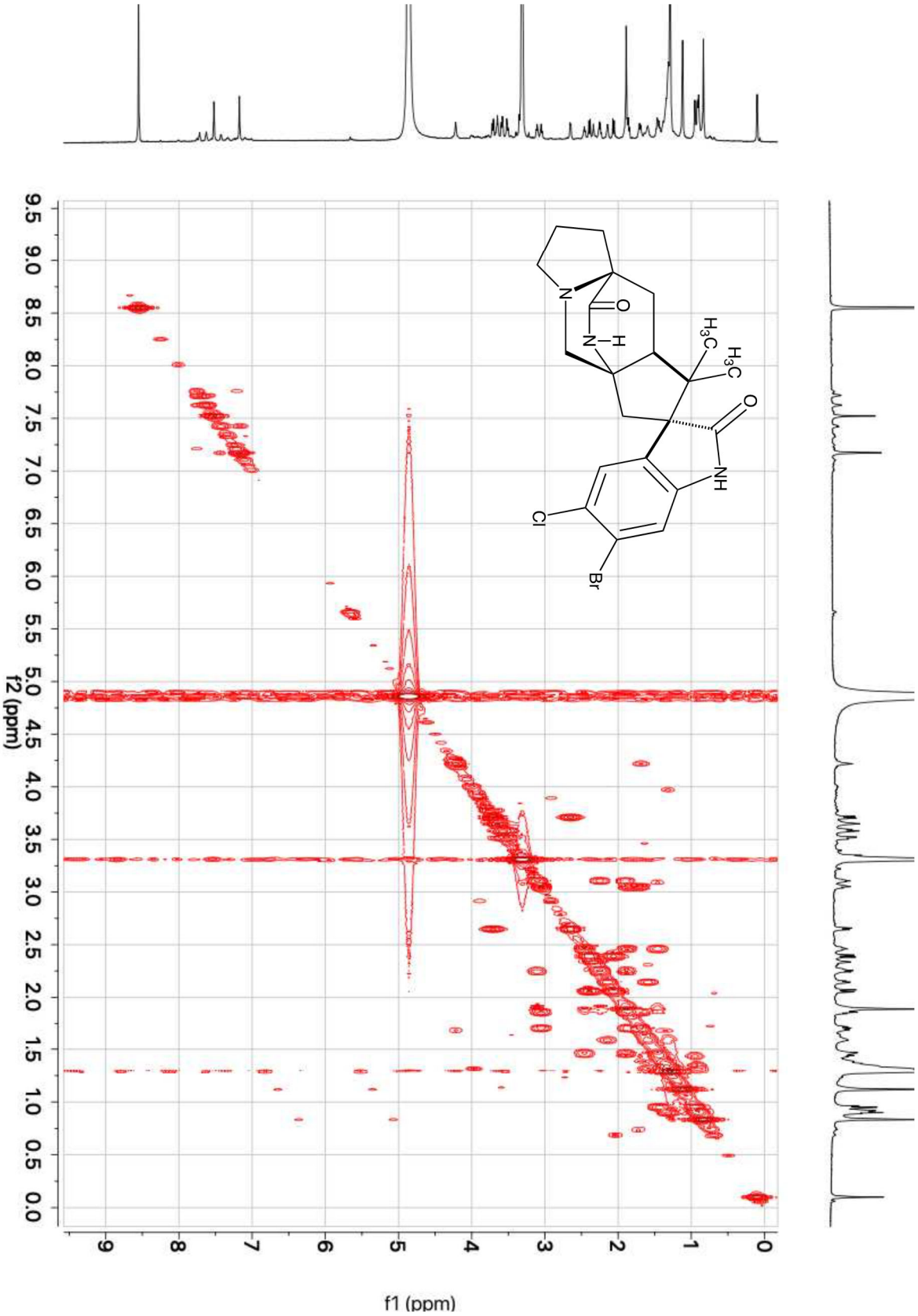

Figure S111. gCOSY correlations of spiroisomalbrancheamide D (**28**) (800 MHz, CD_3OD).

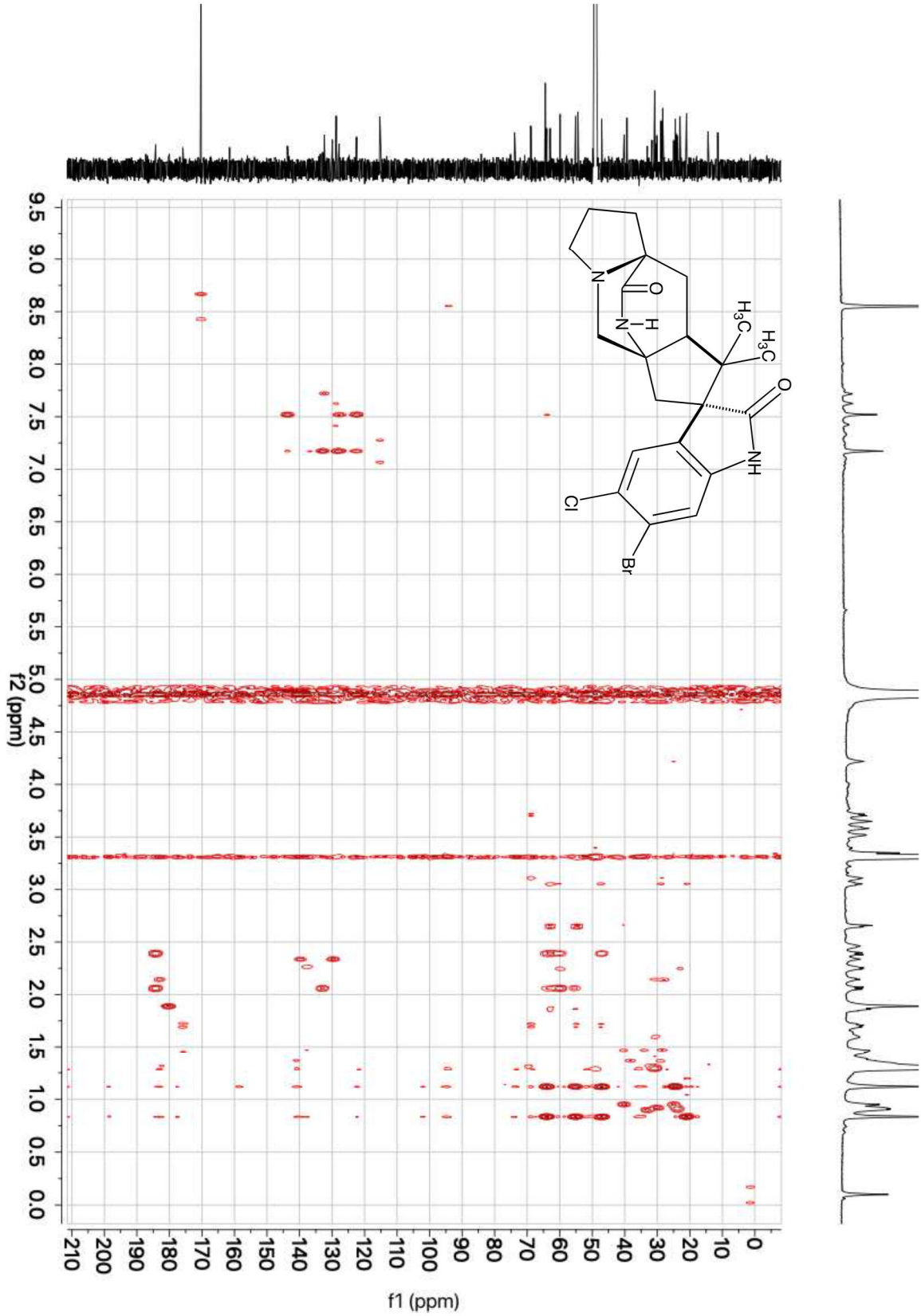

Figure S112. gHMBCAD correlations of spiroisomalbrancheamide D (**28**) (800 MHz, CD_3OD).

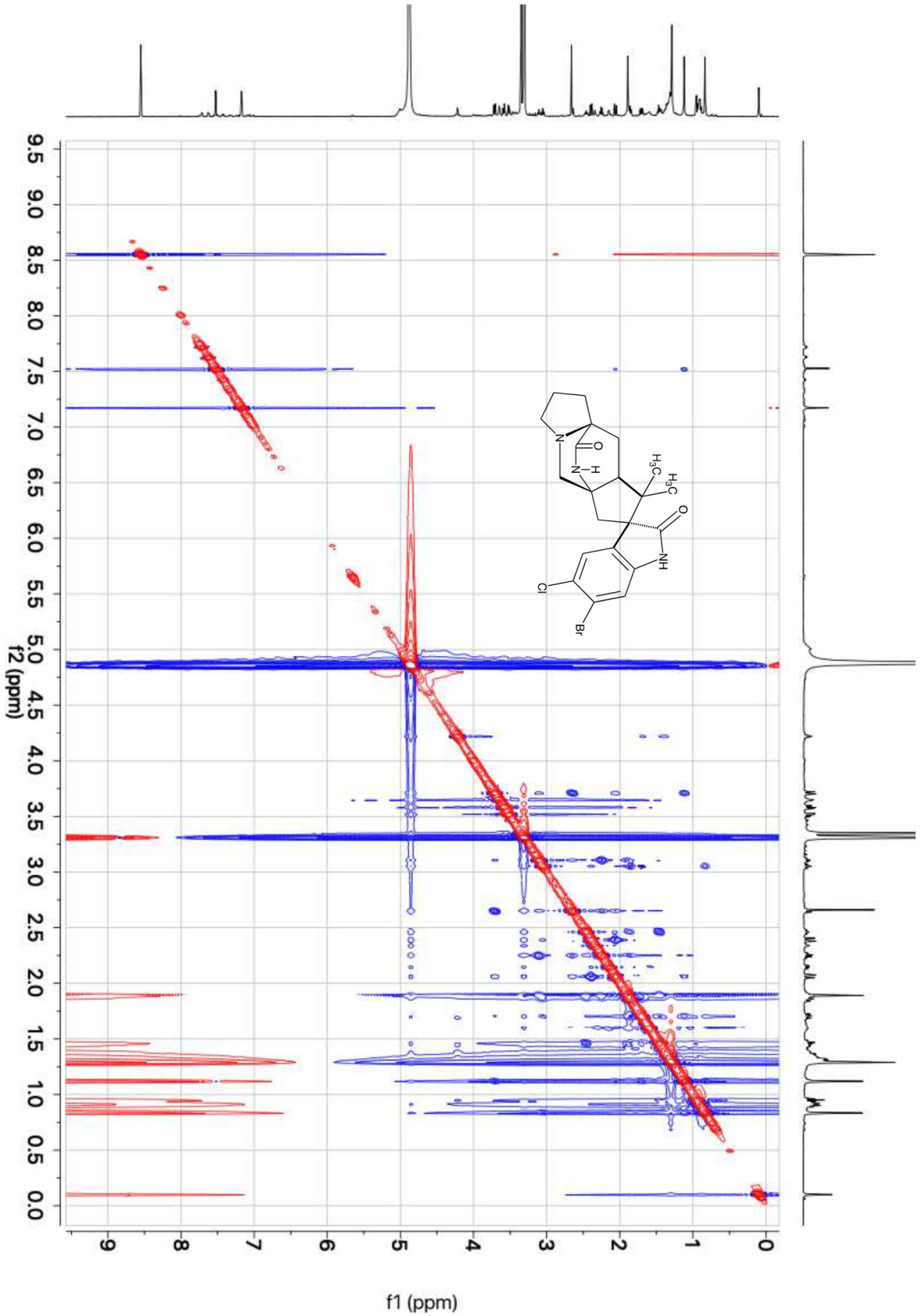

Figure S113. NOESY correlations of spiroisomalbrancheamide D (**28**) (800 MHz, CD_3OD).

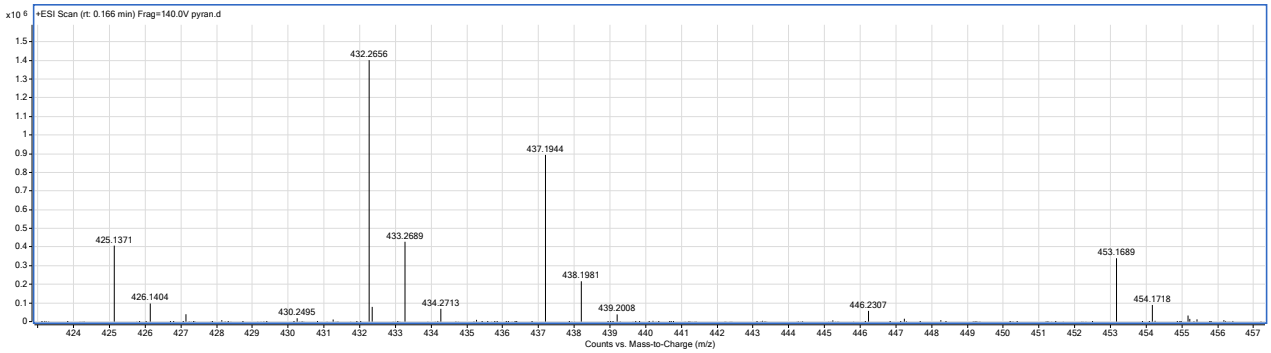

Figure S114. Mass spectrometry (QTOF LC/MS) data for paraherquamide K (**14**).

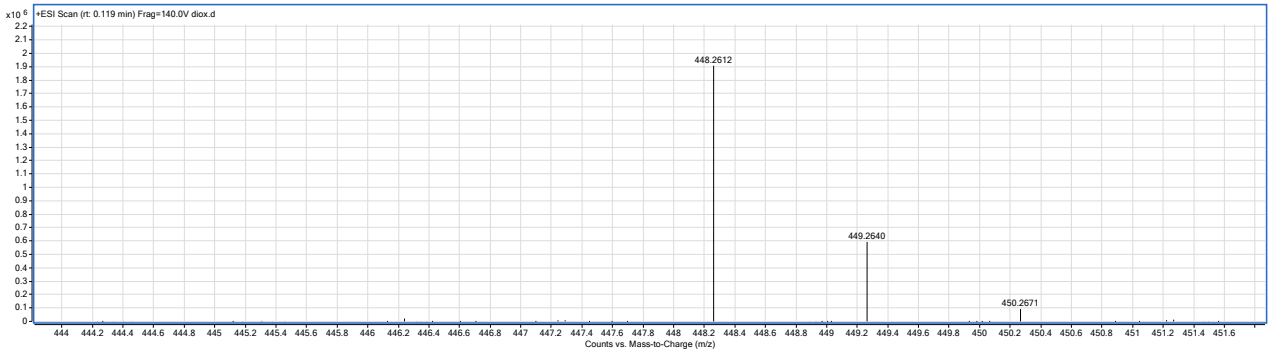

Figure S115. Mass spectrometry (QTOF LC/MS) data for paraherquamide L (**15**).

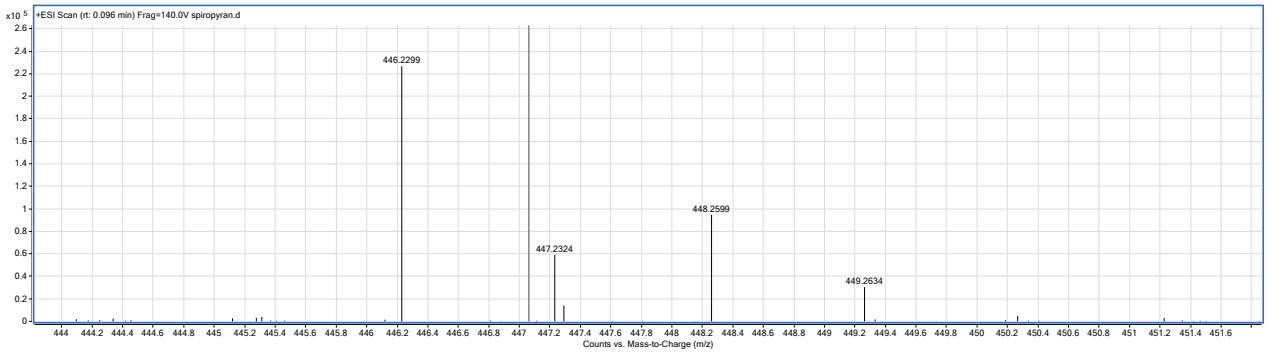

Figure S116. Mass spectrometry (QTOF LC/MS) data for paraherquamide M (**16**).

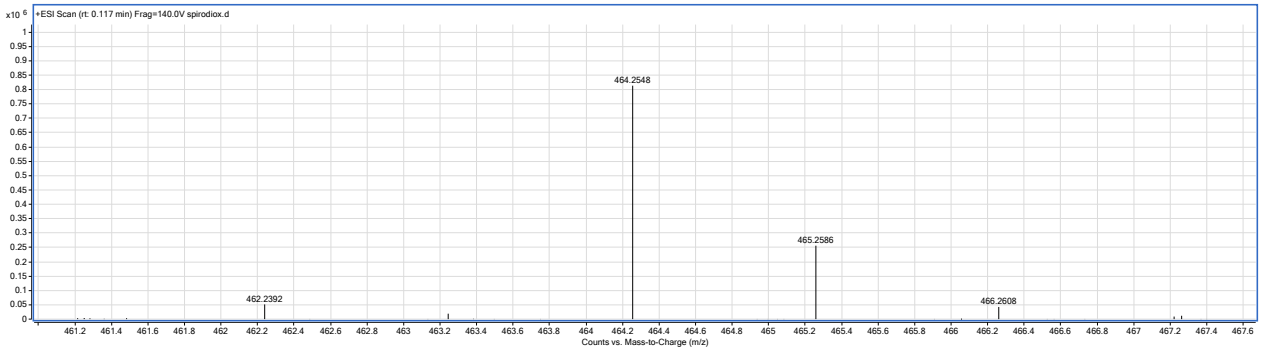

Figure S117. Mass spectrometry (QTOF LC/MS) data for paraherquamide N (**17**).

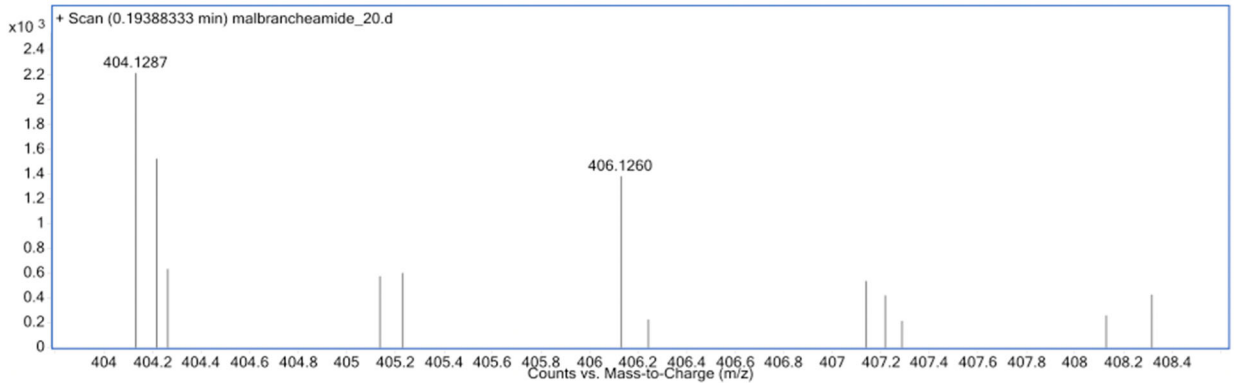

Figure S118. Mass spectrometry (QTOF LC/MS) data for malbrancheamide (**19**).

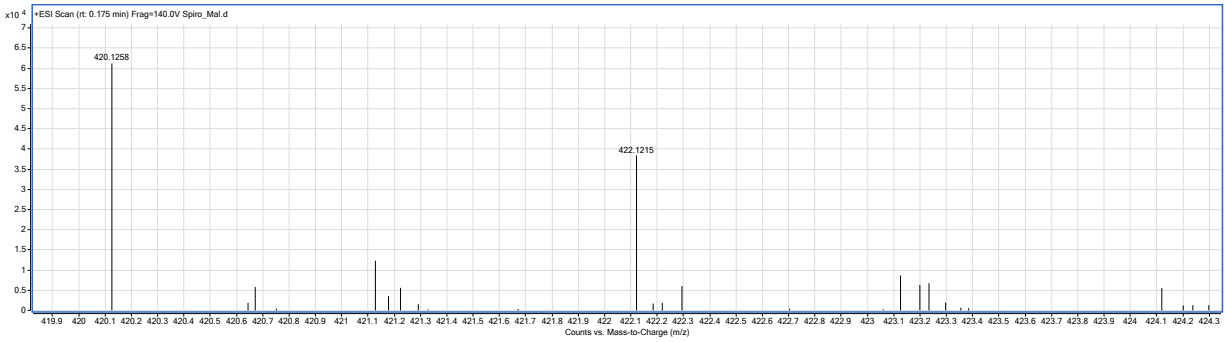

Figure S119. Mass spectrometry (QTOF LC/MS) data for spiromalbramide (**20**).

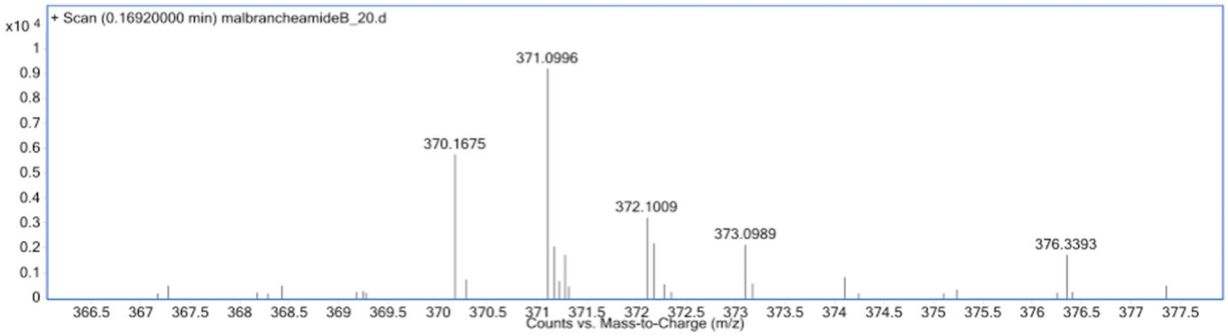

Figure S120. Mass spectrometry (QTOF LC/MS) data for malbrancheamide B (**21**).

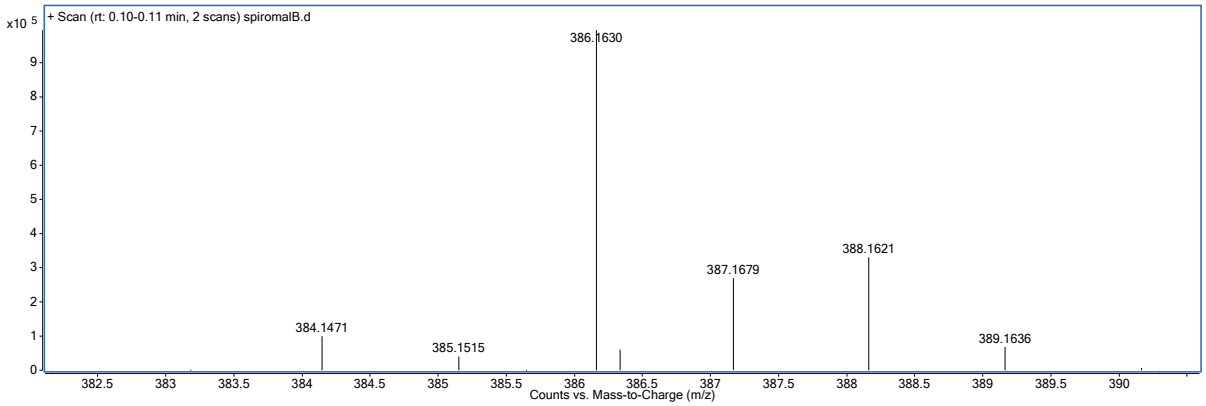

Figure S121. Mass spectrometry(TOF LC/MS) data for spiromalbrancheamide B (**25**).

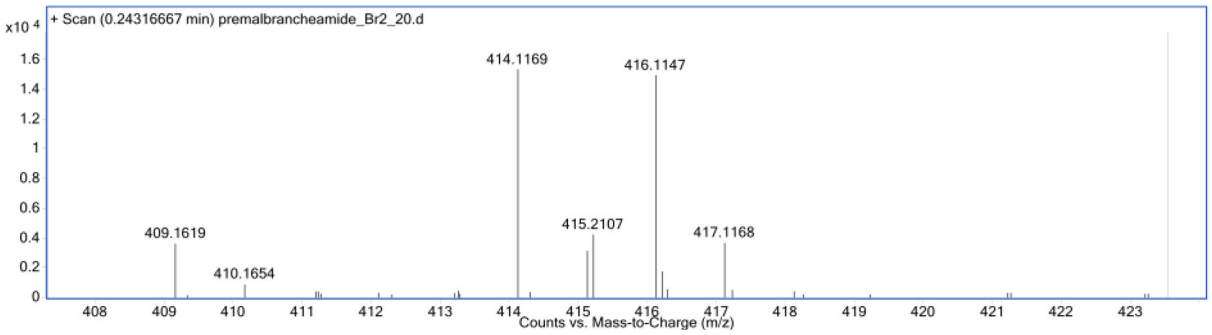

Figure S122. Mass spectrometry (QTOF LC/MS) data for malbrancheamide C (**22**).

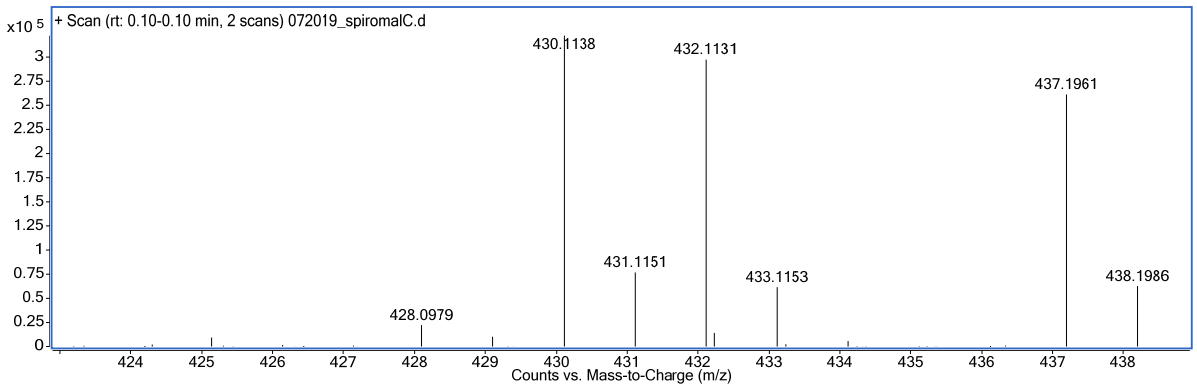

Figure S123. Mass spectrometry (TOF LC/MS) data for spiromalbrancheamide C (**26**).

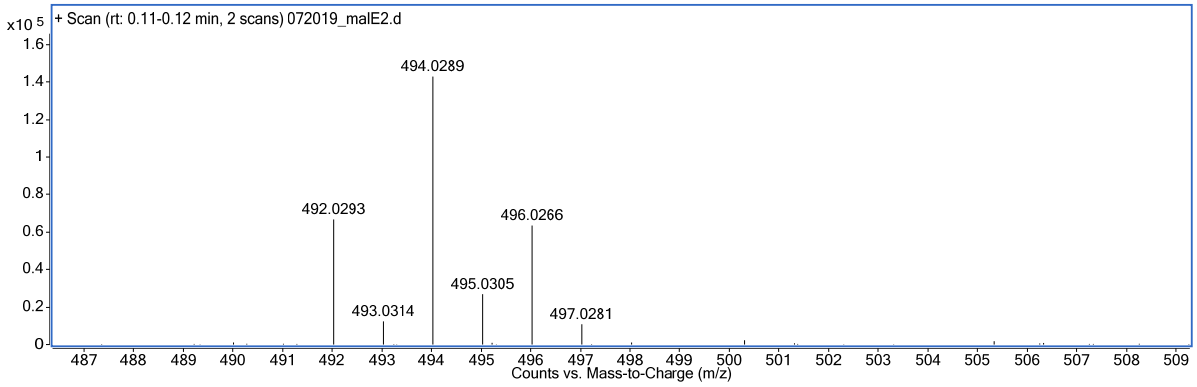

Figure S124. Mass spectrometry (TOF LC/MS) data for malbrancheamide E (**23**).

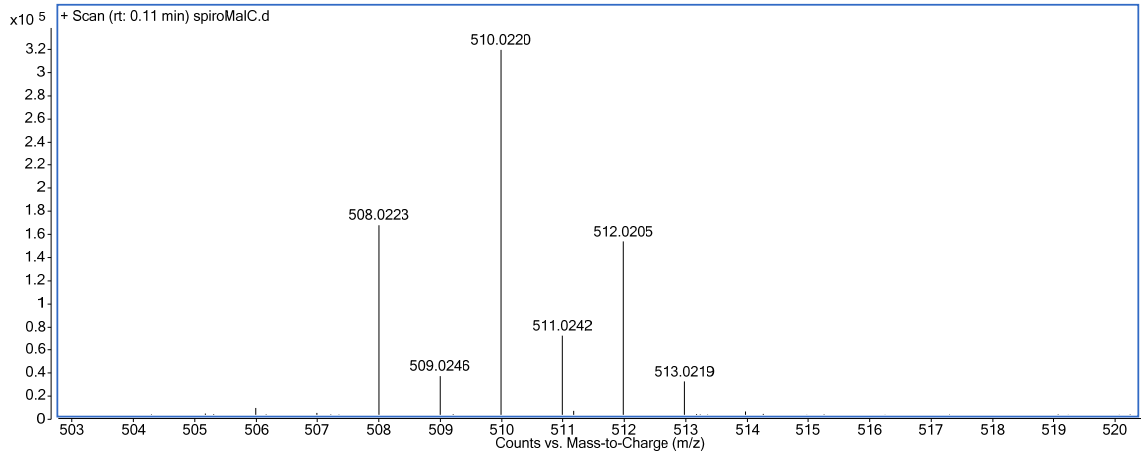

Figure S125. Mass spectrometry (TOF LC/MS) data for spiromalbrancheamide E (**27**).

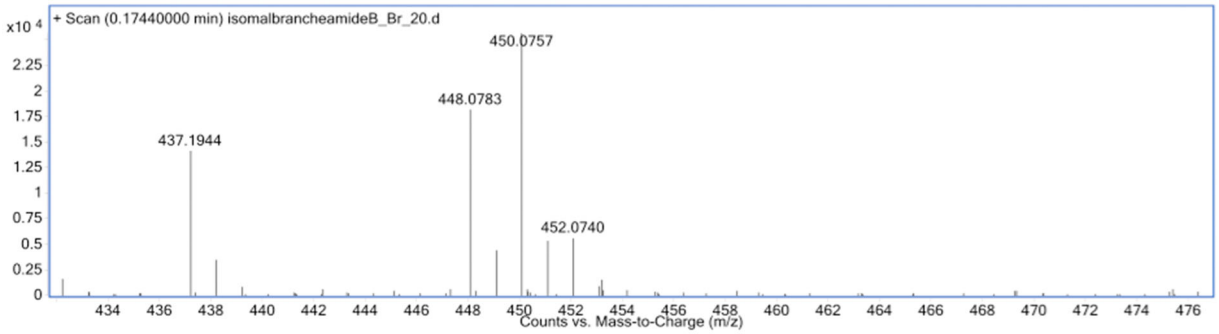

Figure S126. Mass spectrometry (TOF LC/MS) data for isomalbrancheamide D (**24**).

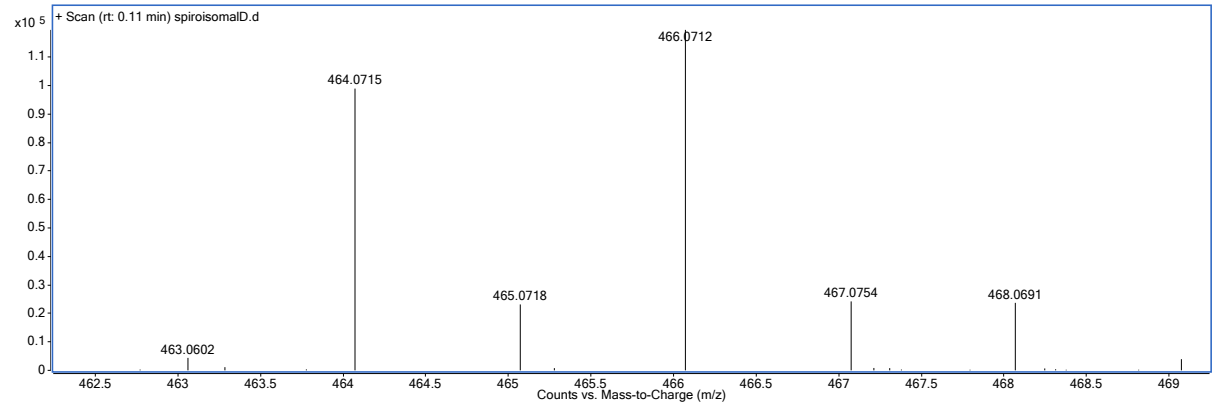

Figure S127. Mass spectrometry (TOF LC/MS) data for spiroisomalbrancheamide D (**28**).

Energies and Cartesian Coordinates of All Optimized Structures

ZPVE = zero-point vibrational energy; TCE = thermal correction to energy; TCH = thermal correction to enthalpy; TCG = thermal correction to Gibbs free energy.

Thermodynamics of 35-41 of R^1=H and R^2=H system

Structure	ZPVE	TCE	TCH	ECG	E	H (E + TCH)	G (E + TCG)
29	0.286687	0.299833	0.300777	0.248339	-673.410745	-673.109967	-673.162405
Guan	0.087548	0.093928	0.094872	0.058614	-205.753171	-205.658299	-205.694557
30	0.377237	0.397168	0.398112	0.330188	-879.182458	-878.784346	-878.852270
31	0.377010	0.396644	0.397589	0.330225	-879.162238	-878.764649	-878.832013
32	0.377032	0.397747	0.398691	0.327513	-879.228330	-878.829639	-878.900817
33	0.286648	0.300287	0.301231	0.247303	-673.456391	-673.155160	-673.209088
34	0.377577	0.397186	0.398130	0.329724	-879.168776	-878.770646	-878.839053
35	0.375908	0.397100	0.398044	0.325511	-879.207054	-878.809009	-878.881543
36	0.286118	0.299924	0.300868	0.246565	-673.436097	-673.135229	-673.189532

Transition States of R^1=H and R^2=H system

Structure	ZPVE	TCE	TCH	ECG	E	H (E + TCH)	G (E + TCG)	Imaginary Frequency
TS-1 C2 1,2 shift	0.374323	0.394276	0.395220	0.326766	-879.152734	-878.757514	-878.825969	-304.137
TS-2 C3 1,2 shift	0.374763	0.394659	0.395603	0.326885	-879.152613	-878.757010	-878.825728	-370.426

Thermodynamics of 35-41 of R^1=OMe and R^2=H system

Structure	ZPVE	TCE	TCH	ECG	E	H (E + TCH)	G (E + TCG)
29	0.319727	0.335542	0.336486	0.277933	-787.890513	-787.554027	-787.612580
30	0.410738	0.433241	0.434185	0.360706	-993.662768	-993.228583	-993.302062
31	0.411123	0.433042	0.433987	0.362171	-993.652737	-993.218750	-993.290566
32	0.410513	0.433735	0.434679	0.357624	-993.707829	-993.273150	-993.350204
33	0.319989	0.336103	0.337047	0.277582	-787.936066	-787.599019	-787.658484
34	0.411215	0.433314	0.434258	0.361025	-993.654278	-993.220020	-993.293252
35	0.409485	0.432952	0.433896	0.356986	-993.690871	-993.256975	-993.333885
36	0.319236	0.335663	0.336607	0.276021	-787.919018	-787.582411	-787.642997

Transition States of R^1=OMe and R^2=H system

Structure	ZPVE	TCE	TCH	ECG	E	H (E + TCH)	G (E + TCG)	Imaginary Frequency
TS-1 C2 1,2 shift	0.406935	0.429593	0.430537	0.355921	-993.634638	-993.204101	-993.278717	-339.945
TS-2 C3 1,2 shift	0.408117	0.430633	0.431577	0.357283	-993.634734	-993.203157	-993.277451	-398.211

Thermodynamics of 35-41 of R^1=OMe and R^2=OMe system

Structure	ZPVE	TCE	TCH	ECG	E	H (E + TCH)	G (E + TCG)
29	0.352331	0.371072	0.372016	0.306774	-902.361653	-901.989637	-902.054878
30	0.443443	0.468904	0.469848	0.388675	-1108.136336	-1107.666488	-1107.747660
31	0.442810	0.468075	0.469019	0.389417	-1108.118215	-1107.649195	-1107.728797
32	0.443220	0.469326	0.470270	0.387162	-1108.179351	-1107.709081	-1107.792189
33	0.352820	0.371931	0.372875	0.306570	-902.407226	-902.034351	-902.100657
34	0.444902	0.469509	0.470453	0.392640	-1108.127085	-1107.656632	-1107.734445
35	0.442565	0.468779	0.469723	0.386880	-1108.160123	-1107.690400	-1107.773243
36	0.351937	0.371276	0.372221	0.304905	-902.388599	-902.016379	-902.083694

Transition States of R^1=OMe and R^2=OMe system

Structure	ZPVE	TCE	TCH	ECG	E	H (E + TCH)	G (E + TCG)	Imaginary Frequency
TS-1 C2 1,2 shift	0.440052	0.465635	0.466580	0.385320	-1108.104717	-1107.638138	-1107.719397	-334.702
TS-2 C3 1,2 shift	0.440974	0.466424	0.467368	0.386601	-1108.101216	-1107.633848	-1107.714615	-370.917

Thermodynamics of R^1=H and R^2=H without Arg model (guan) system

Structure	ZPVE	TCE	TCH	ECG	E	H (E + TCH)	G (E + TCG)
33	0.298803	0.312671	0.313615	0.259908	-673.846908	-673.533293	-673.587000
34	0.286648	0.300287	0.301231	0.247303	-673.456391	-673.155160	-673.209088
35	0.299587	0.313742	0.314687	0.259813	-673.852975	-673.538288	-673.593162
36	0.286118	0.299924	0.300868	0.246565	-673.436097	-673.135229	-673.189532

Transition States of R^1=H and R^2=H without Arg model (guan) system

Structure	ZPVE	TCE	TCH	ECG	E	H (E + TCH)	G (E + TCG)	Imaginary Frequency
TS-1 C2 1,2 shift	0.296770	0.310488	0.311432	0.258210	-673.825694	-673.514262	-673.567484	-287.302
TS-2 C3 1,2 shift	0.297904	0.311526	0.312470	0.258968	-673.822303	-673.509832	-673.563335	-390.426